CYCLONIC ACTIVITY AND ITS INFLUENCES ON ANTARCTICA

DISSERTATION

zur Erlangung des akademischen Grades
eines Doktors der Naturwissenschaften
am Fachbereich für Geowissenschaften
der Freien Universität Berlin

vorgelegt von

Jens Grieger

Berlin, 04. November 2014

1. Gutachter: PD Dr. Gregor C. Leckebusch
School of Geography, Earth and Environmental Sciences,
University of Birmingham

2. Gutachter: Prof. Dr. Uwe Ulbrich
Institut für Meteorologie, Freie Universität Berlin

Tag der Disputation: 04. Mai 2015

Selbstständigkeitserklärung

Hiermit erkläre ich an Eides Statt, dass ich die vorliegende Arbeit selbstständig und ohne fremde Hilfe angefertigt, keine anderen als die angegebenen Quellen und Hilfsmittel benutzt und die den benutzten Quellen wörtlich oder inhaltlich entnommenen Stellen als solche kenntlich gemacht habe. Diese Arbeit hat in gleicher oder ähnlicher Form noch keiner Prüfungsbehörde vorgelegen.

Berlin, 04. November 2014

Contents

Abstract

The Antarctic Ice Sheet is the largest single ice mass on earth. Future change of Antarctic surface mass balance potentially impacts global sea level. Therefore, investigations of future surface mass balance is highly relevant and also discussed by the "Intergovernmental Panel on Climate Change". While the role of future increase of atmospheric moisture content is already analysed in several studies, the influence of changing atmospheric circulation on Antarctic mass balance is underexplored. This thesis contributes to fill this gap.

Extra-tropical cyclones make the main contribution of atmospheric moisture flux in the mid- and high-latitudes. For that reason this work investigates the possibility of objective identification and tracking of extra-tropical cyclones in the Sub-Antarctic region and its influence of moisture transport towards Antarctica. At first this is done for ERA Interim reanalysis. An estimation of methodical dependency of cyclone tracking algorithms is done by means of analysis of 15 different objective methodologies. Strong cyclones were selected and their impact on moisture transport is examined. A strong methodical dependency is found for the absolute number of identified cyclones, whereas spatial patterns of cyclone densities mainly agree. Major disagreements are found in Weddell and Ross Seas, where quasi-stationary systems occur. A good agreement, i.e. small methodical dependency, can be found for the identification of strong cyclones. Poleward moisture transport which is attributed to these strong systems is well represented by the different algorithms.

Investigation of climate change signals of Southern Hemisphere cyclones is done by means of a multi-model ensemble of six coupled atmosphere-ocean general circulation models with nine simulations in total. Strong cyclones are also separately analysed. While each model simulates a significant decrease of cyclone tracks between 20°S and 90°S in the 21st century, seven of nine integrations show increasing strong tracks, whereas three changing signals are significant. For the cyclone track density of all cyclones a robust poleward shift is simulated by the ensemble mean. Strong cyclones show increases on the Eastern Hemisphere.

Antarctic net precipitation is the atmospheric branch of surface mass balance. In this work net precipitation is calculated out of the divergence of the moisture flux vector. This analysis

is also done by means of coupled atmosphere-ocean general circulation model simulations for the 20th and 21st centuries. By means of a scaling approach future changes of net precipitation are split into thermodynamical (atmospheric warming) and dynamical (change of the atmospheric circulation) parts. Dynamical parts are further attributed to different atmospheric mechanisms. This attribution is done by means of a wave decomposition of spatial and temporal variability. As expected the thermodynamical part shows an increasing net precipitation for Antarctica. Although a poleward shift of the Southern Hemisphere stormtrack is found, the dynamical part of the changing signal shows decreases for Antarctica. The stormtrack shift is connected to the climate signal of cyclone activity. The dynamical climate change of moisture flux is found to be decreasing south of 60°S. This is attributed to a weakening of low frequency waves around Antarctica.

Zusammenfassung

Der Antarktische Eisschild bildet die größte zusammenhängende Eismasse der Erde. Zukünftige Änderungen der Massenbilanz haben potentielle Einflüsse auf den globalen Meeresspiegel. Daher ist die Untersuchung zukünftiger Massenbilanzen des Antarktischen Eisschildes von großer Relevanz und wird in den Sachstandberichten des "Intergovernmental Panel on Climate Change" diskutiert. Während die Rolle von zukünftig erhöhtem atmosphärischem Feuchtegehalt in verschieden Studien untersucht ist, ist der Einfluss der Änderung der atmosphärischen Zirkulation wenig erforscht. Dazu leistet diese Promotion einen Beitrag.

In den mittleren und hohen Breiten haben extra-tropische Zyklonen den größten Beitrag am atmosphärischen Feuchtetransport. Daher untersucht diese Arbeit zunächst die Möglichkeiten objektiver Identifikation und Verfolgung extra-tropische Zyklonen in subantarktischen Regionen und deren Einfluss auf den Feuchtetransport in Richtung Antarktis. Dafür werden zunächst ERA Interim Reanalysen untersucht. Zur Abschätzung der Methodenabhängigkeit verschiedener Identifikationsverfahren wird die Reanalyse mit 15 objektiven Algorithmen analysiert. Starke Zyklonen werden hierbei gefiltert und deren Einfluss auf den polwärtigen Feuchtefluss abgeschätzt. Es kann eine starke Methodenabhängigkeit für die absolute Anzahl der identifizierten Zyklonenbahnen festgestellt werden, wobei räumliche Muster der Zyklonendichten im Wesentlichen übereinstimmen. Größte Unterschiede können in den Regionen des Weddell und Ross Meers festgestellt werden. Diese Regionen sind bekannt für das Auftreten quasi-stationärer Systeme. Eine gute Übereinstimmung und somit geringe Methodenabhängigkeit kann für die Identifikation starker Zyklonen festgestellt werden. Der polwärtige Feuchtetransport, der durch diese starken Systeme verursacht wird, lässt sich mit den verschiedenen Algorithmen sehr vergleichbar darstellen.

Zur Untersuchung des Klimaänderungssignals südhemisphärischer Zyklonen wird ein Multi-Modell Ensembles sechs gekoppelter Atmosphäre-Ozean Modelle mit insgesamt neun Simulationen verwendet. Starke Zyklonen werden hier ebenfalls getrennt analysiert. Während im 21. Jahrhundert jedes Modell des Ensembles für den Bereich 20°S bis 90°S eine signifikante Abnahme aller Zyklonen simuliert, zeigen sieben von neun Simulationen eine Zunahme

starker Zyklonen, wobei davon drei signifikant sind. Für die Zyklonenzugbahndichte aller Systeme simuliert das Multi-Modell Ensemble eine robuste Südverschiebung der Zyklonen-Zugbahnen zeigen. Starke Zyklonen zeigen eine erhöhte Aktivität auf der Östlichen Hemisphäre.

Der Antarktische Netto Niederschlag stellt die atmosphärische Komponente der Massenbilanz dar. In dieser Arbeit wird der Netto-Niederschlag aus der Divergenz des Feuchteflussvektors berechnet. Die Analyse des Feuchteflusses findet ebenfalls mit Hilfe eines gekoppelten Atmosphäre-Ozean Modells im 20. und 21. Jahrhundert statt. Mit Hilfe eines Skalierungsansatzes werden zukünftige Änderungen durch thermodynamische (Erwärmung der Atmosphäre) und dynamische (Änderung der Zirkulation) Effekte getrennt, wobei in einem weiterem Schritt die dynamischen Effekte entsprechenden Mechanismen der atmosphärischen Zirkulation zugeordnet werden. Diese Zuordnung findet durch eine Wellenzerlegung räumlicher und zeitlicher Variationen statt. Erwartungsgemäß zeigt die thermodynamische Änderung des Netto Niederschlags eine Erhöhung für die Antarktis. Obwohl eine polwärtige Verschiebung des südhemisphärischen Stormtracks gefunden wird, zeigt der dynamische Anteil der Netto-Niederschlagsänderung eine Abschwächung über der Antarktis. Der Effekt der Verschiebung des Stormtracks kann mit der Änderung von Zyklonen-Zugbahnen in Verbindung gebracht werden. Jedoch zeigt der dynamische Anteil der Feuchteflussänderung eine Abnahme südlich von 60°S. Diese lässt mit der Abschwächung niederfrequenter Wellenaktivität um die Antarktis beschreiben.

1 Introduction

The topic of this thesis is the investigation of Southern Hemisphere (SH) extra-tropical cyclones and its influence on Antarctica. Synoptic activity has various impacts on the climate of Antarctica. Extra-tropical cyclones are the major contributor to meridional moisture transport in the mid- and high latitudes. Poleward moisture flux is an important part of the hydrological cycle of Antarctica. This thesis analyses the impact of extra-tropical cyclones on meridional moisture flux and its influences are discussed with respect to anthropogenic climate change to contribute to a better understanding of the climate change signals of moisture accumulation over Antarctica.

The introduction starts with a motivation why it is relevant to investigate moisture transports into Antarctica in the last and current centuries, and why it is important to better understand the underlying mechanisms. It follows a discussion of the current state of knowledge of atmospheric poleward energy transport and its impacts on moisture budget of Antarctica. Furthermore, literature is discussed with respect to SH cyclone activity and its tools for identification and tracking. Mechanisms leading to the projected climate change signals of Antarctic moisture inflow are not fully understood yet. That fact motivates the research goals of this work. The introduction ends with an outline of the thesis.

1.1 Motivation

The polar regions, and especially the Greenland and Antarctic ice sheets are important for regional and global climate of the Earth' system. The ice sheets are the reason for polar amplification of surface temperature, they are sources for freshwater, and are potential causes of irreversible climate changes (Bindoff et al., 2013). The Antarctic ice shield contains about 90% of the world's ice. This fact makes Antarctica to one of the most important contributors to potential sea level rise, with respect to climate change. During the last century, surface temperature did not change spatially uniform distributed. Whereas the Antarctic Peninsula

shows strong positive surface temperature trends, changes are little and mostly insignificant across the rest of the continent (Turner et al., 2009). The temperature increase at the Peninsula has lead to different ice shelf disintegrations, which in turn speeds up Antarctic glaciers to move in the direction of the Southern Ocean. The transport of moisture from the mid-latitudes into the Antarctic region is the main contributor to ice sheet increase. Decrease takes place by melt-water run-off and glacier movement towards the coast, and interaction with the Southern Ocean. This interplay balances the mass of the Antarctic ice sheet, whereas local differences of temperature changes lead to regional imbalances of ice sheet mass distributions, e.g. the catastrophic disintegration events during the late 20th and early 21st centuries (Turner et al., 2009).

An important contributor to Antarctic ice sheet accumulation rates, is the amount of atmospheric moisture inflow. Surface mass balance (SMB) of the ice sheet can be calculated by means precipitation and evaporation rates as well as melt water run-off. The latter is negligible for the current climate, but it has to be taken into account as well as ice sheet dynamics for an estimation of SMB projections (Church et al., 2013). This in turn is important for an estimation of potential future global sea level rise. That means that a better understanding of mechanisms leading to moisture transport changes, can help for an interpretation of SMB and sea level rise changes.

Climate projections of CMIP3 and CMIP5 models show the Antarctic ice sheet to be a negative contributor to global sea level rise with a various strength spread over the different climate models (Meehl et al., 2007b; Church et al., 2013). This is due to a increased hydrological cycle in a warmer climate. Nevertheless, atmospheric circulation shows also changes in the future climate projections. Both global temperature increase, and thus the feedback of the hydrological cycle and circulation changes, e.g. the poleward shift of the SH storm track, is differently pronounced by the general circulation models (GCMs). For a estimation of the causes for a spread of SMB changes, it is necessary to better understand the mechanisms leading to climate change signals of Antarctic moisture inflow, and to assign it to changing signals of temperature and atmospheric circulation, respectively.

1.2 State of knowledge

1.2.1 Atmospheric energy transport and the hydrological cycle of Antarctica

Antarctica is the driest and coldest continent on earth. Consequently a moderate hydrological cycle is found in the SH high latitudes. In comparison to the Arctic region of the Northern Hemisphere (NH), the Antarctic ice shield is grounded on bedrock. The last time of a completely ice-free continent was more than 33 million years ago (mya). At the Oligozän (33.9 - 23.03 mya) Antarctica split up from South America and Australia. Since then the Antarctic continent was completely surrounded by the Southern Ocean. Thus the Antarctic circumpolar current (ACC) emerged and isolated Antarctica from warm surface water. The continent cooled down and growth of the Antarctic ice shield started. Nowadays about 90% of the world's ice can be found at Antarctica and form its ice shield. The mechanism of ice formation is described in the following passage.

The polar regions generally show an energy deficit. The amount of long wave emission exceeds short wave immission which is connected to solar irradiance, and which has generally less power per unit area at the polar regions in comparison to the tropics. A meridional energy transport has to be fulfilled to locally balance energy budget. A meridional atmospheric circulation emerges, i.e. the Hadley circulation. In mid-latitudes a secondary eddy driven circulation can be found. Due to large temperature gradients mid-latitude climate is dominated by bands of high baroclinicity. This leads to conditions where atmospheric wave disturbances have the possibility to grow. Mean meridional energy transport is low in these bands of latitudes and energy flux is dominated by transient waves.

Different components of atmospheric energy transport is already discussed by Peixoto and Oort (1983). When concerning meridional heat flux, it is possible to distinguish between transport of sensible and latent heat. Meridional moisture flux is proportional to the transport of latent heat. It is possible to analyse the moisture accumulation by means of the flux. It can be shown that the convergence of moisture flux is equal to net precipitation, i.e. the difference between precipitation P and evaporation E (Peixoto and Oort, 1983). For the SH polar region, this relation is valid for seasonal and longer time scales (Bromwich, 1988). It is beneficial to use this approach for high latitudes, since atmospheric energy transport is generally directed polewards. Moisture flux convergence can be defined within a spherical cap centred at pole. Net precipitation is the atmospheric branch of accumulation. For an analysis of accumulation,

the convergence of snow drift as well as melt water runoff have to be taken into account (Bromwich, 1988).

The variation of the Antarctic ice sheet is an interplay between atmospheric inflow and runoff, and ice sheet dynamics, respectively. In equilibrium state, increasing snow accumulation would simultaneously increase ice thickness and thus, increase the ice flow towards the Southern Ocean, where the interaction with the ocean balances the ice sheet (Turner et al., 2009). This state is more a theoretical concept than a description of reality. The different parameters of this interaction are permanently varying, which modifies the equilibrium state. Recent observations show Antarctic net precipitation to be positive for the hole year (cf. Bromwich, 1988; Cullather et al., 1998).

The investigation of moisture flux divergence for the evaluation of net precipitation is commonly used for the Antarctic region due to different reasons (cf. Bromwich, 1988; Bromwich et al., 1995; Cullather et al., 1998). Because of the generally small amount of snow fall over Antarctica and comparably high snow drift, precipitation measurement by means of ground based station standard methods is often impossible (Bromwich, 1988). This technical problems does not exist for numerical analysis, whereas other problems have to be discussed. Although precipitation and evaporation are variables which are calculated by the numerical model of the analysis, it can be even useful to evaluate the hydrological cycle of the numerical data (Cullather et al., 1998). Model physics have to deal with the polar conditions of Antarctica, which can lead to problems for the characterisation of P and E. The analysis of the equations of the hydrological cycle are potentially better represented even in high latitudes (Cullather et al., 1998).

Several studies analyse meridional moisture flux with respect to a splitting of components into mean meridional circulation (MMC) and transient eddies (TE) (cf. Bromwich, 1988; Bromwich et al., 1995; Cullather et al., 1998). This approach can be used to calculate net precipitation with respect to different mechanisms (Cullather et al., 1998). The eddy component of $P - E$ is generally higher than the mean part and positive for different bands of latitude as well as over the Antarctic continent (Cullather et al., 1998; Tietäväinen and Vihma, 2008). On the other hand, the mean component of $P - E$ shows negative values, which can be explained by an equatorward flux direction, due to katabatic winds with high directional constancy (Tietäväinen and Vihma, 2008). In principle, moisture inflow into Antarctica takes place at three coastal areas, i.e. the region of Dronning Maud Land, Wilkes Land and Marie Byrd Land (Cullather et al., 1998; Leckebusch, 1999). SH westerlies interact with the near-surface easterlies off-coast Antarctica, which are a phenomena of katabatic winds. Streamlines of moisture

inflow show that interaction and the corresponding regions of moisture inflow (Leckebusch, 1999).

Future climate projections of coupled atmosphere-ocean general circulation models (AOGCMs) generally show climate warming at the end of the 21st century (Collins et al., 2013). Although impacts are manifold and have to be discussed with respect to different phenomena, it is very likely that atmospheric temperature will increase during the century (Christensen et al., 2013). Following the basic formulation of Clausius-Clapeyron, atmospheric specific humidity will be increase, too, which shows strong feedbacks on atmospheric radiation (cf. Held and Soden, 2000). This implies that there are two potential sources of climate change signals of atmospheric moisture flux, i.e. changes of the general circulation and the content of specific humidity. Held and Soden (2006) analyse the global hydrological cycle with respect to climate change and find robust responses to atmospheric warming. This approach is modified by Lorenz and DeWeaver (2007), since they discuss changes in the hydrological cycle to be a function of zonal mean temperature at 850hPa. For a more detailed discussion of mechanisms, Seager et al. (2010) split MMC part of moisture flux climate change signals into thermodynamical and dynamical parts. Since TE is a covariance, it is not straightforward possible for this component.

Held and Soden (2006) also analyse the response of net precipitation to global warming. Consistent with their finding, thermodynamics also dominate the change of $P-E$ over Antarctica (Uotila et al., 2007). Thermodynamical influences can be attributed to atmospheric temperature increase, whereas dynamical impacts are not refered to the exact phenomena. This is still an open question which will be discussed by this thesis in chapter 4.

1.2.2 Southern Hemisphere extra-tropical cyclones

Synoptic activity is a main feature of mid- and high-latitude atmospheric circulation. At these latitude belts main parts of weather and climate can be referred to extra-tropical cyclones, which are associated to low pressure systems. SH observation of extra-tropical cyclones is attempted to perform since the middle of the last century (e.g. Karelsky, 1963; van Loon, 1965). These early works use weather charts to manually analyse low pressure systems. Although these methods have been very time-consuming and the quality of weather charts has been restricted to the sparse coverage of measurements, results already show qualitative well distributed spatial densities of cyclone activity, with maxima around the Antarctic coastline (e.g. Taljaard, 1967). In the late 1970s, with a come up of SH satellite observations, previous

studies have been supplemented by manually identified cyclone activity by means of satellite data (e.g. Carleton, 1979). In the early 1980s, first studies of extra-tropical cyclones in numerical analysis have been performed (e.g. Silberberg and Bosart, 1982). In the following years, objective methodologies for cyclone identification become established and could be applied to different numerical analysis, such as operational analysis, Reanalysis as well as climate model data (e.g. Lambert, 1988; Murray and Simmonds, 1991a).

When using SH reanalysis data, the sparse observational network in early years has to be taken into account. The quality has been significantly increased once satellite observation can be used since the late 1970s (Bromwich and Fogt, 2004). The first objective analysis of SH extra-tropical cyclone activity for a Reanalysis dataset starting in the middle of the last century is done by Simmonds and Keay (2000) investigating NCEP-NCAR Reanalysis (Kalnay et al., 1996). In further studies, additional state-of-the-art reanalysis data have been investigated by means of different objective cyclone tracking algorithms (Simmonds et al., 2003; Lim and Simmonds, 2007; Bromwich et al., 2007; Ulbrich et al., 2009).

The objective cyclone identification of numerical data enables the possibility to additionally investigate GCM data. So, the application of cyclone trackings to future projections of climate models facilitates the analysis of climate change signals of SH synoptic activity (Geng and Sugi, 2003; Lambert and Fyfe, 2006; Bengtsson et al., 2006). Results robustly suggest poleward shifts of cyclone activity, which will also be examined by this thesis in chapter 3.

Objective cyclone identification

There are several different objective methodologies for the identification and tracking of extra-tropical cyclones (Ulbrich et al., 2009). An extra-tropical cyclone is not uniquely defined. Traditionally cyclones are referred to low pressure systems. Therefore, an automatic identification method should objectively look for pressure minima in the output of any numerical model. Often, extra-tropical cyclones are embedded into the strong pressure gradient field nearby the polar front. Thus, enclosed isobars are not necessarily found although a distinct cyclonic vortex can be identified. Therefore, some objective algorithms are based on the identification of the relative vorticity of the corresponding vortex.

Neu et al. (2013) compared 15 different objective methodologies to discuss similarities and differences of the algorithms investigating the same ERA Interim reanalysis. Therefore, the Intercomparison of mid latitude storm diagnostics (IMILAST)[1] project has been established.

[1] http://www.proclim.ch/imilast/index.html

According on how extra-tropical cyclones are defined and thus, which parameter is identified and tracked, the results have to be interpreted. In general, there is no best algorithm for the identification and tracking of extra-tropical cyclones. Different methodologies have their advantages and disadvantages. Nevertheless, the characterization of the most severe cyclones is more similar represented throughout the different methods (Neu et al., 2013). Well comparable results can also be found for climate change signal of strong cyclones, regarding various algorithms, whereas the general signal is obviously depending on the methodology, since different algorithms are identifying varying numbers of cyclones (Ulbrich et al., 2013). However, natural variability and trends of cyclone densities can be captured by different methods, regarding reanalysis data (Leckebusch et al., 2015).

In chapter 3 and 4 the algorithm of Murray and Simmonds (1991a) is used with the refinements of Simmonds and Murray (1999) and Simmonds et al. (1999). The method is a kind of a hybrid methodology since in a first step a maximum of the quasi-geostrophic relative vorticity is identified following by the assignment of a mean sea level pressure (MSLP) minimum to this vorticity maximum. This is advantageous, since the MSLP field is much smoother than the vorticity field which simplifies the tracking of identified systems. On the other hand, the identification of cyclones by means of the relative vorticity enables the finding of synoptic systems in a state where they do not necessarily show closed isobars, yet (Ulbrich et al., 2009).

1.3 Objectives

The main objective of this thesis is to contribute to a better understanding of the different parts of climate change signals of SH moisture flux and Antarctic net precipitation. Therefore, mechanisms leading to moisture transport will be investigated. It is known, that extra-tropical cyclones play an important role for meridional energy transports. Therefore, the representation of cyclones in the current climate, i.e. by means of reanalysis data, will be analysed as well as climate change signals have to be are investigated. This thesis will propose an approach how to distinguish between temperature and circulation changes for an understanding of the climate change signal of net precipitation. Both the uncertainty of the possible usage of different cyclone methodologies as well as the usage of different AOGCMs for the future climate projection will be discussed.

The following research questions will be discussed by this thesis:

Is the cyclone characterization dependent on the identification algorithm?

- How are Sub-Antarctic extra-tropical cyclones represented by different tracking schemes in reanalysis data?
- How do the identified cyclones contribute to moisture inflow into Antarctica?
- Are the results sensitive on different objective tracking algorithms?

Is the cyclone climate change signal dependent on the dataset?

- How are extra-tropical cyclones represented in a multi-model ensemble (MME)?
- How does the MME simulate climate change of SH extra-tropical cyclones?

Understanding the climate change of Antarctic net precipitation

- How is Antarctic net precipitation represented in an AOGCM?
- How large is the climate change signal of net precipitation?
- What is the role of water vapour increase in a warmer climate for changed net precipitation?
- What is the role of changed atmospheric circulations for changes in Antarctic net precipitation?

1.4 Outline

This thesis is structured into three main chapters, each approaching one research topic defined in section 1.3. Each chapter is written in a the style of a separate scientific article and can be read largely independently of the others. Chapter 2 will be part of a contribution to a special issue in the context of IMILAST, and has still to be submitted, whereas chapter 3 is already published, and chapter 4 has be submitted. If the phrasing "this paper" is used in the following chapters, the corresponding chapter is referred to.

- In chapter 2 ERA Interim reanalysis is investigated by 15 objective cyclone tracking and identification algorithms performed by the IMILAST team. Results are shown for

the evaluation of Sub-Antarctic cyclones represented by the different schemes, whereas strong cyclones are separately examined. The chapter includes an analysis of moisture flux for ERA Interim in relation to the most severe cyclones. This chapter is part of a contribution to a special issue in the context of IMILAST. It will be submitted to *TELLUS-A*[2].

- Chapter 3 deals with the investigation of SH winter cyclone activity analysing a multi-model AOGCM simulations with one algorithm for the identification of extra-tropical cyclones. The climate change signal of all and strong cyclones is analysed, with respect to the multi-model ensemble (MME). Furthermore, mechanisms responsible for the changing signal of all cyclones are discussed. This chapter is published in *International Journal of Climatology* [3].

- Chapter 4 analyses Antarctic net precipitation. An approach is presented how to divide climate change signals of net precipitation into thermodynamical and dynamical parts. Furthermore, the changes of the dynamical component are attributed to atmospheric processes, such as the climate change signal of extra-tropical cyclones. Strong cyclones as well as local Antarctic pressure pattens, i.e. the Amundsen-Bellingshausen Sea Low (ABSL), play an important role. This chapter corresponds to a manuscript which has been submitted to *Journal of Climate*. A revised version of the manuscript is now accepted [4].

- The thesis concludes with a summary, discussion, and outlook in chapter 5.

[2] J. Grieger, G. C. Leckebusch, I. Rudeva, C. C. Raible, and I. Simmonds. Comparison of different tracking algorithms analysing subantarctic cyclones. *in preparation for TELLUS-A*, 2015a

[3] J. Grieger, G.C. Leckebusch, M.G. Donat, M. Schuster, and U. Ulbrich. Southern hemisphere winter cyclone activity under recent and future climate conditions in multi-model aogcm simulations. *Int. J. Climatol.*, 34(12):3400–3416, 2014. ISSN 1097-0088. doi: 10.1002/joc.3917. URL http://dx.doi.org/10.1002/joc.3917

[4] Jens Grieger, Gregor C. Leckebusch, and Uwe Ulbrich. Net precipitation of Antarctica: thermodynamical and dynamical parts of the climate change signal. *J. Climate*, 2015b. doi: 10.1175/JCLI-D-14-00787.1. URL http://dx.doi.org/10.1175/JCLI-D-14-00787.1

2 Cyclones around Antarctica

This chapter will be part of an IMILAST Special Issue which will be submitted to Tellus A.[1].

2.1 Introduction

SH extra-tropical cyclones have major impacts on the climate of Antarctica. Especially the coastal regions of Antarctica are highly influenced by synoptic activity. Atmospheric energy fluxes are strongly influenced by extra-tropical cyclones (Peixoto and Oort, 1983). Thus, they are important for heat and moisture transport into Antarctica. Extra-tropical cyclones can be associated with major SH high latitude precipitation events (Turner et al., 1995). Therefore, cyclones are important for certain parts of snow accumulation over Antarctica. Cyclonic activity has been investigated in several previous studies (e.g. Murray and Simmonds, 1991a; Simmonds and Keay, 2000; Hoskins and Hodges, 2005) as well as in connection with different teleconnections phenomena (Pezza et al., 2008, 2012).

Previous works dealing with extra-tropical cyclones used different datasets and various methodologies for the cyclone identification and tracking. This complicates comparability of results and makes it hard to estimate in how far outcome underlies some uncertainties due to the used method and dataset, respectively. Therefore, the IMILAST project has been brought into being for an intercomparison of different algorithms for the identification and tracking of extra-tropical cyclones (Neu et al., 2013). In this paper the same reanalysis dataset is analysed by 15 objective methodologies for the representation of Sub-Antarctic cyclones.

In the following section the used dataset and the methodologies are discussed. The statistics of Sub-Antarctic cyclones represented by the different schemes is shown in section 2.3. This section also includes an analysis of strong cyclones as well as a discussion in how far these strong systems can be attributed to meridional moisture flux. It is analysed whether the results depend on the used cyclone tracking scheme. Section 2.4 gives a summary and conclusion of

[1] J. Grieger, G. C. Leckebusch, I. Rudeva, C. C. Raible, and I. Simmonds. Comparison of different tracking algorithms analysing subantarctic cyclones. *in preparation for TELLUS-A*, 2015a

the results.

2.2 Data and methods

In this current study, 30 years (1979-2008) of ERA Interim reanalysis (Dee et al., 2011) are investigated for cyclone behaviour around Antarctica. Therefore, output of 15 state-of-the-art methods for mid-latitude cyclone identification and tracking is analysed (details see Neu et al., 2013) for SH winter (JJA) and summer (DJF) seasons. The used ERA Interim parameters are depending on the corresponding methodologies, whereas generally 6-hourly values are taken. Several algorithms use MSLP as input parameter, whereas geopotential height at 1000hPa and 850hPa is also used as well as horizontal winds and vorticity, respectively. An overview of the used methodologies is given in table 2.1. For the whole analysis, a postprocessed dataset has been used, which does not include cyclone tracks over high topography, i.e. all tracks are excluded which have been identified over regions higher than 1500m. This is done to take into account that several methods use MSLP, which has to be extrapolated over orography and can lead to unphysical values and identification of spurious lows.

2.2.1 Filtering subsets of cyclone track data

Temporal and spatial selection

In comparison to previous works of the IMILAST community, this paper has a special focus on the high southern latitudes, i.e. Sub-Antarctic regions. Therefore, the cyclone tracks calculated by the single groups have been temporally and spatially filtered. For the selection of winter (JJA) and summer (DJF) tracks, each cyclone track is chosen which shows at least on time step in the corresponding period. Tracks have not been cut and thus, can be found in the adjacent month of the accordant period. This is similar for the spatial selection, which is performed in this paper. At first, all cyclone tracks have been filtered, which can be identified at least once south of 60°S. These tracks are named “ALL” in the following. Tracks are not cut, i.e. in the statistics of this paper are single cyclone counts which can be found north of 60°S. Additionally, three regions are separately taken into account, East Antarctica (EA), the Amundsen-Bellingshausen Sea (ABS) and the Weddell Sea (WED), by means of a longitudinal criteria. Here, tracks are not cut as well as done for the latitudinal filtering. This implicates several tracks to be attributed to multiple sectors. Hence, the sum of the sectorally

Member	Reference
M02	Murray and Simmonds (1991a); Pinto et al. (2005)
M06	Hewson and Titley (2010)
M07	Manos Flaounas
M08	Trigo (2006)
M09	Serreze (1995); Wang et al. (2006, 2012)
M10	Murray and Simmonds (1991a); Simmonds et al. (2008)
M12	Zolina and Gulev (2002); Rudeva and Gulev (2007)
M14	Kew et al. (2010)
M15	Blender et al. (1997); Raible et al. (2008)
M16	Lionello et al. (2002)
M18	Sinclair (1994, 1997)
M20	Wernli and Schwierz (2006)
M21	Inatsu (2009)
M22	Bardin and Polonsky (2005); Akperov et al. (2007)

Table 2.1: Used methodologies in this paper. Enumeration of the IMILAST members is as that used in Neu et al. (2013). Methods which do *not* provide cyclone core pressure are printed in italics.

filtered dataset includes a higher number of tracks than the sectorally unfiltered data. Spatially filter criteria and the naming of the corresponding dataset can be found in table 2.2.

Selection of strong cyclones

It is possible to define strong cyclones by means of absolute thresholds of intensity parameters, e.g. minimum values of cyclone core pressure (Lambert and Fyfe, 2006; Neu et al., 2013). An analysis of different datasets and a comparison of strong cyclones, which have been defined by absolute thresholds, enables the possibility to extract in how far absolute intensities are

Data	latitudinal criteria	longitudinal criteria
ALL	lat $< 60°$S	none
EA	lat $< 60°$S	$0° <$ lon $< 180°$
ABS	lat $< 60°$S	$180° <$ lon $< 240°$
WED	lat $< 60°$S	$240°$W $<$ lon $< 360°$

Table 2.2: Spatial filter criteria for the different datasets analysed in this study. Note that the definition of the sectoral criteria is done by means of longitudes ranging from 0°to 360°. (240°is equivalent to 60°W, 0°is equivalent to 360°).

represented by different data. Furthermore, strong cyclones can be defined by means of percentile thresholds of a cyclone intensity measure, e.g. the 95th percentile of the Laplacian of MSLP (Leckebusch and Ulbrich, 2004; Leckebusch et al., 2006, 2008; Grieger et al., 2014). This is beneficial if an intensity bias is represented by the analysed data, which can be the case for numerical climate models integrated at different horizontal resolution (e.g. Blender and Schubert, 2000; Pinto et al., 2005; Grieger et al., 2014). This paper investigates one single dataset by means of different algorithms for the identification and tracking of extra-tropical cyclones. Neu et al. (2013) discuss the different representation of intensity distributions of cyclones which are found by various methodologies analysing the same dataset. Although the mean distribution of identified cyclones largely differs, strong cyclones are much more similar characterized. This finding can be confirmed by the analysis of one AOGCM experiment, where strong cyclones are defined by a fixed number of the most severe events (Ulbrich et al., 2013). Following Ulbrich et al. (2013), for the definition of strong cyclones, the most intense 500 cyclone tracks for the 30 year dataset are used, which are about 5.5% of all identified tracks on average. Strong cyclones are calculated for the winter period for all methodologies, which provide cyclone core pressure. On overview can be found in table 2.1.

2.2.2 Meridional moisture flux and attribution to strong cyclones

In this paper it is aimed to attribute extraordinary amounts of moisture flux to the occurrence of strong cyclones. Therefore, vertically integrated moisture flux $\vec{Q}$ has been calculated.

$$\vec{Q} = \frac{1}{g} \int_{p_0}^{p_{sfc}} q_{(p)} \vec{v_{(p)}} dp, \tag{2.1}$$

where g is acceleration of gravity, q is specific humidity and $\vec{v}$ is the horizontal wind vector. Moisture flux is integrated from surface pressure p_{sfc} to $p_0 = 200$ hPa using 6-hourly data on 23 pressure levels. For the assignment of moisture flux to extra-tropical cyclones, which can be attributed to atmospheric transient waves, a Reynolds decomposition of the meridional moisture flux has been performed. The decomposition of meridional moisture flux Q can be written as follows:

$$\overline{Q} = \overline{qv} = \overline{q}\,\overline{v} + \overline{q'v'}, \tag{2.2}$$

whereas the first part is the transport due to MMC and the latter is the component of TE. In the SH extra-tropics, the most important part of meridional transport is due to transient flux perturbations (Peixoto and Oort, 1983). Moisture flux as well as the decomposition of

equation 2.2 is calculated separately for each of the 30 years for the period between April-September. This period is chosen because it is aimed at the attribution of cyclones for the winter season, which possibly can exist in the adjacent months, as described in section 2.2.1. Moisture flux during this period is highly relevant for humidity transport into Antarctica, since net precipitation shows its maximum during this months over the continent (e.g. Bromwich et al., 1995; Cullather et al., 1998).

In the following, daily means of the TE component of Q are used for the comparison with extra-tropical cyclones. For each strong cyclone track, the day of minimum pressure is identified. For each member, these 500 days are used for the calculation of a TE composite. The 30 year mean of the TE component of Q is then subtracted from each composite, to get moisture transport anomalies, which can attributed to the existence of strong cyclones. Statistical significance of the differences is evaluated by means of a t-test, where daily variances of the composites and 30 year mean, respectively are used.

2.3 Results

2.3.1 Cyclone track counts in the different regions

As known from previous studies (cf. Neu et al., 2013), the number of identified cyclones shows large differences with respect to the analysed tracking methods. Table 2.3 shows the number of cyclone counts identified by each method between 1979-2008 with respect to the different regions and seasons. The definition of the regions and the corresponding filter criteria can be found in section 2.2.1.

To assess the similarities and differences of cyclone tracks in certain regions identified by the various methodologies, the anomaly of each identified track number in comparison to the mean of all members is investigated. Figure 2.1 shows the anomaly of tracks in % for winter (JJA) and summer (DJF) for four regions filtered with the criteria of table 2.2. For JJA, there are three methods which generally identify more tracks than the mean (M02, M06, M18), and five methods which generally identify less tracks (M08, M12, M14, M21, M22), whereas the others fluctuate near the mean. Surprisingly, the relative representation of the different number of identified tracks does not depend on the region, whereas the absolute number largely differs between the regions (cf. table 2.3). In summer season, the spread between the various members is less pronounced in comparison to winter season. At first sight, this is counterintuitive, since cyclones generally are of lower intensity in summer and

	winter	(JJA)			summer	(DJF)		
Member	ALL	WED	EA	ABS	ALL	WED	EA	ABS
M02	14040	3336	8493	6510	8848	1793	5324	4179
M06	13101	2608	6936	6285	8257	1422	3935	4019
M07	10892	2107	5567	4946	8172	1439	3981	3963
M08	6989	1499	3987	3212	6587	1359	3615	3033
M09	8088	1817	4539	3759	7337	1673	3805	3642
M10	9848	1989	5827	4409	7545	1523	3924	3561
M12	6725	1555	4036	3320	6126	1472	3375	3164
M14	5345	1233	3176	2467	4644	1163	2631	2273
M15	10212	1943	5498	4719	7344	1359	3882	3421
M16	7862	1913	4230	3802	7381	1740	3790	3674
M18	12822	2887	6807	6202	9592	2043	4941	4683
M20	8456	2101	4662	3926	6963	1592	3736	3427
M21	6503	1261	3663	2933	4348	804	2294	1994
M22	6961	1512	3961	3230	5589	1199	3018	2656
Mean	9131	1982	5098	4265	7052	1470	3732	3406

Table 2.3: Number of identified cyclone tracks for each method for JJA and DJF in the region (all) south of 60°S, (WED) between 60°W - 0°, (EA) 0°- 180°E, and (ABS) 180°E - 60°W.

results of different tracking algorithms are better comparable for intense cyclones (Neu et al., 2013; Ulbrich et al., 2013). As found for winter season, the results do not depend on the different regions.

For a better understanding of the results concerning the identified number of cyclone tracks by different methods, the cyclone track frequency for each region and season is shown as a function of minimum core pressure of the corresponding track (figure 2.2). This analysis is done for each member, which provides cyclone core pressure (cf. table 2.1). Figure 2.2 shows the minimum pressure density function multiplied by the number of identified tracks for each member. Note, that the integral of each curve gives the absolute number for each member, region and season as shown in table 2.3. As expected, core pressures are generally lower for winter season. Here, the largest differences between the methods occur for strength around the peak and for less intense ones, respectively. As supposed by previous studies, the number of stronger cyclones does not largely differ. The picture drawn here, does not strongly depend on the region, whereas the different number of identified for each region can clearly be seen in figure 2.2. For JJA, the intensity distributions show a more bell like shape. Differences between the methods occur mainly at the peak, whereas both more and less intense cyclones

are comparable. The conclusion here is, that the generally broader range of extra-tropical cyclone intensity distributions in winter lead to higher possibilities for differences between the various methodologies. Indeed, the numerous methods mostly differ for shallow cyclones and show better agreements for intense ones. The large intensity range in winter season results in higher discrepancy for identified cyclone tracks, found in figure 2.1.

2.3.2 Horizontal system density

For the further analysis of cyclone frequencies represented by the different methodologies, cyclone system density is calculated. The system density, i.e. the average number of cyclone counts per season in a $(^\circ\text{lat})^2$ area is calculated at each point of an 2.5°grid using a weighting function that is strictly monotonically decreasing and zero for $r > 2.5^\circ$ (c.f. Murray and Simmonds, 1991b). Figure 2.3 and 2.4 show the system density for JJA and DJF, respectively for each member. Note that no cyclones tracks have been identified over Antarctica due to the postprocessed filtering of cyclones over high topography. In general, both figures show the characteristic of the various methods to identify different numbers of cyclones. The system density presented here, shows the number of cyclones counts, which can be assigned to corresponding tracks. Therefore, the total amount of cyclones shown in figure 2.3 and 2.4 is not directly comparable to the number of tracks shown in table 2.3, because each track consists of a different number of cyclone counts. At this point, this gives an additional information about the track length and number of cyclone counts of the tracks, respectively. Most notably is the panel of M06 in figure 2.3 and 2.4. With respect to all members, M06 identifies almost the maximum number of cyclone tracks (cf. table 2.3) but shows the smallest system density. This is due to the high number of short tracks identified by this methodology (not shown). Apart from that, the identification of local maxima is comparable between the members. In principle, methods most agree for the local maxima, which can be identified off-coast Dronning Maud Land at 30°E, near Wilkes Land at 120°E, and at Ross Sea. This maxima can be attributed to climatological MSLP minima, which can be identified in that regions (Schwerdtfeger, 1984). These characteristics are more pronounced for winter season (figure 2.3). Some methods identify additional local maxima of the system density, i.e. mainly the region of Ronne, and Ross ice shelf. At these regions the most pronounced differences occur between the members. Six methodologies show their absolute maximum system density over at least one of the huge ice shelf regions (M02, M07, M14, M16, M20, M21), whereas the others do not show pronounced system densities in these regions. M02 and M15 find another local maximum at the Antarctic

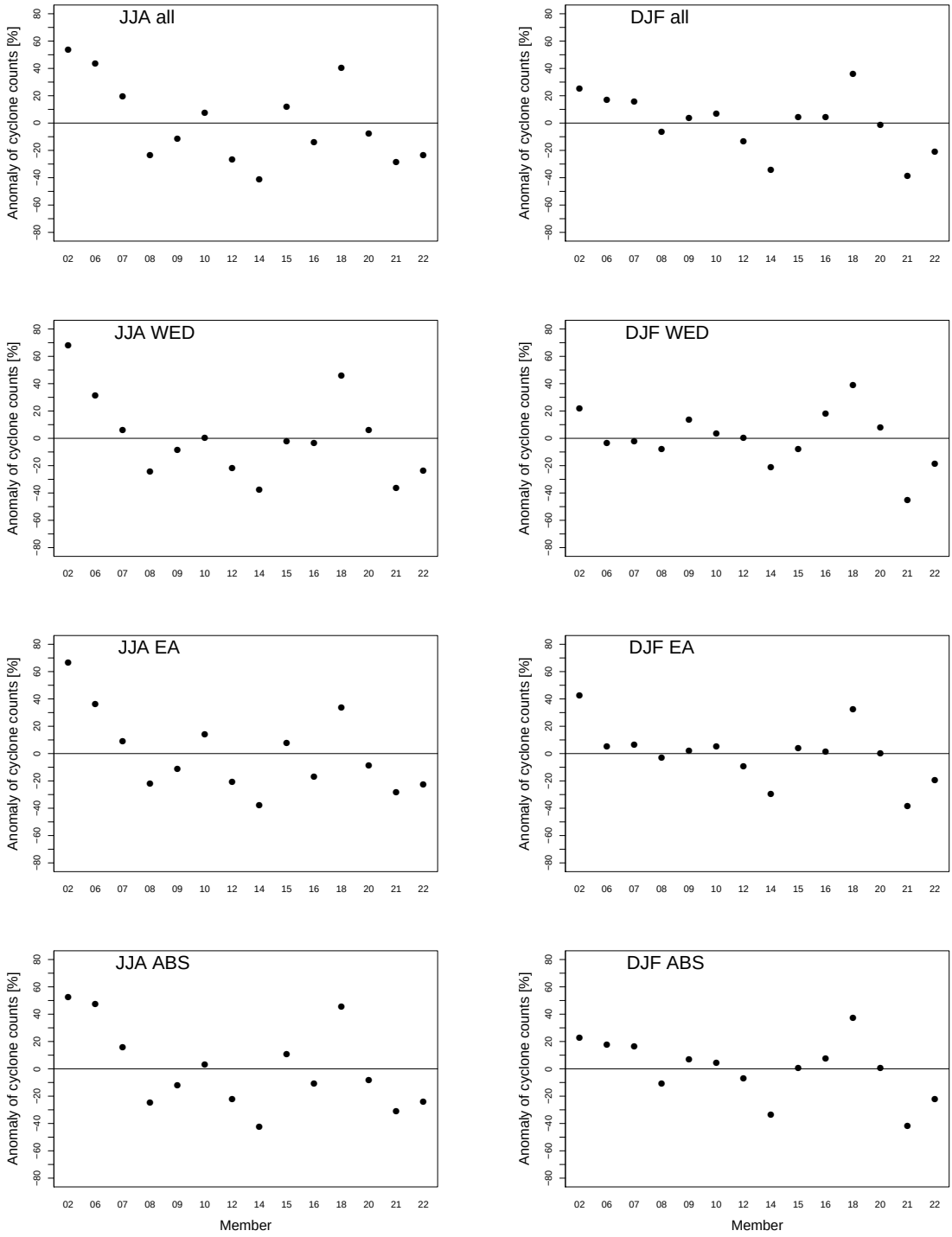

Figure 2.1: Anomaly [%] of identified cyclone tracks with respect to the mean number found per season and region (cf. table 2.3).

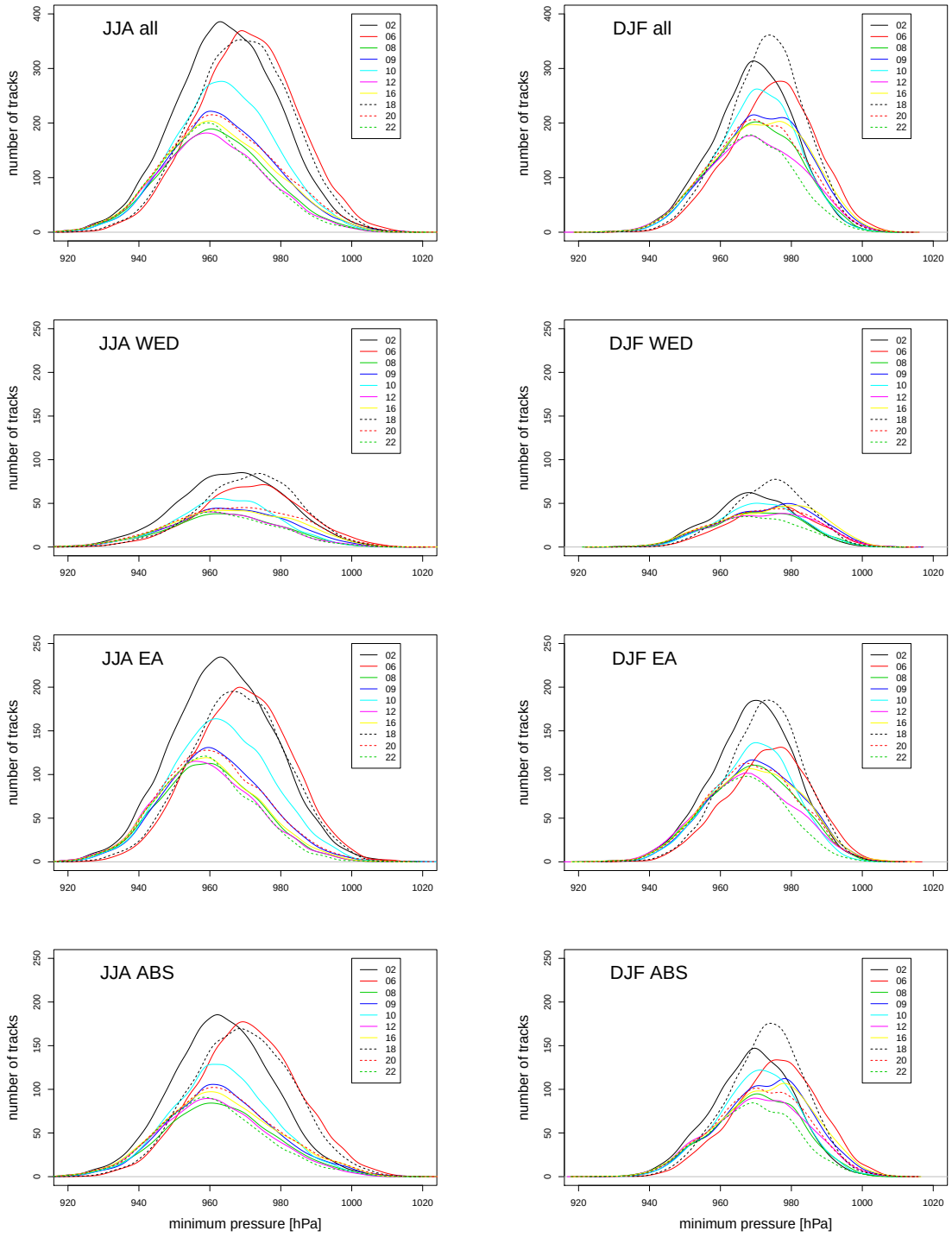

Figure 2.2: Density function for minimum pressure for each cyclone track multiplied by the number of identified tracks for each method found per season and region (cf. table 2.3). Note the different scale of the y-axis for the lower three panels in comparison to the uppermost one.

Peninsula, which is the absolute maximum for M15. M07 is the only method, which shows an extraordinary pronounced maximum at Amery Ice Shelf. Generally, a similar picture can be drawn for summer season (figure 2.4). Additionally to the local maxima, which have been identified for winter season (figure 2.3), highly pronounced system density can be identified throughout the methodologies at Bellingshausen Sea. This is possibly due to the annual cycle of the ABSL, which is shifted in the direction of the Antarctic Peninsula for summer months (Fogt et al., 2012).

Strong cyclone tracks are defined by means of the most intense 500 tracks of each method, with respect to the minimum core pressure. This is done for winter season, when pressure values are generally lower. Figure 2.5 shows the system density of strong cyclones per winter season. This time absolute values of the system density are well comparable, since the same absolute number of 500 tracks is used for the statistics of 30 years. Only methodology M06 shows distinctive lower values of system densities, because of the shorter tracks (not shown). All members identify four local maxima of strong cyclone system density, i.e. a pronounced maximum at the ABSL sector, one at Prime meridian, at 30°E, and at 90°E. At this point it can be concluded that strong cyclones are well comparably represented by various methodologies in comparison to the characteristic of all cyclones. Nevertheless, the different identification of track length has to be taken into account.

2.3.3 Attribution of moisture flux to strong cyclones

Extra-tropical cyclones are an important source for meridional energy transport towards Antarctica Peixoto and Oort (1983); Tietäväinen and Vihma (2008). For an analysis in how far strong cyclones are responsible for an extraordinary meridional moisture flux Q, the TE component of Q is evaluated by means of a composite study. Therefore, all days are taken into account, where each strong cyclone for the 30 year period shows its maximum intensity (minimum core pressure). The 30 year mean of TE was subtracted from each composite corresponding to one member to get the anomaly of moisture flux, which can be attributed to strong cyclone activity. SH poleward moisture transport is generally negative because of the definition of the meridional component of the wind vector v. For an easier interpretation of anomaly fields, poleward transports are defined to be positive here. Hence, a positive anomaly means more poleward transport.

Figure 2.6 shows the moisture flux anomaly due to strong cyclone activity for each methodology. As expected, anomalies are mainly positive since strong cyclones have major impacts

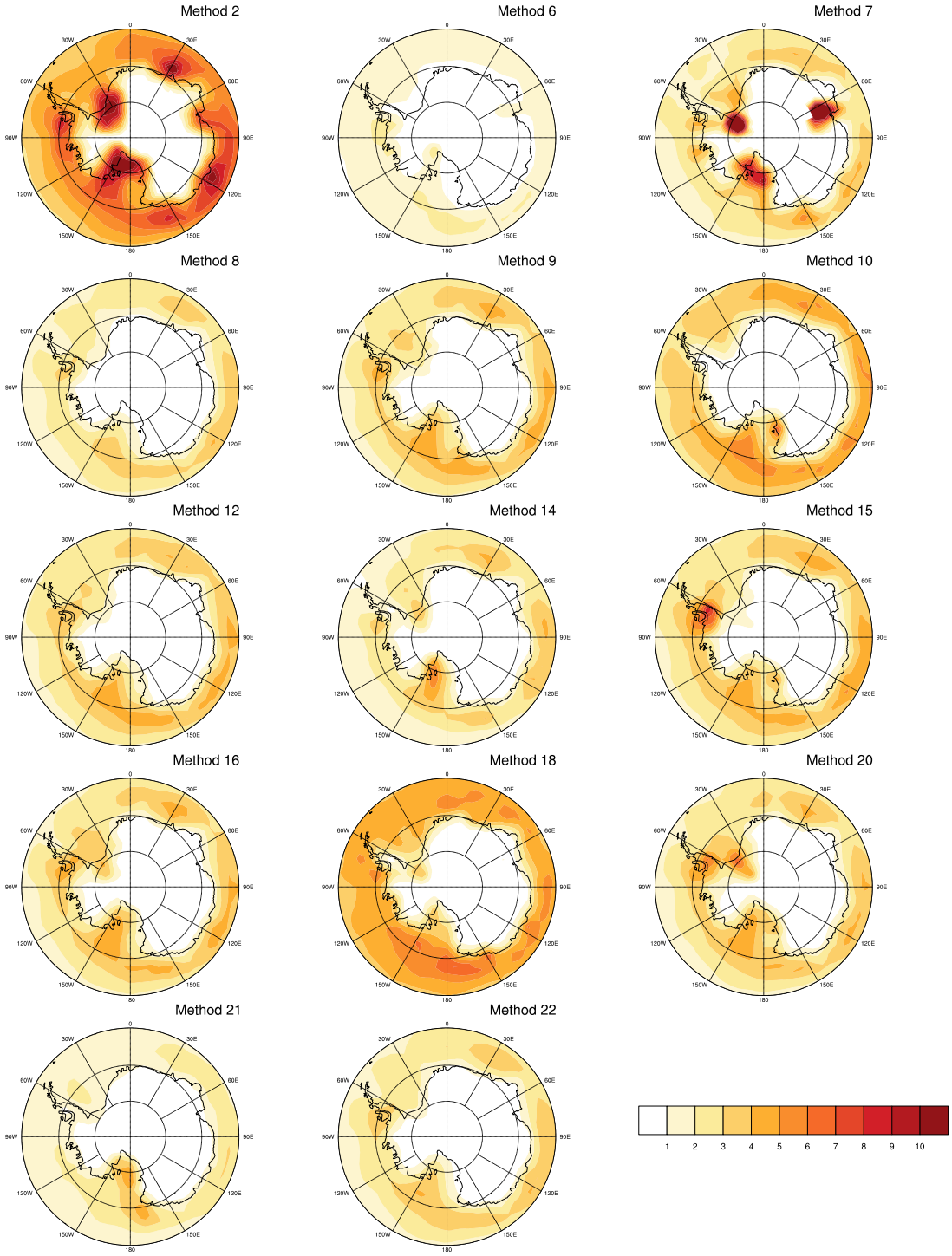

Figure 2.3: System density for winter (JJA) [cyclones per $10^3(^\circ\text{lat})^2$ area, and season].

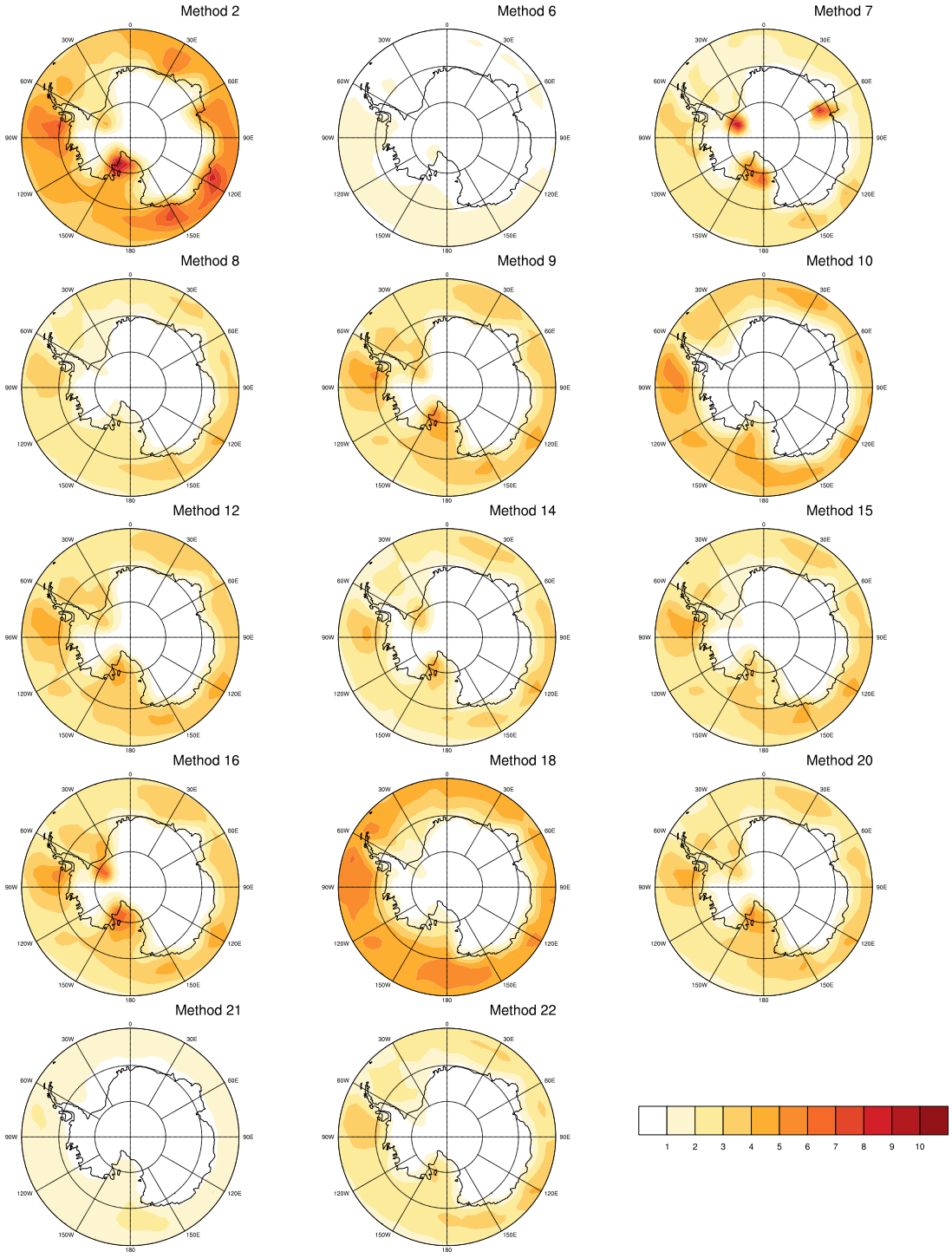

Figure 2.4: System density for summer (DJF) [cyclones per $10^3(°\text{lat})^2$ area, and season].

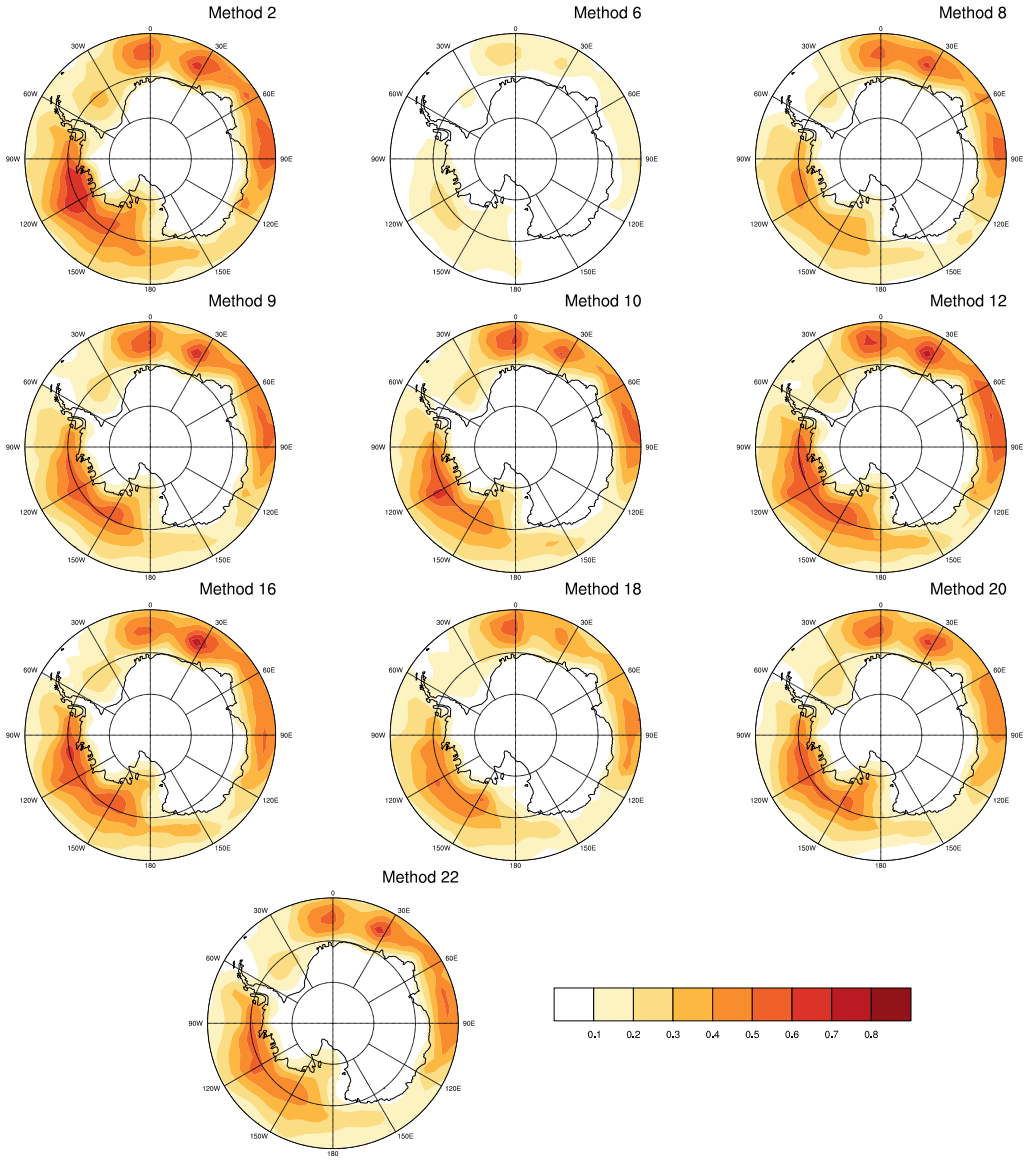

Figure 2.5: Strong system density for winter (JJA) [cyclones per $10^3(^\circ\text{lat})^2$ area, and season].

on poleward moisture transports. Generally, the different members show similar results of flux anomalies. For all methods, the most pronounced region is at Prime meridian, whereas significant positive anomalies are further found around East Antarctica up to 90°E. With respect to zonal symmetry, an interruption of significant positive anomalies can be identified between 90°E and 120°E. Again all methodologies show significant positive anomalies at Wilkes Land. Here, some members find significant values over the continent, whereas the absolute values of the anomalies seem to be very small. This is due to the general low amounts of moisture flux over Antarctica. Furthermore, north of the Ammundsen-Bellingshausen Sea significant positive values are found up to 90°W. Small insignificant negative anomalies are also identified by some members in the region of Bellingshausen Sea. This delimits moisture flux in the direction of West Antarctica, where strong cyclones are steered under the influence of the ABSL. Obviously, the regions of increased moisture flux are related to the occurrence of strong cyclone activity as discussed in section 2.3.2. In principle, there are three major regions of moisture inflow into Antarctica, i.e. the region of Dronning Maud Land, Wilkes Land and Marie Byrd Land (Cullather et al., 1998; Leckebusch, 1999). This evaluation of the attribution of transient moisture flux to strong cyclones shows the importance of these severe synoptic systems for Antarctic moisture transport at least at Dronning Maud Land and Wilkes Land.

2.4 Summary

This study analysed Sub-Antarctic cyclones identified by 15 objective identification and tracking algorithms for extra-tropical cyclones. Therefore, SH winter (JJA) and summer (DJF) season is investigated. By means of a spatially filtering postprocess, four regional subsets of data were produced and analysed. As suggested by previous studies (Neu et al., 2013), the number of identified cyclones varies for the different methodologies. Although a largely different number of cyclone tracks is identified for the four regions, the general behaviour weather a methodology identifies more or less cyclones tracks is very similar. Interestingly, the spread of identified cyclone track numbers between the methodologies is larger in winter than in summer, where cyclones are generally less intense. This is explained by the smaller range of cyclone intensity.

For the representation of horizontal cyclone distributions, the cyclone system density is calculated for each member and season. At first sight, the results of the different identified cyclone tracks are characterized by the system density, as well. There is especially one ex-

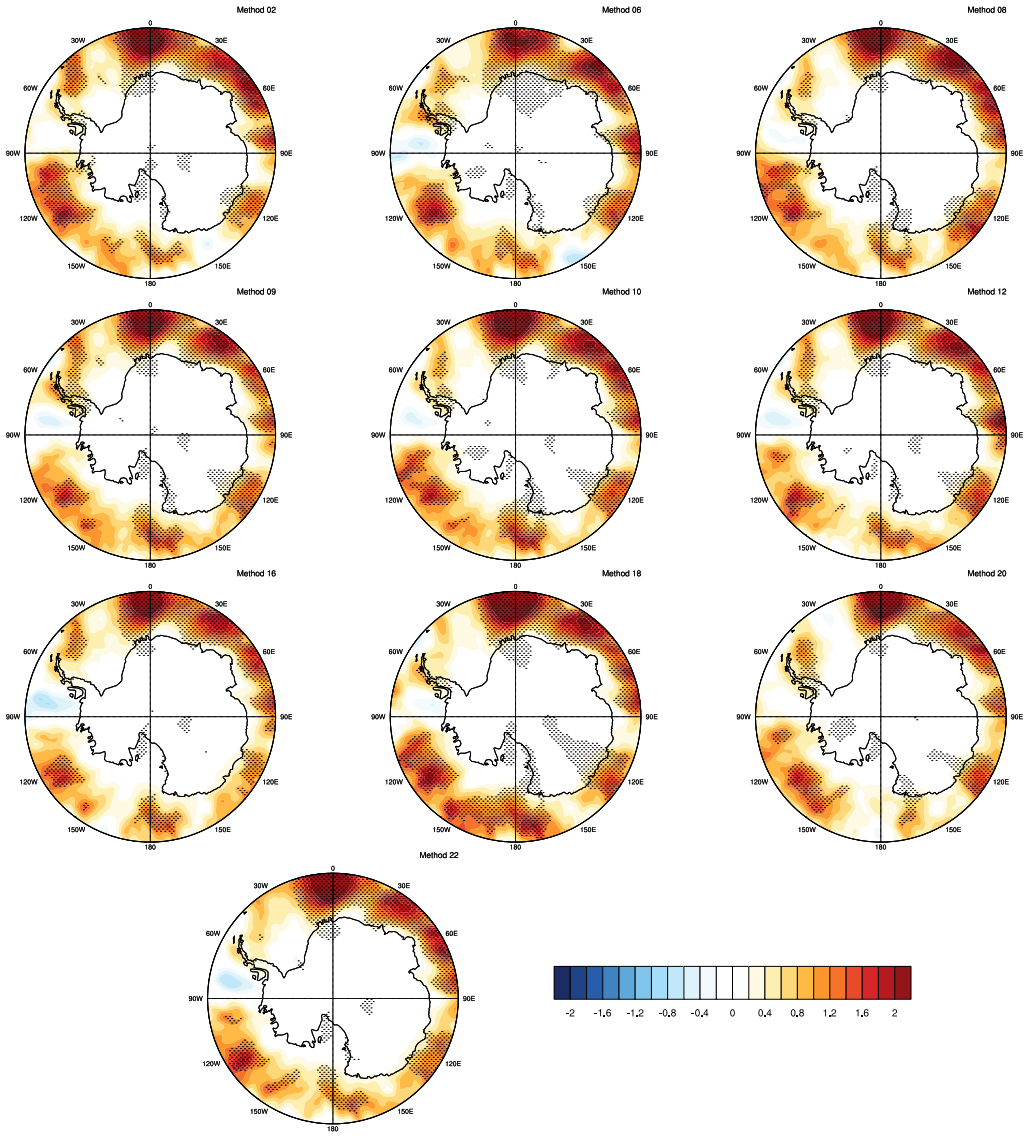

Figure 2.6: Composite of transient meridional moisture flux anomaly for all days where the maximum intensity of strong winter (JJA) cyclones is identified. Anomalies are calculated with respect to the long term (1979-2008) mean for April-September. Stipples show 95% significance with respect to daily mean and variance. Note that poleward moisture flux is defined to be positive.

ception (M06), which identifies a huge number of tracks, but is underrepresented in system density. This is due to the extraordinary short tracks, found by this method.

The most severe cyclones are well comparable between the methods. Both absolute values as well as the location of relative maxima are well represented by the methods.

The study investigated transient moisture transports for an attribution of these fluxes to strong cyclones. Therefore, a composite analysis were performed, where all days of maximum intensity of strong cyclones were used for a calculation of moisture flux composites. Anomalies were computed by means of the difference between the composite and the long term mean. A generally positive anomaly of increased poleward moisture flux can be found and attributed to the regions of strong cyclone density. The major locations of moisture inflow to Antarctica are characterized by the composite study. With respect to the different methodologies, the results are robust.

3 Southern Hemisphere winter cyclone activity under recent and future climate conditions in multi-model AOGCM simulations

This chapter has been published in International Journal of Climatology[1]*.*
Section 3.3.5 results out of the Master Thesis of Mareike Schuster (Schuster, 2012).
The co-authors supervised the work on the manuscript. All the rest was done by Jens Grieger.

3.1 Introduction

Extra-tropical cyclones have major influences on mid-latitude weather and climate. In the Southern Hemisphere (SH) mid-latitudes, synoptic systems have a substantial impact on poleward energy transport (Peixoto and Oort, 1983) and a potential influence on the energy balance of certain regions of Antarctica (Turner et al., 2009 and references therein). The meridional temperature gradient between the tropics and the polar regions in the SH is associated with numerous cyclonic systems over the Southern Ocean, forming a low-pressure band around the Antarctic continent (King and Turner, 1997).

Several studies analyse varieties of characteristics of SH cyclone activity in reanalysis data (e.g. Simmonds and Keay, 2000; Simmonds et al., 2003; Hoskins and Hodges, 2005;

[1] J. Grieger, G.C. Leckebusch, M.G. Donat, M. Schuster, and U. Ulbrich. Southern hemisphere winter cyclone activity under recent and future climate conditions in multi-model aogcm simulations. *Int. J. Climatol.*, 34(12):3400–3416, 2014. ISSN 1097-0088. doi: 10.1002/joc.3917. URL http://dx.doi.org/10.1002/joc.3917

Lim and Simmonds, 2007). Results agree with peak winter track density in the Indian and Australian sectors of the Southern Ocean around 60°S whereas cyclone activity especially at Ross Sea and Weddell Sea is differently pronounced depending on the reanalysis dataset used.

Yin (2005) investigates baroclinic wave activity calculated from the bandpass-filtered eddy kinetic energy in a multi-model ensemble (MME) of coupled atmosphere-ocean general circulation models (AOGCM). He finds a poleward shift of the winter season storm tracks in the future scenario simulations. Lambert and Fyfe (2006) analyse low-pressure events in a similar set of AOGCMs using the daily averaged mean sea level pressure (MSLP) in a 120-day winter season. Robust results are shown in terms of the analysed multi-model ensemble; for example, a reduction in the total number of all events and an increase in the number of intense events are identified in all AOGCMs with respect to the SRES A1B scenario (Nakicenovic et al., 2000). However, their study did not find any shift of cyclonic activity. Bengtsson et al. (2006) analyse cyclonic activity in three integrations of the ECHAM5 coupled climate model with respect to the SRES A1B scenario and identify an increase of track density in the high latitudes and a reduction around 40°S in the winter season. Furthermore, an intensification of cyclones in terms of their vorticity is found in the regions of enhanced activity. The intensification is suggested to be caused by the more poleward position of the tracks which possibly enables cyclonic access to cold air masses from Antarctica. In a subsequent study, Bengtsson et al. (2009) investigate different parameters representing cyclonic intensity in terms of their impacts, e.g. wind speed and precipitation. They use a high-resolution AOGCM and conclude that they cannot identify a clear intensification in the future climate forcing scenario. Geng and Sugi (2003) analyse the difference of two 20-year time-slices representing a control experiment and greenhouse gas forcing for the 2050s. They identify a decrease of cyclone activity in SH mid-latitudes and explain the reduction with decreased baroclinicity due to enhanced static stability mainly caused by relatively little warmings over the SH extra-tropical oceans. Furthermore, Geng and Sugi (2003) find an increase of strong cyclones with respect to the experiment with enhanced greenhouse gases and suggest increasing atmospheric moisture due to global warming to be the reason for this changed intensity distribution. Lim and Simmonds (2009) have performed idealised temperature forcing experiments for a better understanding of SH change of cyclone tracks with respect to climate change scenarios. In their study, the decrease of identified cyclones is also discussed to be caused by an enhancement of static stability but due to increasing temperature of the upper tropospheric tropics. To describe the poleward shift of synoptic activity, Bengtsson et al. (2006) discuss the influence of changing sea surface temperature (SST) gradients that was also investigated in previous studies (e.g.

Inatsu et al., 2002). Inatsu et al. (2002) have performed aqua-planet simulations with idealized SST gradients for the analysis of storm tracks. They found baroclinicity to be influenced in their idealized simulations mainly due to variations of vertical wind shear. Kidston and Gerber (2010) analyse SH jet stream in CMIP3 simulations and find a correlation between the bias in the location of the 20C forcing and the strength of the shift in future projections. Chang et al. (2012) investigate storm tracks and cyclone activity in a CMIP5 multi-model ensemble and find a consistent poleward shift of track locations with respect to the RCP8.5 scenario. However, the decrease of SH winter cyclone track frequency is not a consistent results in their investigation of the CMIP5 AOGCMs, whereas the increasing number of extreme events is a robust finding.

While the general picture of SH winter cyclonic climate change is discussed in several studies, quantitative comparisons are hardly reasonable. A huge number of cyclone identification and tracking methodologies and data-sets enable a lot of different investigations of cyclone characteristics (Ulbrich et al., 2009). Furthermore, different definitions of strong cyclones have been used in several previous studies (e.g., Leckebusch and Ulbrich, 2004; Lambert and Fyfe, 2006; Chang et al., 2012). Neu et al. (2013) compared different cyclone identification and tracking algorithms for the investigation of an identical reanalysis data set. While absolute numbers of detected cyclones show large spreads between the methods, trends of track densities are well captured across the algorithms. Major climate change signals seem to be robust independently of the used method (Ulbrich et al., 2013). The representation of different intensity classes of extra-tropical cyclones by AOGCMs and possible influences on climate change signals are still an open scientific question. While different studies discuss the reasons for the projected change of extra-tropical cyclone behaviour, detailed mechanisms are not fully understood yet.

Our current study principally focuses on potential future changes of the SH cyclonic activity in simulations following the SRES A1B forcing scenario compared to simulations of recent climate conditions. To this end, a multi-model ensemble of AOGCMs is analysed by means of an objective cyclone identification and tracking algorithm to investigate how the change of cyclone characteristics is represented in this multi-model ensemble. Therefore, we present a scaling technique for a fair combination of simulated cyclones by AOGCMs of different horizontal resolutions. Specific thresholds for the definition of strong cyclones and calculation of climate change signals are analysed and the sensitivity of changes in intense cyclones with regard to natural variability is investigated. Furthermore, two possible mechanisms driving the change of SH winter cyclone activity are discussed.

The following section describes the ensemble of analysed AOGCMs and the objective algorithm for cyclone identification and tracking. The representation of cyclone characteristics in the multi-model ensemble simulations of the 20th and 21st centuries is shown in section 4.3. This also includes investigations of the sensitivity of the results regarding different intensity thresholds, natural variability, different model contributors to the ensemble mean and possible mechanisms relevant for the climate change signals. Section 3.4 gives a summary, discussion and conclusion of our findings.

3.2 Data and methods

3.2.1 Data

This study investigates an ensemble of nine coupled AOGCM integrations from six different models (Table 3.1) performed in the ENSEMBLES project (van der Linden and Mitchell, 2009). SH cyclonic parameters are analysed in simulations representing the climate of the 20th century and future projections of the SRES A1B forcing for the 21st century, hereafter denoted by 20C and A1B, respectively. In all model integrations analysis is done for a 20-year time period at the end of the 20th and 21st centuries, respectively. Because of these short periods multidecadal variability may influence both, the climate change signal and inter-annual standard deviation of the corresponding parameter. The multi-model ensemble approach investigates climate signals of all model years (180 years for 20C and 180 years for A1B) and uses the inter-annual standard deviation of the whole ensemble for the calculation of statistical significance. Thus, it is ruled out that signals and their significance are strongly influenced by multi- decadal variability. Nevertheless for three integrations of one climate model, for which 6-hourly data could be made available over longer time periods, we also use time series of transient 200 years to discuss the identified climate change signals in comparison with multi-decadal variability (cf. Table 3.1).

In the multi-model ensemble used here, the ECHAM5 model is over-represented (four of nine ensemble members). The same ensemble of GCM simulations was also used in previous studies investigating changes in European storminess conditions (Donat et al., 2010) and storm losses related to extreme wind speeds (Donat et al., 2011). These studies have shown that even different simulations with the same model, starting from different states with regard to internal variability, may lead to different climate change signals with respect to the occurrence of extreme events. As it was our aim to include as many members as possible in the ensemble

Model	Institute	Resolution	20C	A1B	References
BCCR-BCM2	Bjerkness Centre for Climate Research	T42, L45	1980-1999	2080-2099	Furevik et al. (2003)
CNRM-CM3	Meteo France/Centre National de Recherches Meteorologiques	T42, L31	1981-2000	2081-2100	Salas-Mélia et al. (2005)
DMI-ECHAM5	Danish Meteorological Institute	T63, L31	1981-2000	2081-2100	Jungclaus et al. (2006)
FUB-EGMAM	Freie Universität Berlin Institute of Meteorology	T30, L39	1981-2000	2081-2100	Manzini and McFarlane (1998) Legutke and Voss (1999) Huebener et al. (2007)
IPSL-CM4	Institut Pierre Simon Laplace	2.5°×3.75°, L19	1981-2000	2081-2100	Marti et al. (2005)
METO-HC-HadGEM1 Ringer et al. (2006)	UK Met Office Hadley Center	1.25°×1.875°, L38	1980-1999	2080-2099	Johns et al. (2006) Martin et al. (2006)
MPI-ECHAM5	Max Planck Institute for Meteorology	T63, L31	1981-2000 1901-2000*	2081-2100 2001-2100*	Jungclaus et al. (2006)

Table 3.1: AOGCMs analysed in this study. Datasets marked * are used for additional investigations in section 3.3.3.

representing different models and different phases of climate variability, we generally used all nine available model integrations to compute the ensemble mean. Nevertheless, the outcome is also discussed using only one integration of each model (Section 3.3.4).

Reanalysis data is used as a reference to validate the capability of the AOGCMs to simulate SH parameters that are identified by an objective cyclone tracking algorithm. Compared to station observations, reanalysis products had problems producing realistic MSLP datasets, before the incorporation of satellite data in the late 1970s (Bromwich and Fogt, 2004), particularly on Southern Hemisphere. Bromwich and Fogt (2004) found ERA40 to perform well in the modern satellite era. Hence, in this study we use 20 years of ERA40 reanalysis data (Uppala et al., 2005) from the end of the 20th century, namely 1981-2000, on a spatial resolution of 2.5°× 2.5°. This horizontal resolution is in a similar order of magnitude as in most analysed AOGCMs.

For the analysis of cyclone tracks, we use 6-hourly values of mean sea level pressure (MSLP) from all models. Cyclones are less frequent and generally weaker in summer (Simmonds and Keay, 2000). Their impact on poleward energy transport is reduced in that season (Peixoto and Oort, 1983). Therefore, we restrict our study to SH extended winter season (April-September). Extra-tropical cyclones are analysed between 20°S and 90°S.

3.2.2 Cyclone identification and tracking algorithm

We apply an algorithm for identification and tracking of extra-tropical cyclones that was developed by Murray and Simmonds (1991a) with the modifications specified in Simmonds and Murray (1999) and Simmonds et al. (1999). A short description of the algorithm is given here. According to Simmonds and Murray (1999) a multi-pass smoother is used as a first step of the algorithm to the MSLP field. Thereafter, this field is interpolated by means of a bicubic spline to a polar stereographic grid centred at the south pole. Areas where the orography exceeds 1000m are disregarded because MSLP is derived from extrapolation of the lowest model-level pressure to sea level and may be inexact especially in regions with high orography. On the new grid the Laplacian of the MSLP, $\nabla^2 p$, is calculated which is proportional to the quasi-geostrophic relative vorticity. This field of the Laplacian is scanned for local maxima compared to eight surrounding grid points. Local minima of the MSLP field are assigned to the maximum values of $\nabla^2 p$.

The core of a cyclone with closed isobars is identified if the assignment is successful. If this is not the case within a radius of 6°lat, a search of the pressure inflection point is performed. This point is related to the minimum gradient of the pressure field and determines the location of an open depression. The Laplacian of MSLP can be used as a measure of the intensity of the identified low-pressure systems since it is physically related to wind speed by means of the quasi-geostrophic approximation. Therefore, for each identified low pressure system, $\nabla^2 p$ is averaged over a radius of 2°lat around its maximum value.

For the cyclone tracking procedure, a subsequent position of each identified cyclone is predicted and compared to identified candidates in the following time step.

The identification and tracking scheme may also identify spurious cyclone tracks that have to be filtered off. The requirements for each track are a lifetime of more than one day, i.e. at least five time-steps, and the criteria of closed isolines and high-intensity classification ($\nabla^2 p > 0.7\text{hPa}(^\circ\text{lat})^{-2}$ in our case) once in its life cycle (Leckebusch and Ulbrich, 2004).

Various statistical characteristics of the cyclones are calculated. A more detailed description is given in Murray and Simmonds (1991b). In our current study, horizontal cyclone statistics are calculated on a $2.5^\circ \times 2.5^\circ$ grid using a distance weighting function that is monotonically decreasing and zero for distances $r > 7.5^\circ$lat.

3.2.3 Scaling the cyclone characteristics from different models for ensemble mean analysis

The analysed AOGCMs have been integrated at different spatial resolutions (Table 3.1). Pinto et al. (2005) have demonstrated how spectral reduction of horizontal data resolution leads to a decreased number of identified shallow systems, whereas the distribution of strong systems remains unaffected. Bengtsson et al. (2009) compared cyclone activity in the same GCM integrated at different horizontal resolutions. They find a similar number of cyclone tracks after homogenisation of the model output. Nevertheless, the high-resolution dataset shows much higher intensities in terms of the vorticity and the core pressure.

Indeed, the various model integrations in our study hold a large spread in numbers of low-pressure systems and cyclone tracks (Figure 3.1). To make sure that all simulations are equally weighted when calculating the multi-model ensemble mean of the cyclone track density (e.g. Figure 3.2d), a scaling is performed. For each AOGCM i, a temporally independent scaling factor c_i is derived, specifying the proportion between the total number of identified lows in ERA40 l_{era} relative to the cyclone number in the 20C run of each model l_i.

$$c_i = \frac{l_{era}}{l_i} \tag{3.1}$$

The track density at each grid point of model integration i is then multiplied by the hemispheric model-specific scaling factor c_i. This scaling assures conservation of individual model specific spatial patterns of the track density while standardising all model outputs to the same order of magnitude with regard to total hemispheric cyclone counts. Hence, there is no overestimation of individual model integrations featuring high absolute track density values when calculating the ensemble averages. In contrast to track density, scaling is not used for the intensity measures. The scaling factor is derived for the 20C runs in comparison to the reanalysis data, but also applied to the A1B runs. Consequently, the relative climate change signal of each model integration is unaffected by this scaling technique.

3.2.4 Definition of strong cyclone tracks

In this paper, following the approach of previous studies (Leckebusch and Ulbrich, 2004; Leckebusch et al., 2006, 2008), strong cyclone tracks are defined by means of the 95th percentile of the Laplacian of MSLP with respect to the maximum along-track distribution. This threshold is calculated for each model individually over the considered temporal period in

Model	$\nabla^2 p_{P95}$ [hPa$(^\circ lat)^{-2}$]
ERA40	3.642
BCCR BCM2	2.011
CNRM CM3	2.019
DMI ECHAM5	3.924
FUB EGMAM	2.544
IPSL CM4	2.955
METO HC HadGEM1	3.828
MPI ECHAM5 run 1	3.969
MPI ECHAM5 run 2	3.950
MPI ECHAM5 run 3	3.950

Table 3.2: 95th percentile of the Laplacian of MSLP related to all identified tracks in the 20C runs on the SH. For each model, this value is used as the threshold to define tracks of strong cyclones.

20C (Table 3.2). Only cyclonic systems that exceed the threshold at least once in their lifetime are chosen. The threshold for the Laplacian is calculated for the 20C period and fixed for A1B. Hence, it is possible to discuss the change of strong cyclones in terms of their individual representation in the 20C integration. For each AOGCM this is a consideration of strongest cyclonic activity independently of arguable absolute thresholds.

The Laplacian is a cyclonic intensity measure reflecting the curvature of the pressure field. It is proportional to relative vorticity in terms of the quasi-geostrophic approximation. Several studies use this intensity parameter (e.g. Simmonds et al., 1999; Simmonds and Keay, 2000; Simmonds et al., 2003; Leckebusch and Ulbrich, 2004; Pinto et al., 2005; Leckebusch et al., 2006; Lim and Simmonds, 2007; Pinto et al., 2007; Nissen et al., 2010) whereas there is a large number of alternative possibilities for the definition of cyclone intensity (Neu et al., 2013). In comparison to vorticity the Laplacian is varying for different latitudes with the inconstant coriolis parameter.

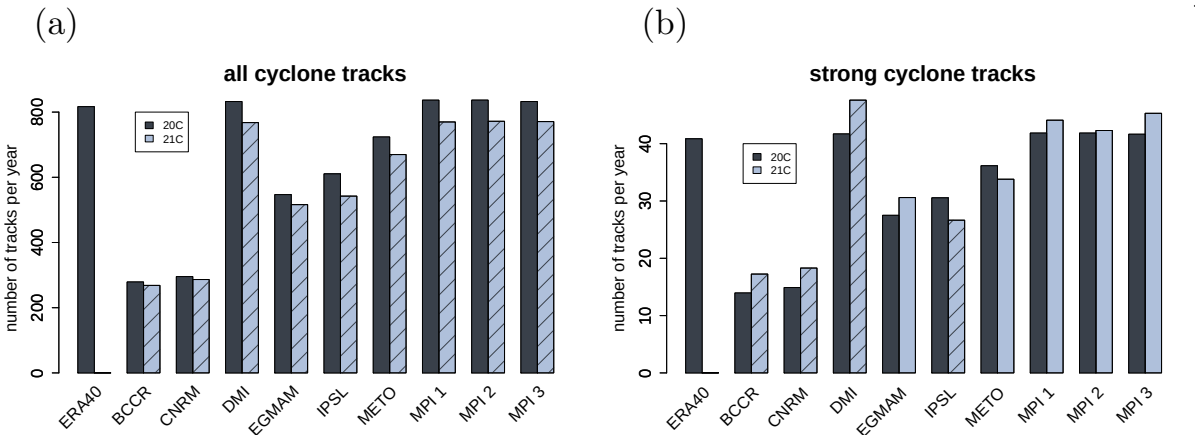

Figure 3.1: Cyclone tracks per year in the SH extra-tropics (20°S-90°S) in reanalysis and the AOGCMs data for a) the number of all identified tracks and b) the number of strong tracks. Hatching of the bars indicate significant changes at the 95% level.

3.3 Results

3.3.1 Cyclone tracks and their changes in a multi-model perspective

Validation of the AOGCMs (20C) with ERA40

For the SH extra-tropics (20°S - 90°S) an average number of 816.7 tracks per extended winter season can be found for ERA40 (Figure 3.1). Note that the absolute number of identified cyclone tracks is dependent of the used identification methodology (Neu et al., 2013). Between the ensemble members, a large spread is detected regarding the total number of identified cyclones, as to be expected given the different spatial resolutions and specific representations of the atmospheric GCM. For the analysed ensemble, models with a coarse resolution (e.g. BCCR, CNRM, FUB) tend to simulate fewer cyclone position counts than the other ones (e.g. DMI, IPSL, MPI, METO). The ratio of cyclone counts between the models holding fewest counts (BCCR) and most counts (DMI) is about 2 (not shown). The ratio is even larger, i.e. about 3 for the number of cyclone tracks, BCCR and MPI-2, respectively (Figure 3.1). Although the influence of horizontal resolution on the number of identified cyclones was shown in previous studies for individual models (e.g. Blender and Schubert, 2000; Pinto et al., 2005), for the analysed multi-model ensemble, it is not possible to identify a functional relationship between the horizontal resolution of the model data and the number of identified cyclones.

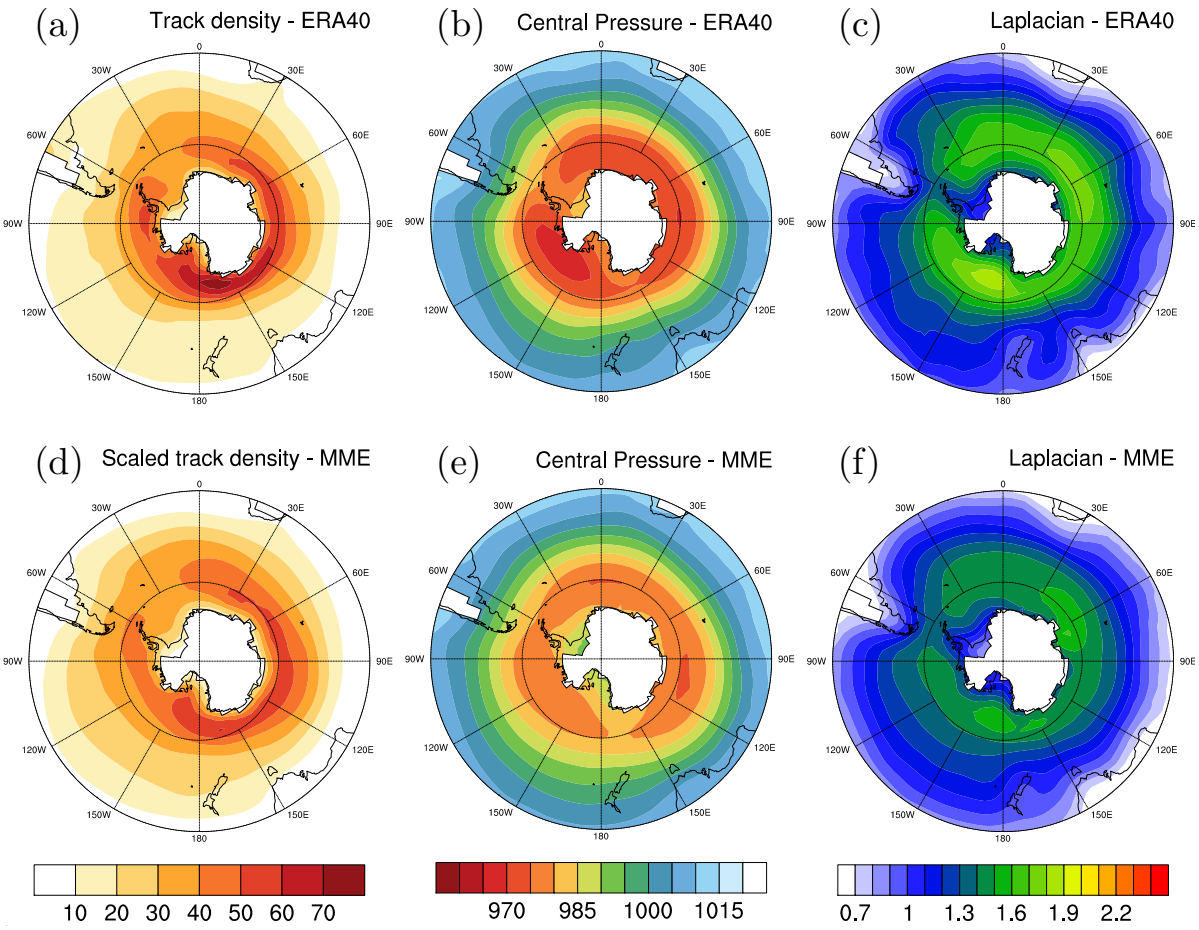

Figure 3.2: Cyclone climatology (April-September) of all cyclones: ERA40 (a) Track Density [tracks/winter $°\text{lat}^{-2}$] (b) Core Pressure [hPa] (c) $\nabla^2 p$ [hPa $°\text{lat}^{-2}$] and MME (d) scaled Track Density [tracks/winter $°\text{lat}^{-2}$] (e) Core Pressure [hPa] (f) $\nabla^2 p$ [hPa $°\text{lat}^{-2}$].

Horizontal distributions of cyclonic characteristics calculated from ERA40 reanalysis are discussed for model validation. The main characteristics are in agreement with earlier studies (Simmonds and Keay, 2000; Simmonds et al., 2003; Lim and Simmonds, 2007; Hoskins and Hodges, 2005). Maximum track density can be identified south of 60°S (Figure 3.2a). Highest values are found in the Australian sector of the Southern Ocean with more than 70 tracks per winter season per $(°\text{lat})^2$. Core pressure and the Laplacian of MSLP represent two different intensity measures related to the statistic of identified cyclone tracks (Figure 3.2b and c). Maximum intensity is found at 60°S in Ross Sea and in the Indian sector, whereas values are lower in the Drake Passage concerning this band of latitude.

The spatial patterns of ERA40 and the GCM ensemble mean show similar cyclone characteristics. Regions of highest track density south of 60°S are consistent, and the absence of circumpolar maximum track density around 60°S north of Weddell Sea is simulated correctly (Figure 3.2d). Compared to reanalysis, the scaled track density of the ensemble mean has higher values in the mid-latitudes of the Pacific. The scaling approach makes sure that for reanalysis and each AOGCM the total number of cyclones is the same in the entire analysed area. Especially in the Atlantic and Pacific sectors of the Southern Ocean (around 40°S and 50°S), the ensemble mean of the scaled track density shows higher values than ERA40 reanalysis. This overestimation of the scaled track density at certain regions leads to an underestimation of peak values south of 60°S. While the track density of ERA40 has maximum values up to 70 tracks per winter per $(°\text{lat})^2$ in the Australian sector of the Southern Ocean, in the multi-model ensemble mean only 60 tracks per winter per $(°\text{lat})^2$ can be identified in this region. Particularly for core pressure, some differences are apparent between model ensemble and reanalysis. In the climate model simulations, minimum values of core pressure are identified in the Atlantic and Indian sectors. Different to ERA40 reanalysis, the minimum in the Pacific sector is less pronounced. The horizontal distribution of $\nabla^2 p$ is well simulated by the ensemble mean. Highest cyclonic intensity can be identified in the Indian sector of the Southern Ocean and at Ross Sea, whereas the characteristics of intense cyclones at Tasman Sea are not as distinctive. Several integrations (DMI, MPI, IPSL) show another maximum of $\nabla^2 p$ at Bellingshausen Sea, which cannot be identified after averaging AOGCMs to the model mean. ERA40 reanalysis does not feature this additional intensity maximum west of the Antarctic Peninsula. In general, ERA40 reanalysis shows higher intensities, i.e. lower values of the core pressure and higher Laplacian per cyclone track, than the multi-model ensemble mean. The AOGCMs in the analysed model ensemble with the highest spatial resolutions (DMI, MPI, METO) hold values in the same order of magnitude as ERA40, whereas the underestimation of the mean is mainly due to lower cyclone intensities in BCCR and CNRM.

Strong cyclone activity according to the 95th percentile of $\nabla^2 p$ and the total distribution feature similar properties in ERA40. Differences are pronounced in the occurrence of an additional maximum of strong track density in the Indian sector at 60°S (Figure 3.3a). The characteristics are shifted to the direction of the Indian Ocean and especially to the Atlantic, whereas the track density in the Pacific is only slightly pronounced. Obviously, the intensity measures of strong cyclones are more pronounced than the mean ones related to all cyclone tracks (Figure 3.3b and c). Both measures show wavelike irregularity patterns where strong track density becomes small. Since these measures are given per number of tracks, the patterns

are based on a small sample. In general, the characteristics of the intensity are comparable to those of all cyclones. In comparison to all cyclones, the local maximum of the Indian sector expands further into the Atlantic sector towards lower latitudes (Figure 3.3c).

With regard to strong cyclone track density, the shift in direction of the Atlantic sector is even stronger in the AOGCMs than in ERA40. The ensemble mean shows a pronounced maximum of strong scaled cyclone track density in the Indian sector (30°E-90°E) of the Southern Ocean at 60°S (Figure 3.3d). This shift is distinguishable in all single AOGCMs, except METO. The intensity of strong cyclonic activity in the multi-model ensemble mean represents the more distinctive characteristic of strong cyclones in direction of the Atlantic sector, whereas peak values are not as pronounced as in the case of ERA40 reanalysis (Figure 3.3e and f). In addition, the same model integrations which show further maxima at Bellingshausen Sea for all cyclones (DMI, MPI, IPSL) reveal this characteristic in the statistics of strong cyclone activity. As found for all cyclones this intensity maximum cannot be seen in the MME mean.

Changes in the SRES A1B scenario

The climate change signal of the cyclone parameters discussed in the previous section is analysed for the multi-model ensemble mean, whereas the changes of the track density are also discussed for single model integrations in terms of their consistency. Changes in the parameters are investigated in terms of the difference between the mean values in the 20-year periods at the end of the 21st and 20th centuries and the relative change is normalised by the mean of the 20th century. To compute the mean and inter-annual standard deviation of the accordant period, all 180 model years (Table 3.1) of the multi-model ensemble are used. Statistical significance of the changes is estimated by applying Student's t-test.

A systematic significant decrease of identified cyclone tracks is found in the future scenario simulations with each analysed AOGCM (Figure 3.1a). While absolute numbers of the cyclone track decrease show an obvious spread since the total amount of identified cyclones has huge differences in the single AOGCMs, the relative changes of the number of cyclone tracks are much closer, ranging between about -3% and -11% (Table 3.3).

Regarding the A1B scenario, most model integrations in this study indicate an increase in the identified number of strong cyclone tracks as defined in section 3.2.4 (Figure 3.1b). On the other hand, only three AOGCMs show increases which are significant at the 95% level. Different to the majority of simulations, two integrations show a decrease of strong cyclone

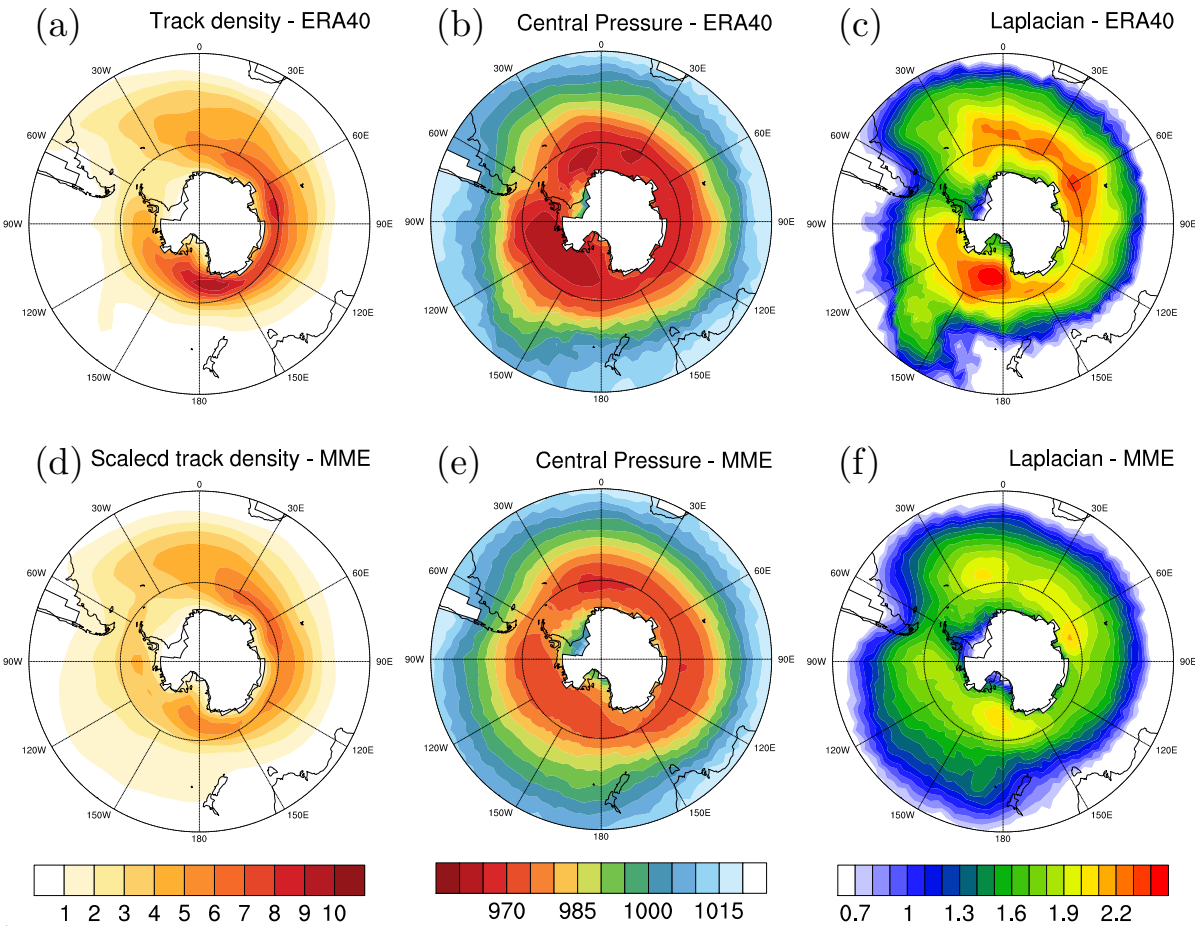

Figure 3.3: Same as Figure 3.2, but for strong cyclones.

Model	relative change [%] of all cyclone tracks	strong cyclone tracks
BCCR-BCM2	-3.8	23.7
CNRM-CM3	-3.1	22.8
DMI-ECHAM5	-7.8	14.1
FUB-EGMAM	-5.6	11.3
IPSL-CM4	-11.2	-12.8
METO-HC-HadGEM1	-7.5	-7.0
MPI-ECHAM5 1	-8.0	5.4
MPI-ECHAM5 2	-7.8	1.1
MPI-ECHAM5 3	-7.4	8.8

Table 3.3: Relative change of cyclone tracks of each model integration in the future scenario simulation (A1B) compared to 20C. Parameters are investigated in the whole analysed area, i.e. the SH between 20°S and 90°S, excluding locations higher than 1000m.

tracks, namely IPSL, METO (Figure 3.1b) with relative changes of about -7% and -12%. The decreasing number of strong tracks is significant for IPSL but not for METO.

The climate change signal of the horizontal distribution of scaled cyclone track density shows significant increases of up to 20% in the Atlantic-Indian sector at the Antarctic coast line, whereas decreasing values are distinctive north of about 50°S in a hemispheric perspective (Figure 3.4a). While there is no increase off the Antarctic coast in the Pacific sector, a weak signal of increase can be found around 50°S south of Australia. The climate change signal in the single model integrations shows slightly different specifications in this region, whereas the signal in the Atlantic and Indian sectors is more robust. All single integrations of the analysed ensemble show a significant reduction of scaled track density in several regions north of 40°S, whereas a completely consistent significant decrease can be identified in the Indian sector, at Tasman Sea, and east of New Zealand (Figure 3.5b). All models also show a higher amount of track density in the high latitudes, whereas significantly increasing track densities are found around East Antarctica. This leads to a robustness of increasing cyclone track density in up to six of nine integrations at Davis Sea (Figure 3.5a).

The intensity measures discussed above show a cyclonic intensification in certain regions in the ensemble mean for the future scenario simulations (Figure 3.4b and c). South of about 55°S, a decrease of core pressure, i.e. an intensification, can be identified in a band around Antarctica (Figure 3.4b); this is related to the general lowering of the ambient pressure in these bands of latitude (Niehörster et al., 2008). Regions of maximum decrease of core pressure are found in the Atlantic and Australian sectors south of 60°S up to 0.5%, i.e. 5hPa deeper in the multi-model ensemble mean. A weak but significant increase of the cyclonic core pressure is found north of 40°S in the multi-model ensemble mean. $\nabla^2 p$ considers the shape of the pressure field. It is proportional to quasi-geostrophic vorticity and thus is an intensity measure related to wind speed. This quantity shows slight increases in the Indian and Australian sectors of the Southern Ocean, whereas the only area with significant increase is found in the south of Tasman Sea (Figure 3.4c), where no changes of scaled cyclone track density were identified. Nearby this location, meridional SST gradients are simulated to increase in the future projection (Figure 3.10c). It indicates an enhancement of low level atmospheric temperature gradients and thus increasing baroclinicity.

Despite reduced total cyclone counts, strong cyclone activity is simulated to increase in the future scenario in the majority of analysed model integrations (Figure 3.1). This characteristic is confirmed by investigations of the horizontal track density distributions (Figure 3.4d). Changing patterns of strong cyclones are dominated by an increase of the scaled track density

in the Indian and Australian sectors of the Southern Ocean with local maximum values up to 40% south of Tasman Sea and up to 50% in southern Australia. Further spots of increasing scaled track density are east of South America, where a maximum of strong cyclones' genesis is detected (not shown) and the southern tip of Africa. It is noticeable that different integrations of the same ECHAM5 model show marked differences in the change of strong cyclone tracks. While the DMI run holds distinctive areas of increasing values in the Indian and Australian sectors higher than 50%, the MPI-1 integration shows only small insignificant increase in this region (not shown). Investigation of consistency shows an increase of scaled strong cyclone track density for all integrations in a large-scale area of the Indian sector as well as for the region south of Tasman Sea. These increases south of Tasman Sea and in the Indian sector of the Southern Ocean are statistically significant for three and five integrations, respectively (Figure 3.5c). In terms of increasingly strong cyclone tracks in all integrations, these regions of complete consistency are comparable with the areas of significant increase of the ensemble mean (Figure 3.4d). In contrast to all cyclone tracks, the climate change signal of the strong ones is not as zonally symmetric. The number of changing strong tracks in a hemispheric point of view is somewhat ambiguous, whereas results become more robust in the Eastern Hemisphere. With respect to a significant decrease of scaled strong track density, only one location can be found in the multi-model ensemble mean, namely the Pacific region north of New Zealand (Figure 3.4d). Two of nine single model integrations show significant decreases of strong tracks in this region (Figure 3.5d). Furthermore, one model shows a significant decrease of strong tracks in the Amundsen-Bellingshausen Sea. This signal is not significant in the MME perspective.

With respect to the climate change signal, almost no pressure increase per strong cyclone track, i.e. weakening of systems, is found in the SH (Figure 3.4e). In the low latitudes, where statistics of all cyclones showed an increase in core pressure, almost no strong cyclone tracks are identifiable (cf. Figure 3.3d). Nevertheless, core pressure for strong cyclones is reduced at almost the same locations as in the statistics of all cyclone systems, even if the decrease of up to 0.8%, i.e. 8hPa, is more intense with respect to the maxima located south of Tasman Sea and south of Ross Sea. For the strong cyclonic intensity in terms of the Laplacian of MSLP, a significant increase can be identified in three regions, namely south of Ross Sea, south of Tasman Sea, and southern Australia (Figure 3.4f). The latter two are related to maximum increase in scaled strong track density. Intensification is up to 15% south of Tasmania and more than 50% south of Australia. Thus these locations represent regions with potentially high impacts with respect to strong cyclone activity in the investigated future climate scenario.

Single model integrations show even stronger intensifications. But these results cannot be found in the multi-model ensemble perspective.

3.3.2 Intensity threshold sensitivity of changes in cyclone tracks

In contrast to the robust finding of fewer cyclone tracks in the future simulations, the changes in strong cyclones are somewhat inconclusive. To gain a clearer picture of changes related to extreme cyclones, we investigate the changing number of cyclone tracks as a function of different intensity thresholds. To calculate the number of cyclone tracks exceeding the intensity of a certain value of Laplacian, an empirical cumulative density function (ECDF) is used. The function for each period is multiplied by the average number of cyclone tracks per year according to the 20C and A1B, respectively. Hence, the value of the ECDF holds the number of tracks exceeding the threshold represented by the value on the x-axis in Figure 3.6a, which shows the difference of the ECDF between A1B and 20C. Due to our criterion to filter the cyclone tracks (Section 3.2.4), there are no cyclone tracks with a maximum $\nabla^2 p$ value lower than $0.7\text{hPa}(^\circ\text{lat})^{-2}$. Figure 3.6b shows the same differences of the ECDF between A1B and 20C dependent on percentile of the Laplacian threshold.

The leftmost value of Figure 3.6 shows the difference of all cyclone tracks between A1B and 20C (cf. Figure 3.1a). Differences become smaller with increasing intensity thresholds and change sign in four of six models (seven of nine simulations). The percentile of the threshold for which the number of tracks increases is around the 50th for BCCR and CNRM and between 70th and 90th for EGMAM and the four ECHAM5 runs. Only IPSL and METO have no intensity range in which the number of cyclone tracks shows an increase. The general climate change characteristic (less strong tracks in the future projection) of these two models is independent of the intensity threshold. The other integrations show huge differences for the thresholds where strong cyclone tracks become more frequent. Absolute values as well as absolute thresholds of the Laplacian are generally lower for the models with a coarser resolution (cf. Table 3.1 and Table 3.2). Furthermore, the spread of the percentile of intensity thresholds implies a different representation of cyclone strength classes by the AOGCMs.

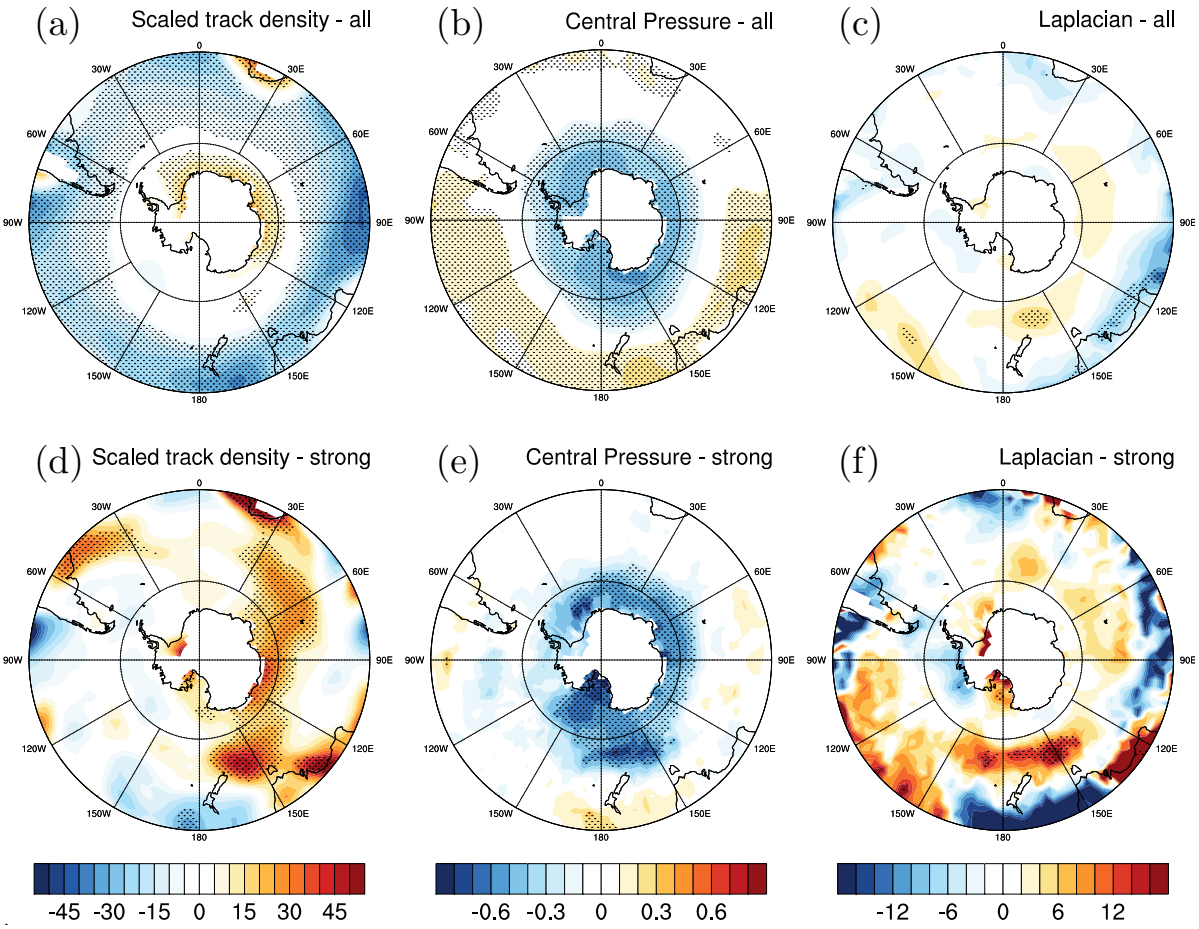

Figure 3.4: Relative climate change signal of the multi-model ensemble (April-September). Change of all cyclones (a) Scaled track density [%] (b) Core Pressure [%] (c) $\nabla^2 p$ [%]. Change of strong cyclones (d) Scaled track density [%] (e) Core Pressure [%] (f) $\nabla^2 p$ [%]. Stippled areas indicate regions where the statistical significance of change exceeds 95% confidence level.

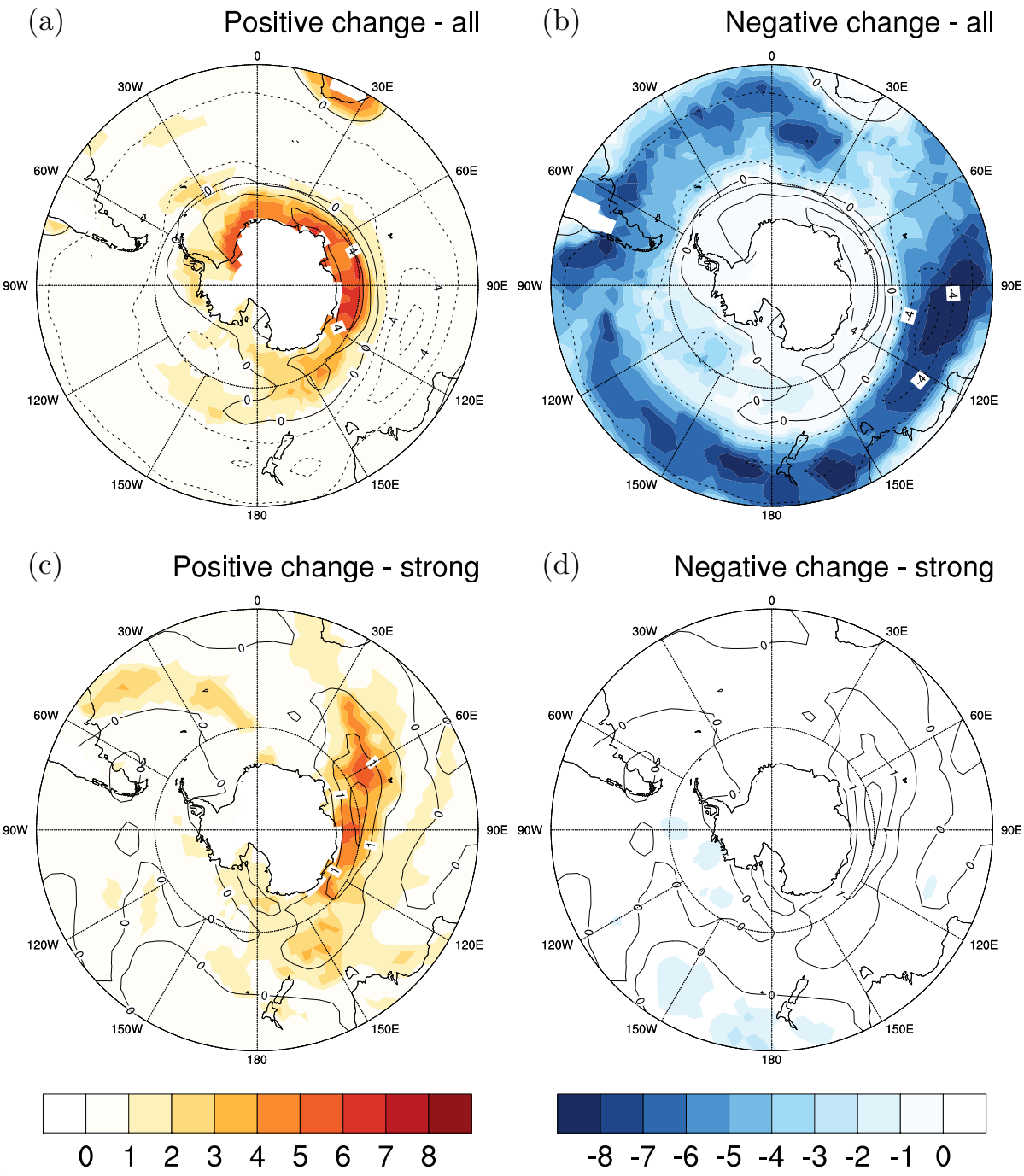

Figure 3.5: Number of model integrations with significant ($p < 0.05$) changes in cyclone track density for (a,b) all and (c,d) strong cyclones. Number of integrations are shaded in colours for (a,c) positive and (b,d) negative changes. The magnitude of the climate change signal of the ensemble mean is shown by isolines with an interval of one [track/winter], whereas dashed lines indicate negative changes.

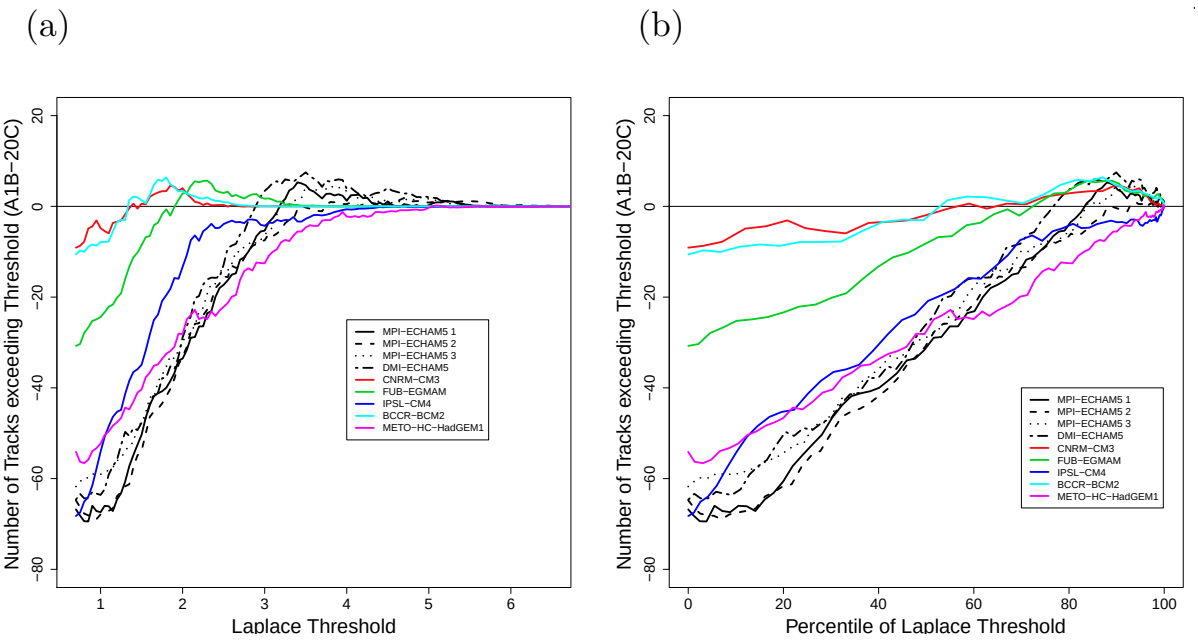

Figure 3.6: Difference of cyclone tracks between A1B and 20C exceeding the varying intensity threshold of (a) Laplacian and (b) percentile of Laplacian, calculated from a ECDF.

3.3.3 Sensitivity of increase in strong cyclones to multi-decadal variability

The presented analysis was performed for a 20-year period at the end of the 20th and the 21st centuries (Table 3.1). Climate change signals calculated from these short time periods are liable to be influenced by natural variability on multi-decadal time-scales. However, since all investigated AOGCMs show the same signal of decreasing cyclone tracks, there is only a small chance that the robust signal is just caused by natural variability. This is different in the case of strong cyclone tracks, where only four of six models show increasing numbers. For a better understanding whether future changes of strong cyclones are possibly influenced by natural variability, long-term time series of strong tracks are also investigated.

Because 6-hourly MSLP fields could not be made available from all models over the entire transient forcing period during 20C and A1B, this analysis is restricted to the three realisations of the MPI model. Figure 3.7 shows the number of strong cyclone tracks (according to $\nabla^2 p$ exceeding the 95th percentile of the 1981-2000 period) in the SH for a 20 year time window. Horizontal lines represent the mean frequency in the 1981-2000 period, i.e. the dif-

ference between the red curve and the black horizontal line at the end of time series shows the climate change signal discussed before. In contrast to the climate change behaviours of all cyclones, which show clearly decreasing numbers, signals of strong cyclone activity are more superimposed by natural variability. For MPI1 a small increasing number of strong cyclones is identified, whereas the higher frequency is more pronounced if the beginning of the 20th century is considered (3.7a). For the MPI2 simulation, a high number of strong cyclone tracks is found at the beginning of the 20th century and at following mid-century (3.7b). Natural variability leads to almost no changing signals at the end of the 21st century. In MPI3 an increasing frequency can be found in the middle of the 21st century resulting in the clearest climate signal across the three MPI integrations (3.7c).

3.3.4 Sensitivity of the multi-model ensemble to different model selections

Here we investigate the sensitivity of the ensemble mean results if only one of the four available simulations of the ECHAM5 integrations was used, to find out whether the presented results may be biased by the inclusion of different realisations of the same climate model. With respect to the future climate scenario, the change of the scaled cyclone track density is unequally represented in the different model integrations, in particular when investigating the characteristics of strong cyclone tracks. The multi-model ensemble mean using four integrations of the same ECHAM5 model is compared to four different sub-ensembles, which all contain only one of the ECHAM5 simulations. Horizontal structure as well as absolute values of climate change signals are similar in the four sub-ensembles (Figure 3.8). Small differences are mostly remarkable in terms of significance. For the statistics of all cyclones, the sub-ensemble containing run 2 of the MPI and integration of the DMI shows the most contiguous region of significant increase of track density south of 60°S (Figure 3.8b and d). Variations between the different sub-ensembles are more pronounced in the case of strong cyclone activity, whereas changing signals are robust in large areas of the SH (Figure 3.9). Differences are mostly pronounced for statistical significance here, too. The most robust signal is found in the Indian sector of the Southern Ocean and south of Tasman Sea in all sub-ensembles.

In conclusion, consideration of different sub-ensembles that contain only one realisation of each climate model shows that the multi-model results would be similar to the ensemble including all available simulations (Section 3.3.1), even though the different integrations of ECHAM5 show a considerable spread. Apparently the ensemble mean results presented above

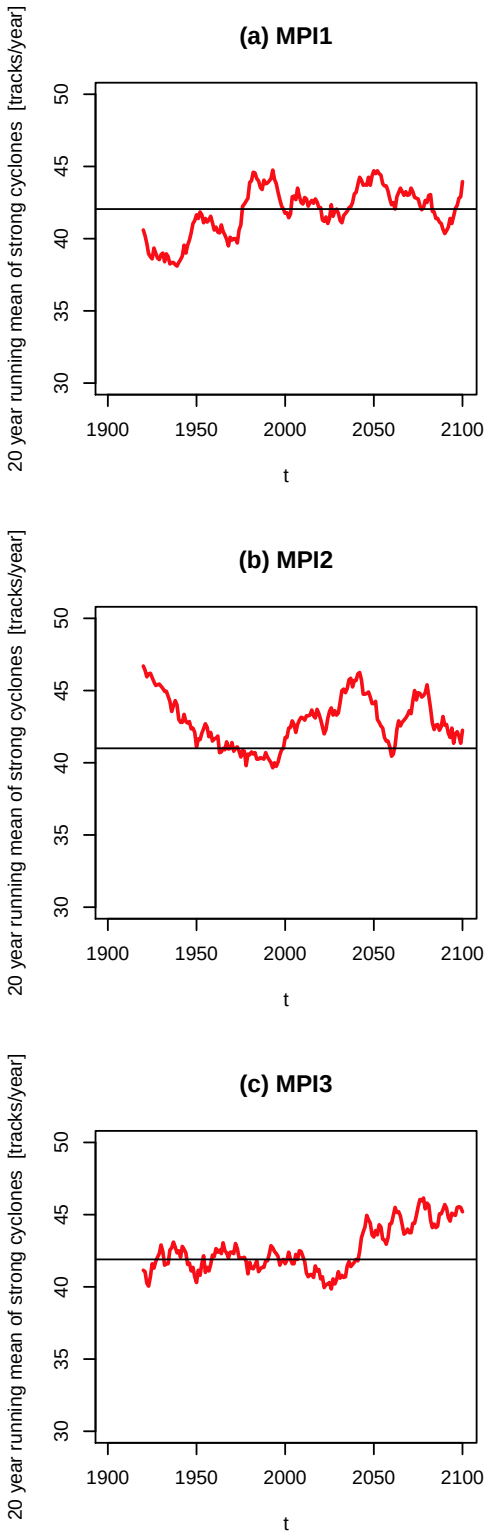

Figure 3.7: Time series of long-term variability of the hemispheric number of strong cyclone tracks for MPI(1-3). Red lines show the running mean of the previous 20 years. Black horizontal line indicates the average of the 1981-2000 period.

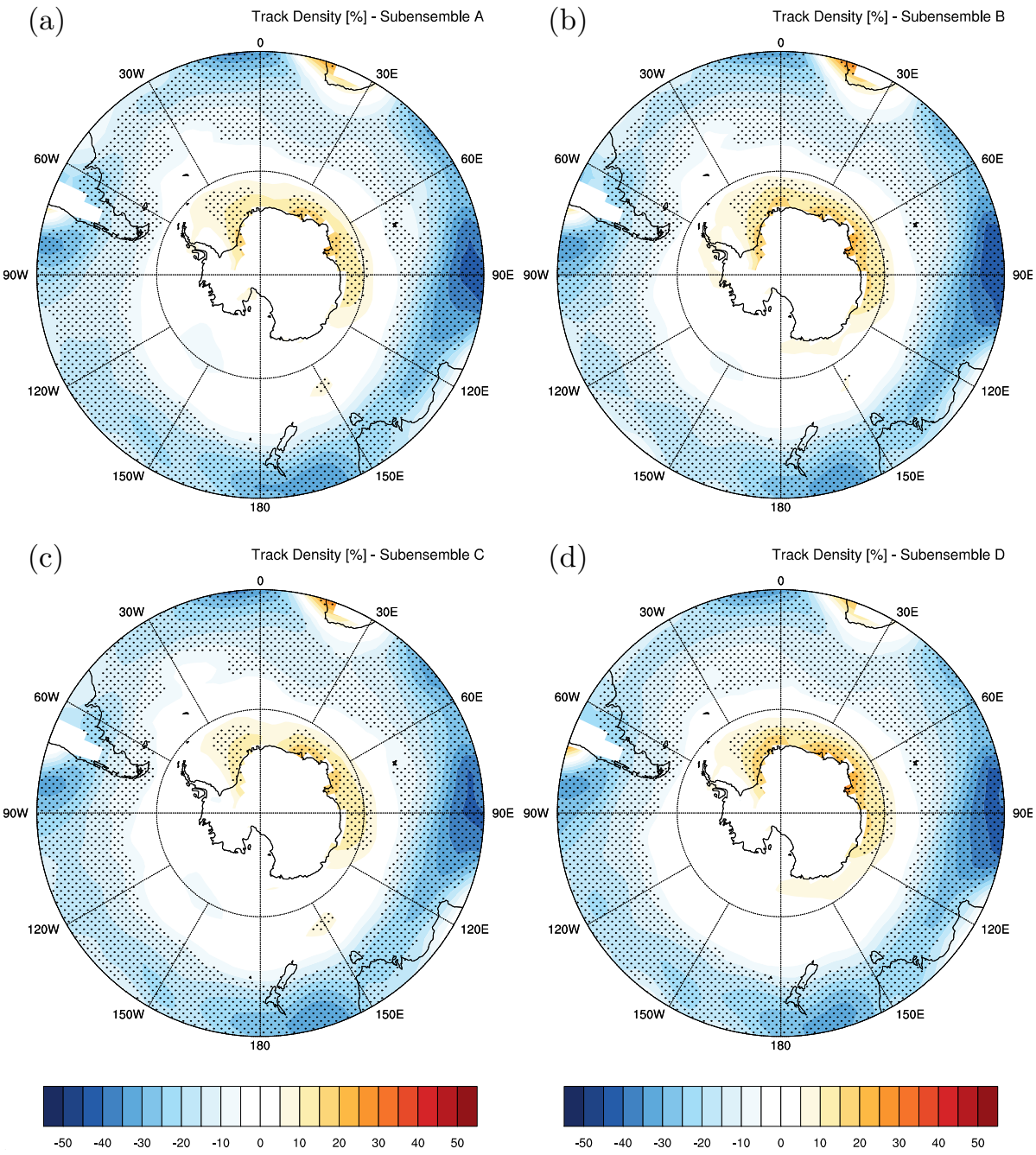

Figure 3.8: Relative climate change signal of Track Density of all cyclones in terms of sub-ensemble containing the integration of a)MPI-1, b)MPI-2, c)MPI-3, d)DMI. Stippled areas indicate regions where the statistical significance of change exceeds 95% confidence level.

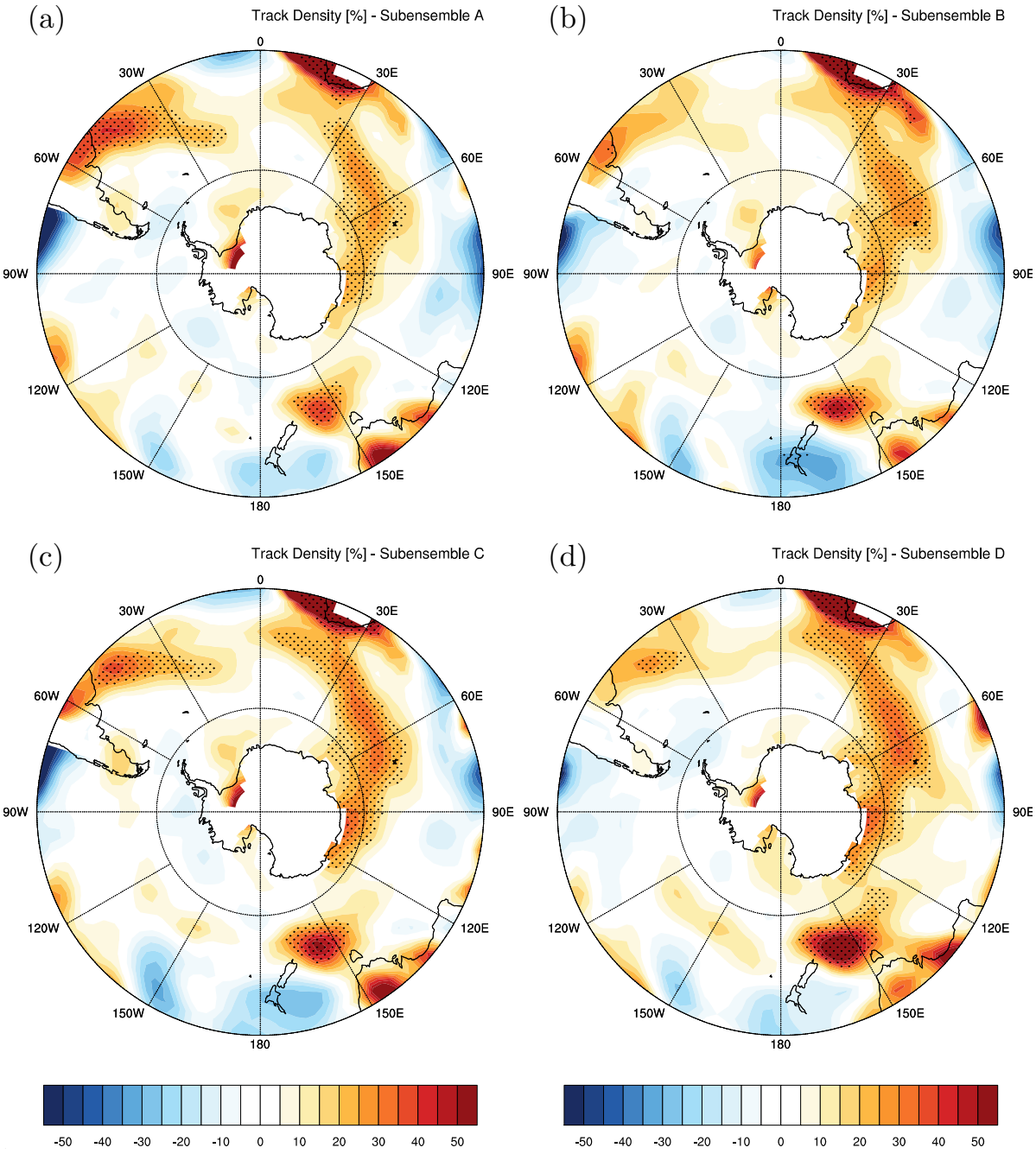

Figure 3.9: Same as Figure 3.8, but for strong cyclones.

are not significantly biased by including several runs of the same model. As this study aims to investigate the robustness of the change signals and given the considerable spread between the different ECHAM5 simulations, it seems preferable to include a larger number of simulations, even if the multi-model ensemble contains different numbers of realisations from the different models.

3.3.5 Possible mechanisms driving the shift of cyclone tracks

As to the poleward shift of cyclone activity, different mechanisms are discussed in literature as possible causes. On the one hand, upper tropospheric warming in the tropics, which is a marked temperature signal in climate change projections (Meehl et al., 2007b), leads to modifications of meridional temperature gradients and changing conditions of atmospheric stability as suggested by Lim and Simmonds (2009). On the other hand, the shift of the meridional temperature gradients of the SST in the Southern Ocean was also shown to affect atmospheric baroclinicity, and hence the storm tracks (Inatsu et al., 2002; Bengtsson et al., 2006). Here, we are investigating for both effects how they relate to the reported poleward shift of cyclone activity. Due to limited availability of suitable data from the different models (see also Section 3.3.3), we perform here an exemplary analysis of three ECHAM5 model runs each containing 200 years (1901-2100) of transient forcing.

Internal variability is investigated to select certain years (winter seasons) for that the discussed possible reasons for cyclone shifts are highly pronounced. These years are used for a composite study of cyclone track density. We select seasons that show a characteristic comparable with the long-term climate change signals, i.e. years are chosen which show a high anomaly of the upper tropospheric temperature in the tropics or high anomaly of the meridional SST gradient in the Southern Ocean, respectively. By means of track density composites for these seasons, it is analysed in how far the two described effects contributes to shifts in cyclone activity. Note that it is not possible to compare the magnitudes of the composites with those of climate change signals as for the composites the detrended time series were used. However, the track density anomalies at different locations of one composite pattern allow a qualitative discussion of the role of the corresponding physical mechanism in relation to the changes in cyclone activity.

Figure 3.10 shows the climate change signal of the ensemble of three MPI runs for (a) the zonally averaged atmospheric temperature and (c) the meridional SST gradient. The upper tropospheric warming in the tropics was previously discussed to enhance static stability in

mid-latitudes and increase meridional temperature gradients (Lim and Simmonds, 2009). This leads to lower baroclinicity in the mid-latitudes while it is possibly increasing in the high latitudes. The climate change signal of the meridional SST gradient is characterised by a poleward shift mainly in the regions where the maximum gradients are located in the 20C simulations. This variation of SST gradients possibly influences atmospheric temperature gradients and thus lead to a poleward shift of the cyclone track density (Bengtsson et al., 2006).

Two different indices are defined to capture the essence of two possible reasons of the cyclonic climate change signal: a) the tropical upper tropospheric warming and b) the shift of the meridional SST gradient. Relating the indices to cyclone track density will then help to examine the response of cyclonic activity due to possible mechanisms. In general, for each winter from 1901 to 2100 an anomaly of the current winter mean relative to the average during the 1981-2000 period is calculated, for the respective variable. Then the index is defined as an area average of this anomaly over a specific region, where a strong climate change signal is apparent. In detail, the Temperature Anomaly Index (TAI) represents the change of zonal mean temperature in the upper tropospheric tropics. It is defined as the mean winter temperature anomaly between 25°S to 25°N and 300hPa to 200hPa. The SST Gradient Anomaly Index (SGI) is a measure for the modification of the meridional SST gradient at the Southern Ocean. It is defined as the sum of the mean winter anomalies of the meridional SST gradient in three sectors of the Southern Ocean. As both indices are calculated within a specific area, they therefore only depict the winter anomaly of the corresponding variable inside these regions (Figure 3.10a and 3.10c, black boxes). Time series of TAI and SGI show distinctively increasing characteristics with the beginning of the A1B forcing (grey curves in figure 3.10e and f). The index time series are linearly detrended with a breakpoint at year 2000 (three colours in figure 3.10e and f). For each index and each integration, winter seasons are selected in which the value of the detrended index exceeds its long term standard deviation. These years represent exceptional high index values, in the same direction as expected from the future scenario GHG forcing. Composites of the detrended temperature and the detrended meridional SST gradient for exceptional years of the TAI and SGI, respectively, show the major spatial patterns of the climate change signal of the corresponding variable (Figure 3.10b and d). The comparison between the climate change signal (Figure 3.10a and c) and the composites (Figure 3.10b and d) give information in how far exceptional TAI and SGI values, respectively, are qualitatively able to represent the climate change of the corresponding variable. Quantitative comparisons are not meaningful here. Furthermore, we use composites of seasons with particularly high

TAI and SGI values to investigate the response of the cyclone tracks to increased index values. The seasonal response of cyclone statistics allows then to infer on potential mechanisms causing the shift in the future climate simulations.

Out of all winter seasons of the three MPI integrations which exceed one standard deviation of TAI (96 seasons) and SGI (95 seasons), composites of the cyclone track density are calculated. Therefore, anomalies of the detrended track density relative to the reference period 1981-2000 are used. The zonal mean of these composites as well as the climate change signal (difference of 2081-2100 and 1981-2000 for the MPI ensemble) is shown in figure 3.11. Both composites show that in years with particularly strong TAI and SGI anomalies, there is a poleward shift of cyclone track density. However, the shift of the SGI/TAI composite is located further in the direction of low/high latitudes. The SGI composite shows increased cyclone track density (about 50°-70°S) poleward of the latitude belts where the maximum SST gradients tend to shift to (about 35°-55°S). In high latitudes (70°-90°S), the track density difference is negative with respect to the SGI composite. Only in these high latitudes the TAI composite shows a positive anomaly. While it is not necessarily meaningful to match the magnitudes of the composites with the climate change signal, it is possible to compare the shape of each curve itself with its peak values. The climate change signal is characterised by a distinct decrease of cyclone track density between 30°S and 60°S, while the peak of increasing track density holds about half of the magnitude of the decrease. This relation is partly represented by the TAI composite. For the SGI composite the peak of increasing track density is dominating the shape of the curve.

This analysis leads to the conclusion that both mechanisms, warming in the tropical upper-troposphere and shifting SST gradients, seem to play a role in order to explain the poleward shift in cyclone activity. The TAI composite shows a negative track density anomaly over the entire mid-latitudes. The relevant mechanism is likely to be the increasing static stability. Here it is mainly affecting cyclone tracks density in the belts south of 60°S. Increasing meridional temperature gradients represented by SGI especially affect the increase of track density in latitudes between 55°S and 75°S. A latitude dependent superposition of both mechanisms potentially can describe parts of the climate change signal in terms of a poleward shift of cyclone track density.

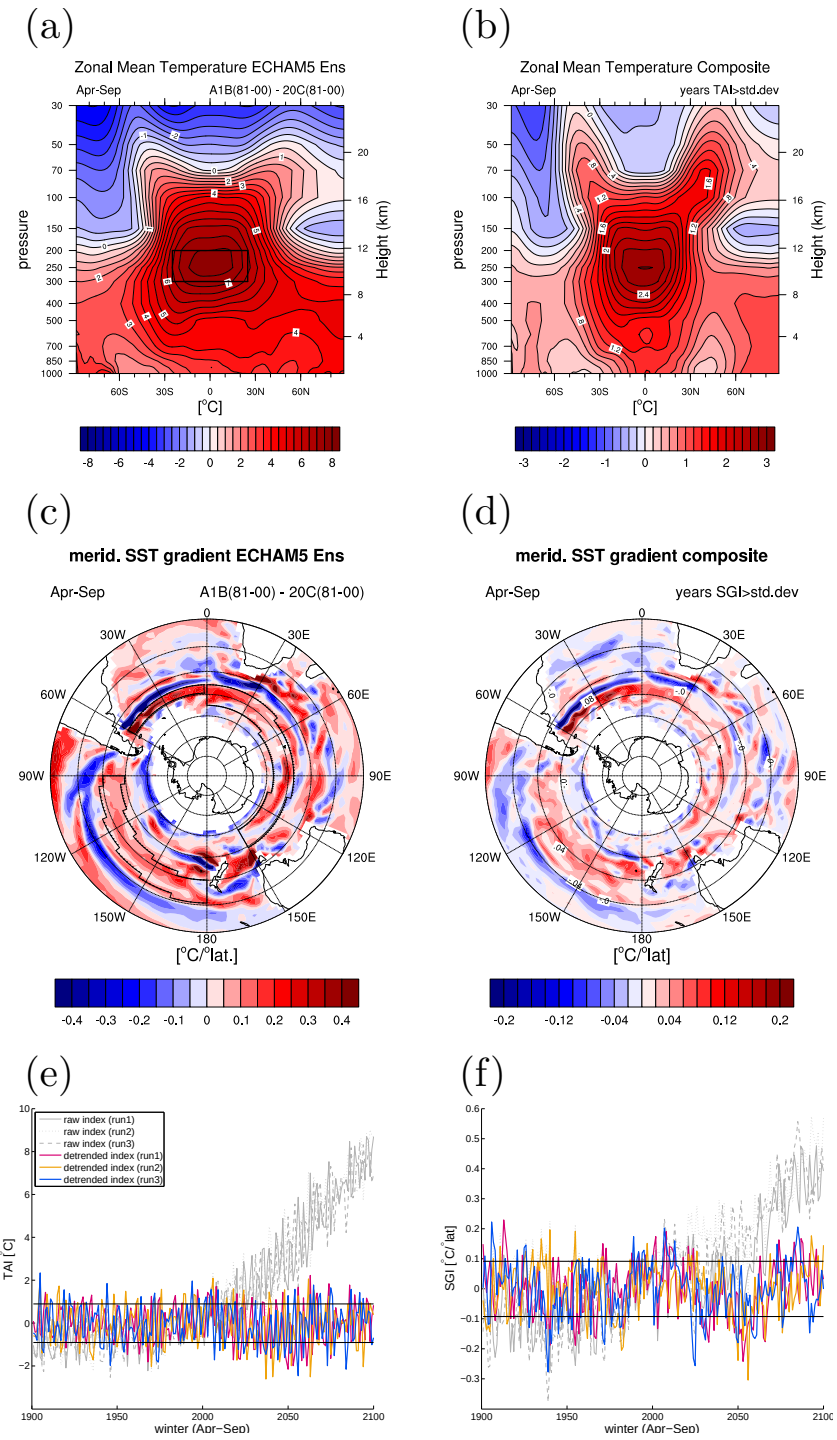

Figure 3.10: Climate change signal (difference between 2081-2100 and 1981-2000) of three MPI ECHAM5 runs: (a) zonally averaged atmospheric temperature, (c) meridional SST gradient. Black boxes indicate regions for the definition of (a) TAI and (c) SGI. Composites of detrended (b) temperature and (d) meridional SST gradient for exceptional TAI and SGI values, respectively. Time series of (e) TAI and (f) SGI. Grey curves show the raw index. Three colours represent the detrended time series of three MPI runs.

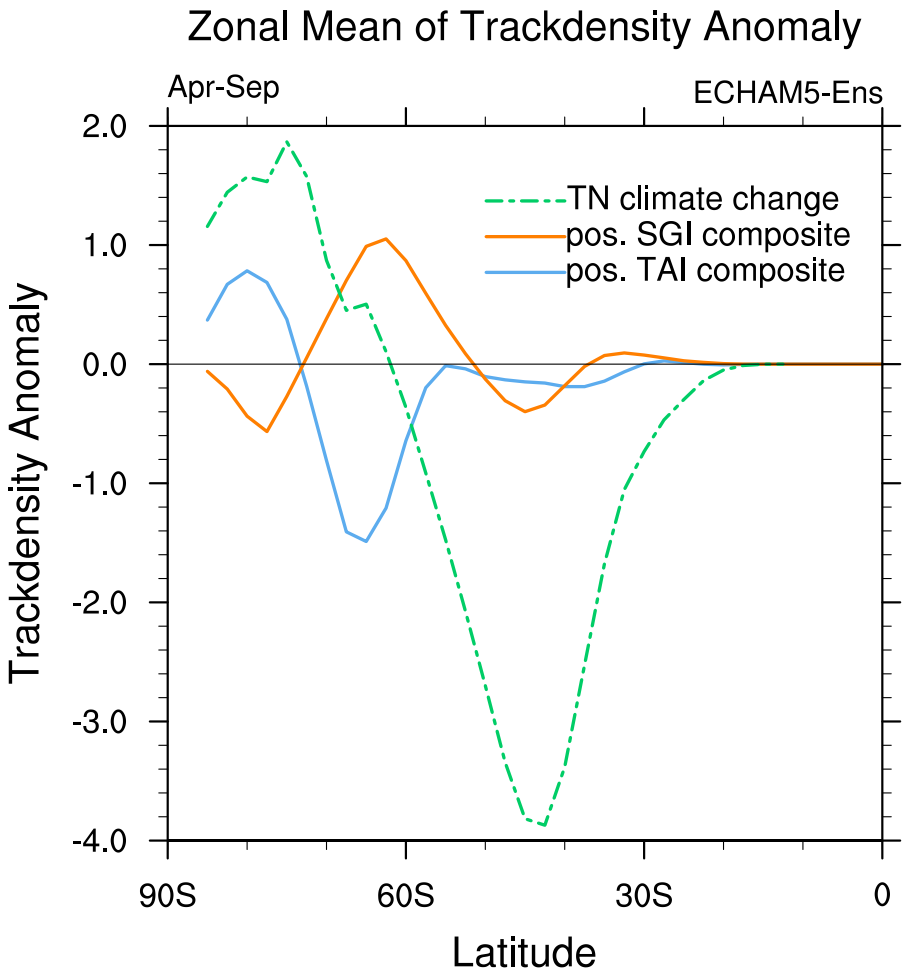

Figure 3.11: Zonal mean for MPI ensemble of (green) cyclone track density climate change signal (difference between 2081-2100 and 1981-2000), detrended cyclone track density composite for exceptional (red) SGI and (blue) TAI values.

3.4 Summary, Discussion and Conclusions

This study analysed extra-tropical cyclones in the SH in climate model simulations under recent and potential future climate conditions according to the SRES A1B forcing scenario. For this purpose, six coupled AOGCMs were used to perform a multi-model ensemble of nine integrations. With respect to climatological features of cyclone activity, horizontal distribution of cyclone track density patterns of ERA40 reanalysis are in good agreement with the model simulations, whereas absolute numbers of identified cyclones differ a lot for certain models. A scaling approach was performed to calculate an equally weighted multi-model ensemble mean. Especially AOGCMs with coarse horizontal resolutions show too low values in their cyclonic strength distribution. This leads to an underestimation of horizontal intensity patterns for the multi-model ensemble mean in comparison to ERA40.

For the future climate scenario (SRES A1B), the multi-model ensemble simulates a poleward shift of the scaled cyclone track density and a significant reduction of the number of cyclone tracks is identified in the ensemble mean and all individual models. The climate change signal of strong cyclones defined by the 5% strongest tracks in terms of the Laplacian of MSLP is not as distinctive. Increasing numbers of strong cyclone tracks are simulated by four of six models, i.e. seven of nine integrations. For three MPI integrations, a study of long-term variability shows multi-decadal influences especially for strong cyclones. It is found that results of climate change signals for strong track numbers are highly influenced by the state of the climate model within its internal variability. This analysis casts doubt on the robustness of the signal of increasing activity of strong cyclone tracks. On the other hand, the sensitivity of the signal to different thresholds of the Laplacian of MSLP has no influence on the general climate change signal since two models show decreases for cyclone tracks at each intensity class. For seven integrations the thresholds for the changing sign in the differences between A1B and 20C forcings are identified between the 50th and 90th percentile. Hence, it is hardly possible to quantify the climate change signal of strong cyclone frequency due to the different representation of cyclonic intensity by the AOGCMs shown by this study of threshold dependency. The climate change signal of strong cyclone track density becomes more consistent for a constraint on the Eastern Hemisphere where all integrations show an increase for certain regions.

We also discuss two different mechanisms as possible causes of the poleward shifts of SH winter cyclone activity in the future projections, based on three integrations of the ECHAM5 model. On the one hand, warming of the upper tropospheric tropics increases meridional

temperature gradients in the high latitudes and also enhances static stability of mid-latitudes. As a result, baroclinicity decreases in the regions of enhanced stability and increases in the polar regions (Lim and Simmonds, 2009). On the other hand, the shift of the meridional SST gradients in the Southern Ocean is analysed for its influences on cyclonic activity, since modification of SST gradients was shown to have influences on storm tracks (Inatsu et al., 2002). We find that both mechanisms seem to play a role for the explanation of SH cyclonic climate change. Upper tropospheric warming tends to mainly influence the general decreases in lower latitudes, whereas SST shifts mainly lead to increase of cyclone track density in the higher latitudes.

Lambert and Fyfe (2006) do not identify "large changes in the position of the storm tracks" calculated out of horizontal distributions of cyclone counts and by means of the 500hPa meridional wind in a multi-model ensemble of IPCC AR4 AOGCMs. In agreement with our results, Bengtsson et al. (2006) find a significant poleward shift of track density in three coupled atmosphere-ocean model integrations of ECHAM5. Furthermore, a consistent poleward shift of cyclone tracks is also found by Chang et al. (2012) in their analysed CMIP5 ensemble forced by the RCP8.5 scenario.

Kidston and Gerber (2010) analysed the differences of CMIP3 AOGCMs in their projection of the magnitude of future poleward shift of SH jet stream. They find correlations between the bias in the latitude of 20th century jet simulations and the magnitude of the shift. Similar results are shown by Chang et al. (2012) investigating storm tracks as well as extra-tropical cyclones in CMIP5 AOGCM simulations. It is possible to find this relationship in our model ensemble, too, although the correlation is not significant for the whole sample of AOGCM integrations possibly due to the smaller sample size in comparison to previous studies (Kidston and Gerber, 2010; Chang et al., 2012).

Lambert and Fyfe (2006) find a reduction of low-pressure systems in their analysed multi-model ensemble investigating different future climate scenarios. With respect to the SRES A1B scenario, they find an increase of strong cyclones in all analysed models at the end of the 21st century. They use the threshold of 960 hPa to define intense low-pressure systems. The model ensemble of our study shows similar behaviour since the climatology of MSLP is reduced in high latitudes in all models (Niehörster et al., 2008). For CMIP5 AOGCMs, the climate change signal of cyclone frequency does not seem to have a consensus, whereas extreme cyclones significantly increase in the future projection (Chang et al., 2012).

Bengtsson et al. (2006) for ECHAM5 as well as Chang et al. (2012) for several CMIP5 AOGCMs find cyclone intensities which are simulated generally weaker than their ERA40

counterparts. With respect to the SRES A1B scenario, Bengtsson et al. (2006) detect an increase of cyclone intensity, in terms of vorticity, in similar regions where they find an increasing track density and suggest the increase of cyclone intensity is due to the more poleward position of tracks and thus enhanced cyclonic access to cold air masses from Antarctica which possibly facilitates cyclone development. In our study, the analysed single model integrations confirm these findings in relation to their identified track density but in the multi-model ensemble perspective the behaviour of increasing intensity, in terms of $\nabla^2 p$, is less robust and mainly insignificant.

Bengtsson et al. (2009) discuss the strength of extra-tropical cyclones with respect to the same SRES A1B forcing scenario in a high-resolution (T213) run with the ECHAM5 model. Their analysis of the 99.5 percentile of 925 hPa wind speed reflects a distinctive maximum increase south of Tasman Sea with respect to the climate change scenario. The enhancement of strong cyclone frequency and intensity in this region which is a robust result of the MME of our study agrees with the finding of wind speed intensification by Bengtsson et al. (2009).

Major results of our study are the characteristic of climate change signals of all and strong SH cyclone tracks in the analysed AOGCMs. Our scaling technique for the ensemble mean as well as the definition of strong cyclones by means of a percentile approach has been taken into account the general bias of models with coarser horizontal resolution to simulate less cyclones which additionally have lower intensities in comparison to AOGCMs with higher resolutions. The study of intensity threshold dependency on the climate change signal of strong cyclone track frequency illustrates the different representation of cyclone intensities by the analysed AOGCMs. While we suggest mechanisms for the changing behaviour of all cyclones, causes for increasing strong cyclone track density which is mainly apparent on the Eastern Hemisphere is not fully understood yet. Our study provides SH cyclone investigations for the "ENSEMBLES" AOGCMs which has not been done so far and helps for a better understanding of SH cyclone climate change signals. Physical mechanisms for the climate change of cyclone intensity distributions as well as model sensitivities are still open questions and call for further research.

Acknowledgements

This work was supported by the SACAI project (LE 1865/1-1), funded by the DFG Priority Programme 1158 "Antarctic Research". The model simulations were made available in the

framework of the ENSEMBLES project, funded by the European Commission's 6th Framework Programme (contract number GOCECT-2003-505539). We thank ECMWF and DWD (German Weather Service) for ERA-40 data use and availability. Markus Donat was partly supported by Australian Research Council grant LP100200690.

4 Net precipitation of Antarctica: thermodynamical and dynamical parts of the climate change signal

This chapter corresponds to a manuscript which has been submitted to Journal of Climate. A revised version of the manuscript is now accepted[1].

4.1 Introduction

The general energy deficit of the polar regions is compensated by poleward energy fluxes, such as atmospheric transports of latent and sensible heat (Peixoto and Oort, 1992). Southern hemisphere (SH) poleward atmospheric fluxes have major impacts on the Antarctic climate, i.e. temperature and moisture accumulation (e.g. Yamazaki, 1992; Turner et al., 1995; Connolley and King, 1993; Bromwich et al., 1995; Cullather et al., 1998). Concerning this, the transient component of moisture flux is the dominating part of SH mid-latitudes (Peixoto and Oort, 1983). The amount of moisture, which is transported towards Antarctica is an important part of the atmospheric contribution to Antarctic surface mass balance (SMB). Estimation of SMB can be done by in-situ observations, remote sensing, and atmospheric modelling, whereas each technique has to deal with its own difficulties regarding the extreme weather conditions of Antarctica (Turner et al., 2009 and references therein). Previous studies have analysed the precipitation and evaporation of Antarctica by means of climate models and reanalysis products, respectively (Bromwich et al., 2004; Monaghan et al., 2006; Tietäväinen and Vihma, 2008). Differences of results depend on the different datasets and methods as well

[1] Jens Grieger, Gregor C. Leckebusch, and Uwe Ulbrich. Net precipitation of Antarctica: thermodynamical and dynamical parts of the climate change signal. *J. Climate*, 2015b. doi: 10.1175/JCLI-D-14-00787.1. URL http://dx.doi.org/10.1175/JCLI-D-14-00787.1

as varying time periods for the analysis (Tietäväinen and Vihma, 2008).

Understanding processes of the SMB variations of Antarctica in recent and future climate is an important issue since the Antarctic ice sheet provides enormous potential for the contribution on sea level rise. Antarctica is likely to be a negative contributor to sea level rise in the 21st century, which is a result of CMIP3 and CMIP5 future projections of global climate models (Meehl et al., 2007b; Church et al., 2013).

Uotila et al. (2007) investigates Antarctic net precipitation, i.e. precipitation minus evaporation (P-E), by means of an ensemble of CMIP3 coupled atmosphere-ocean general circulation models (AOGCM). With respect to the climate change signal at the end of the 21st century, they find an increase for almost all models. Using the approach of the identification of circulation weather types, they distinguish between thermodynamical and dynamical effects. Uotila et al. (2007) conclude that thermodynamics dominate the climate change signal, and the dynamical part has small impact on the increase, especially for the whole Antarctica.

Held and Soden (2006) analyse the climate change of the hydrological cycle simulated by an ensemble of CMIP3 AOGCMs and discuss changing net precipitation to be a function of changes of global near surface temperature. They found a robust intensification of the hydrological cycle due to global warming simulated by their analysed multi-model ensemble. Seager et al. (2010) analyse different components of moisture transport. They split the mean meridional flux into thermodynamical and dynamical parts, but discuss that it is not straightforwardly possible for the transient component of transport since it is a covariance. Lorenz and DeWeaver (2007) discuss changes in the hydrological cycle to be a function of zonal mean temperature at 850hPa. In comparison to Held and Soden (2006), this is a more local response of humidity change to temperature variations.

This work discusses the change of SH moisture transport simulated by three members of one AOGCM. Therefore, an approach is presented to distinguish between thermodynamical and dynamical influences on moisture flux. Furthermore, decomposing atmospheric waves into different length scales and temporal variations, a physical interpretaion of the transport changes is adressed and compared with fluctuations of geopotential height fields as well as climate signals of extra-tropical cyclones.

The following section describes the analysed AOGCM and reanalysis data as well as the methodology used for the flux investigation, and the objective algorithm for cyclone identification. The validation of model precipitation with reanalysis as well as the evaluation of SH moisture transport is done in section 4.3. It also includes the discussion of the climate change signals of moisture flux, geopotential height variations, with respect to their different decom-

positions, as well as cyclone activity. At the end of this section, the change of net precipitation within the Antarctic Circle is adressed. Section 4.4 gives a conclusion of our findings.

4.2 Data and methods

4.2.1 Coupled atmosphere-ocean general circulation model and reanalysis

Analysis is done with three members of a one AOGCM, which has been evaluated within the Coupled Model Intercomparison Project phase 3 (CMIP3) (Meehl et al., 2007a). The AOGCM consists of the atmospheric component ECHAM5 (Roeckner et al., 2003) computed at a horizontal resolution, which is triangular truncated at wavenumber 63 (T63) and the oceanic model MPIOM (Marsland et al., 2003). Validation is performed with ERA40 reanalysis data (Uppala et al., 2005).

SH reanalysis has to deal with sparse observational data, especially in the pre-satellite era. ERA40 is discussed to perform well since satellite products have been used for the reanalysis in the late 1970s (Bromwich and Fogt, 2004). Therefore, 20 years of ERA40 (1981-2000) are used in this study, on a horizontal resolution of 2.5°$\times$ 2.5°, which seems to be a fairer comparison with AOGCM data, especially for the identification of extra-tropical cyclones (Grieger et al., 2014). The three AOGCM members have also been analysed between 1981-2000, and between 2081-2100 following the SRES A1B scenario (Nakicenovic et al., 2000). In principle, the whole investigation has been done for extended austral winter season, i.e. April-September. Primary analysis of precipitation as well as the discussion of annual cycles has been done for the whole year.

For a good representation of vertically integrated moisture transport as well as possibilities to distinguish between mean an transient flux components, CMIP3 standard data availability of 3-dimensional daily variables, which consists of 9 pressure levels between 1000 hPa and 200 hPa is discussed to be insufficient (Uotila et al., 2007). Also CMIP5 model output standards are not adequate. To emphasize the analysis of this current study, 6-hourly data on 11 pressure levels between 1000 hPa and 200 hPa (1000, 925, 850, 775, 700, 600, 500, 400, 300, 250, 200) has been used. This data availability could be achieved for that model run.

For the calculation of atmospheric moisture flux 3-d data of horizontal wind and specific humidity has been analysed. Method validation of calculation net precipitation by means of

moisture flux convergence is done by an evaluation of direct AOGCM output of large scale and convective precipitation, and evaporation. The stormtrack is investigated by means of the 500hPa geopotential height. The objective algorithm for the identification and tracking of extra-tropical cyclones uses mean sea level pressure (MSLP) as input.

4.2.2 Hydrological cycle, moisture flux and flux divergence

Net precipitation can be computed by means of the evaluation of the hydrological cycle (e.g. Bromwich et al., 1995; Cullather et al., 1998). We start with vertically integrated moisture flux vector $\mathbf{Q}$. Generally, moisture flux is defined to be positive in northward direction. This study deals with SH moisture transport and its relevance for Antarctica, i.e. poleward moisture flux is an important quantity, here. For the whole paper, *poleward* moisture flux is defined to be *positive* to make it easier to interpret climate change signals of poleward moisture transports.

$$\mathbf{Q} = \frac{1}{g} \int_{p_{sfc}}^{p_0} q_{(p)} \mathbf{v}_{(p)} dp, \tag{4.1}$$

where g is acceleration of gravity, q is specific humidity and $\mathbf{v}$ is the horizontal wind vector. Moisture flux is integrated from surface pressure p_{sfc} to $p_0 = 200$ hPa. The divergence of $\mathbf{Q}$ can be written as

$$\langle E - P \rangle = \langle \nabla \cdot \mathbf{Q} \rangle + \left\langle \frac{\partial W}{\partial t} \right\rangle, \tag{4.2}$$

where $\langle . \rangle$ denotes areal averaging and W is total column water vapour (TCWV). Temporal mean $\overline{(.)}$ of eqation 4.2 can be written as

$$\overline{\langle E - P \rangle} = \overline{\langle \nabla \cdot \mathbf{Q} \rangle}, \tag{4.3}$$

since $\overline{\left\langle \frac{\partial W}{\partial t} \right\rangle}$ is small for seasonal and longer time scales (Bromwich, 1988).

Equation 4.3 can be written as a line integral using Gauss's theorem (Bromwich and Robasky, 1993). This simplifies the calculation of net precipitation south of an arbitrary polar cap for gridded data sets, since the zonal component u of wind vector $\mathbf{v}$ is no longer needed for the evaluation:

$$\overline{\langle E - P \rangle} = \frac{1}{A} \frac{1}{g} \oint \left\{ \int_{p_{sfc}}^{p_0} q_{(p)} v_{(p)} dp \right\} dl, \tag{4.4}$$

where A is the area of the polar cap and dl is the increment of the line around the cap.

4.2.3 Reynolds decomposition

Reynolds decomposition can be performed to distinguish between mean and eddy flux components. Any quantity A can be separated into average $\overline{A}$ and pertubation A':

$$A\left(t\right) = \overline{A} + A'\left(t\right). \tag{4.5}$$

Using equation 4.5 for moisture flux Q which is the product of specific humidity q and horizontal wind v, decomposition can be written as follows:

$$\overline{Q} = \overline{qv} = \underbrace{\overline{q}\,\overline{v}}_{\text{MME}} + \underbrace{\overline{q'v'}}_{\text{TE}}, \tag{4.6}$$

whereas the first part is the transport due to the mean meridional circulation (MMC) and the latter is the component of transient eddies (TE). In the SH extra-tropics, the most important part of meridional transport is due to transient flux perturbations (Peixoto and Oort, 1983), which are also highly relevant for the Antarctic region (Bromwich et al., 1995; Cullather et al., 1998).

This decomposition is done for each winter season (April-September) separately, to have the possibility of analysing inter-annual variabilities.

4.2.4 Wave decomposition

For an assignment of atmospheric wave components to different physical mechanisms, we follow the approach of Blackmon (1976), who has investigated 500hPa geopotential height fields for the Northern Hemisphere (NH). The methodology is straightforwardly adapted for the used AOGCM and reanalysis data for the objectives of this current study. Following Wu et al. (2011), who have been applied bandpass filtering on different energy flux components, little refinements for the bandpass filter are done.

Transient moisture transport $(q'v')$ as well geopotential height anomalies $(z'z')$ are divided into spacial waves of long transient and synoptic length scales by means of a triangular truncation. For the long wave scale, wavenumbers greater than 7 are truncated, whereas the residuum of the field is used as the synoptic scale. Furthermore, a 21 point low pass filtering is used to

distinguish between low and high frequency fluctuations. Referring to Blackmon (1976), the SH stormtrack is defined as the square of synoptic scale, high frequency fluctuations of the 500hPa geopotential height anomaly. Straightforwardly, the transient component of the vertically integrated meridional moisture flux is divided into long transient and synoptic waves of both, low and high frequency fluctuations. In the following, especially the synoptic scale is discussed, since this component dominates poleward atmospheric moisture transport.

4.2.5 Splitting thermodynamical and dynamical parts of moisture flux

If the climate change signal of moisture flux is investigated, it is often to be discussed mainly influenced by atmospheric temperature increase, since the hydrological cycle is strengthened in a warmer climate (e.g. Held and Soden, 2006; Lorenz and DeWeaver, 2007). Nevertheless, atmospheric circulation is changing in the future projections, generally and for regions which are important for atmospheric poleward moisture transport, i.e. the tropospheric mid-latitudes (e.g. Bengtsson et al., 2006; Grieger et al., 2014). Therefore, it is meaningful to perform an investigation of both thermodynamical and dynamical parts of the climate change signal of moisture transport and to distinguish between these parts.

We start with the results of previous studies that climate changes of net precipitation can be discussed as a function of projected temperature changes, since general circulation is unchanged (Held and Soden, 2006; Lorenz and DeWeaver, 2007). Held and Soden (2006) evaluate net precipitation to be a function of changes of global near surface temperature, whereas Lorenz and DeWeaver (2007) use the approach of analysing changes in the hydrological cycle as a function of zonal mean temperature at 850hPa. Since we investigate moisture flux in the SH mid- and high-latitudes, it is meaningful to follow the approach of Lorenz and DeWeaver (2007). At first, we define the future projection of transient moisture flux TE_{A1B} due to thermodynamics as a function of temperature change:

$$\mathrm{TE}_{A1B} = \mathrm{TE}_{20C} \exp\left[\alpha \left(T_{A1B} - T_{20C}\right)\right], \tag{4.7}$$

where TE_{20C} and TE_{A1B} are transient moisture flux, and T_{20C} and T_{A1B} are zonal mean temperatures in the 20$^{\text{th}}$ and 21$^{\text{st}}$ centuries and α is a proportionality constant. The exponential function can be expressed by the quotient of TCWV for the 21$^{\text{st}}$ and 20$^{\text{th}}$ centuries. Equation 4.7 becomes

$$\mathrm{TE}_{A1B} = \mathrm{TE}_{20C} \exp\left[\alpha \left(T_{A1B} - T_{20C}\right)\right] = \mathrm{TE}_{20C} \frac{W_{A1B}}{W_{20C}}, \tag{4.8}$$

wheras $W = W(\phi)$ is zonal mean of TCWV. Out of equation 4.8, a scaled transient flux $\mathrm{TE}_{A1B}^{scaled}$ can be defined:

$$\mathrm{TE}_{A1B}^{scaled} = \mathrm{TE}_{A1B} \frac{W_{20C}}{W_{A1B}}. \tag{4.9}$$

The climate change signal due to a dynamical change signal can be written with equation 4.9 as the difference between scaled transient flux in the 21st and the flux in the 20th century.

$$\delta\mathrm{TE}^{dynamical} = \mathrm{TE}_{A1B}^{scaled} - \mathrm{TE}_{20C} \tag{4.10}$$

4.2.6 Objective cyclone tracking algorithm

For the comparison of the stormtrack with statistics of extra-tropical cyclones, an objective algorithm for cyclone identification and tracking is used. A description of the methodology can be found in Murray and Simmonds (1991a), whereas modifications are specified by Simmonds and Murray (1999) and Simmonds et al. (1999). A more detailed description of the setting can be found in Grieger et al. (2014).

4.3 Results

4.3.1 Reanalysis and AOGCM 20C

Precipitation and net Precipitation

At first, precipitation (P) and net precipitation ($P - E$), respectively will be investigated for ERA40 and the ECHAM5 AOGCM integration. Therefore, reanalysis and AOGCM model output of precipitation and evaporation is analysed on the same 2.5×2.5 horizontal grid as used for ERA40 in this study, i.e. P and E are regridded by a conservative remapping.

SH precipitation patterns of ERA40 reanalysis show a distinctive gradient of high precipitation values over the Southern Ocean towards lower values over Antarctica (Figure 4.1a). This general behaviour is already discussed in previous studies (e.g. Bromwich, 1988; Tietäväinen and Vihma, 2008). The regions at the coast line of Amundsen and Bellingshausen Seas show maximum values of precipitation off coast of Antarctica. For net precipitation, positive values, i.e. precipitation predominates evaporation, can be found at nearly every location between 50°S and 90°S (Figure 4.1b), but downstream the southern tip of South America and south of Ross Sea. Remarkable are maximum values at the Antarctic coast line of Amundsen-

Bellingshausen Seas and west of the Antarctic Peninsula, which are already be found for precipitation.

General behaviour of precipitation and net precipitation can be simulated by the investigated AOGCM runs (Figure 4.1c and d), although differences are found in some details. The amount of precipitation over the Southern Ocean is generally higher in the AOGCM, whereas precipitation as well as net precipitation is underestimated west of the Antarctic Peninsula, which is likely due to the smoother topography of the AOGCM (cf. Bromwich et al., 2004). Lower orography of the Antarctic peninsula also leads to a less pronounced minimum at Weddell Sea, which is due to blocking of moist air (cf. Tietäväinen and Vihma, 2008). On the other hand, there are additional remarkable locations of high net precipitation off coast the Antarctic continent, namely north of Enderby Land and north of Adelie Land (Figure 4.1d). Although, modelled P and E seem to be a bit more noisy in comparison to ERA40 the AOGCM generally simulates patterns for precipitation and net precipitation, which are well comparable with reanalysis. This is not obvious for a GCM integrated at T63 (cf. Genthon and Krinner, 2001).

Precipitation south of 67.5°S

The reanalysis and the AOGCM analysed in this study use different land sea masks (LSM) as well as a different orography, which complicates fair comparison of precipitation since it is largely influenced of the representation of the Antarctic continent. Therefore, the region of interest is objectified to the spherical cap south of 67.5°S. By this choice additional regridding is not necessary. To ensure that the new area is an acceptable representation of Antarctica, in terms of net precipitation, correlation between $E - P$, given as model output, of both areas is calculated. For monthly values of the analysed period (1981-2000), correlations for the three members of the AOGCM are 0.88, 0.87, and 0.87, respectively.

Figure 4.2 shows the annual cycle for precipitation, evaporation, and the difference of both, i.e. net precipitation, south of 67.5°S for (a) ERA40 and (b) ECHAM5. Precipitation peaks at March for ERA40 with slightly decreasing values for the following months with respect to the annual cycle. Maximum values for evaporation can be found for austral summer (DJF), whereas it is almost zero in winter (JJA). Combination of both leads to an annual cycle of net precipitation, which is maximal for the extended winter season (April-September).

This general behaviour can be found in previous studies (Bromwich et al., 1995; Cullather et al., 1998). The annual cycle simulated by ECHAM5 is shifted towards winter season, i.e. maximum values of evaporation can be found in March and April, and precipitation peaks at

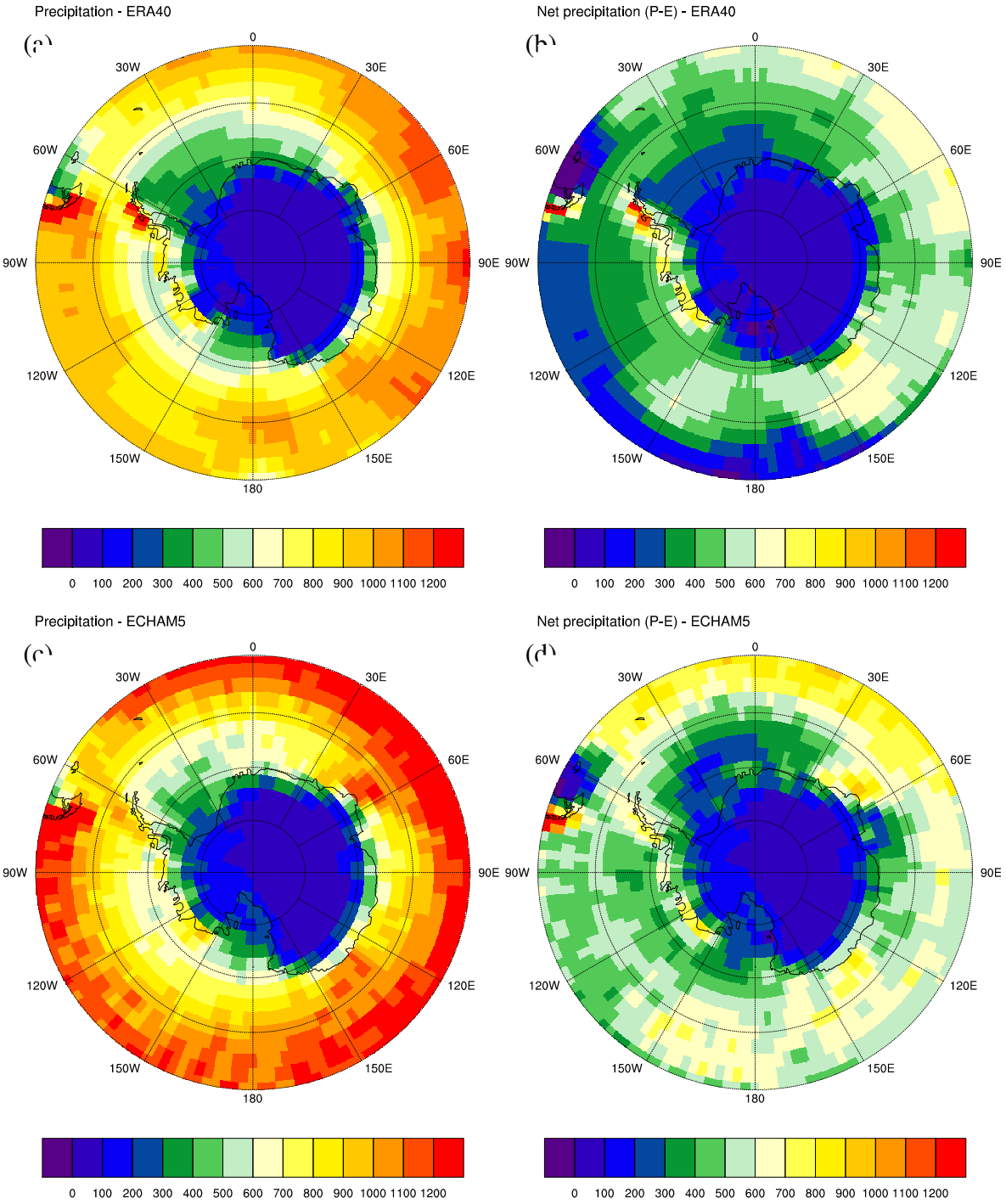

Figure 4.1: Precipitation for (a) ERA40 and (c) ECHAM5 (ensemble of three runs), and net precipitation (P-E) for (b) ERA40 and (d) ECHAM5 (ensemble of three runs) between 1981-2000. Both ERA40 and ECHAM5 have been regridded to the same $2.5° \times 2.5°$ grid.

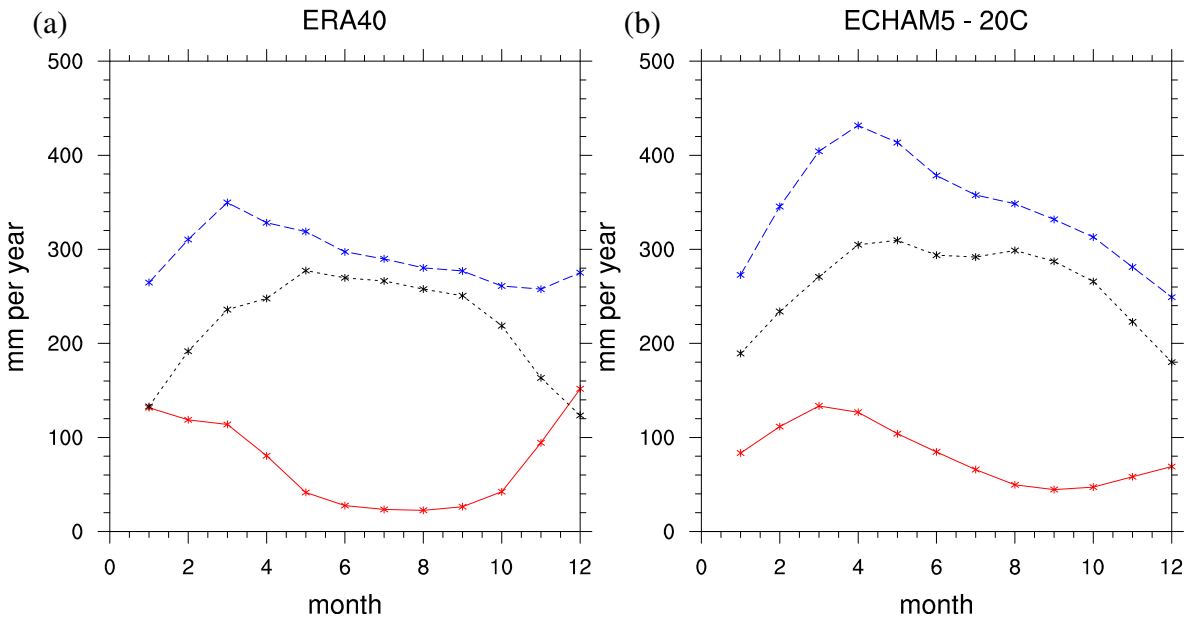

Figure 4.2: Monthly climatology of precipitation (dashed blue), evaporation (solid red), and net precipitation (dotted black) for (a) ERA40 and (b) ECHAM5 (ensemble of three runs) between 1981-2000 south of 67.5°S.

April (Figure 4.2b). As expected by the general characteristic of an higher amount of SH precipitation, in comparison to ERA40 (Figure 4.1), simulated net precipitation over Antarctica is generally higher (Figure 4.2). Nevertheless, the annual cycle of net precipitation shows its maximum throughout extended winter season, as found for ERA40.

Comparison between net precipitation and flux divergence

Following equation 4.4, the divergence inside a spherical cap calculated by moisture flux through the boundary, i.e. latitude of 67.5°S. Using the regridded data on the same $2.5° \times 2.5°$ grid, $P - E$ and moisture flux convergence can easily be compared for the same region. Table 4.1 shows this comparison between net precipitation and flux convergence for ERA40 and ECHAM5 from 1981 to 2000 for the whole year. Results for ERA40 match very well, possibly even better than in the study of Tietäväinen and Vihma (2008). Maybe this is due to the coarser grid used for our calculation, which leads to a smoother representation of the values, which can be beneficial for precipitation. Differences are higher for ECHAM5, i.e. $P - E$ is about 15% higher than flux convergence. This is consistent for each run. Therefore, it seems more to be a systematic bias than a general discrepancy. It is possible that the temporal and vertical

	$P - E$ [mm/year]	$-\overline{\langle \nabla \cdot Q \rangle}$ [mm/year]
ERA40	219.6	215.2
Run 1	264.0	228.9
Run 2	258.2	223.6
Run 3	264.9	229.6

Table 4.1: Net precipitation and flux divergence for ERA40 and the three runs of ECHAM5 south of 67.5°S from 1981 to 2000 for the whole year.

resolution has been still insufficient for an correct calculation of moisture flux convergence (Uotila et al., 2007). On the other hand, $E - P$ values have to be carefully discussed, since it is known that climate models have difficulties in their representation of Antarctic precipitation (Genthon and Krinner, 2001). Generally, it is assumed that the approach of moisture flux convergence can lead to more realistic results for certain regions, if vertical and temporal resolution is sufficiently high.

Splitting moisture flux into components of MMC and TE by means of Eq. 4.6 results in a dominating role of TE for SH moisture flux in the mid- and high-latitudes, as shown by previous studies (e.g. Peixoto and Oort, 1983; Bromwich et al., 1995; Cullather et al., 1998). At the latitude belts covering the Antarctic ice shield, MMC turns into eqatorward direction. This is due to katabatic winds which play a dominant role for the near surface wind system of Antarctica, and are known to show high directional constancy (Tietäväinen and Vihma, 2008). In this current work, further investigation of moisture flux is done for the transient component, since this study focus on the understanding of transport mechanisms from mid- and high-latitudes towards the Antarctic continent. In the following, this paper concentrates on the extended winter season (April-September), since $P - E$ shows maximum values for these month (Fig. 4.2). Figure 4.3 a) and b) show the transient component of vertically integrated meridional moisture flux for ERA40 and the AOGCM runs. The values are negative everywhere which implies a poleward transport on the SH. As shown by previous studies (e.g. Peixoto and Oort, 1983), maximum flux can be identified around 40°S downstream of the continents at the Atlantic, Indian Ocean and Pacific. In comparison to ERA40, it can be stated that the TE component of moisture flux is well characterized by ECHAM5.

Circulation - cyclones and geopotential variations

Transient moisture flux is the transport component due to atmospheric eddies. While the meridional wind component is increasing by height through the troposphere, specific humid-

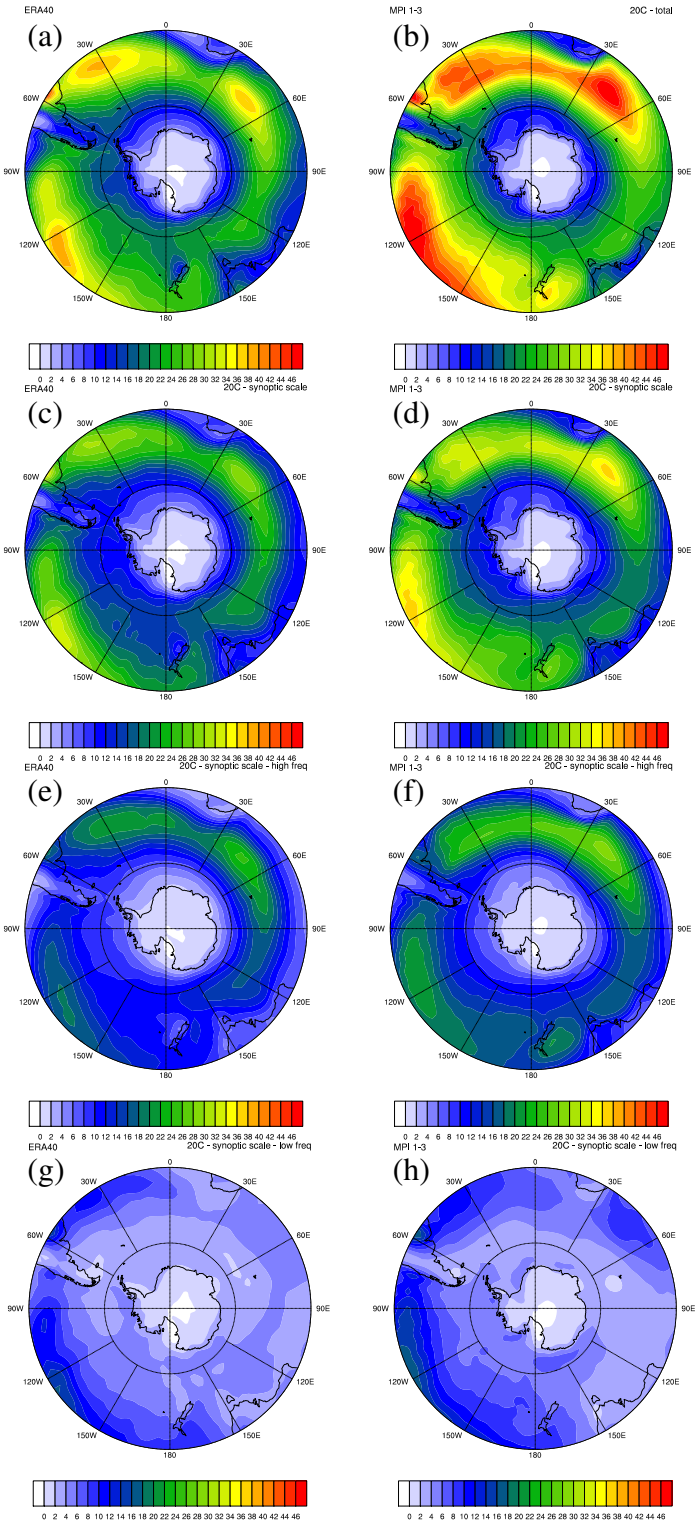

Figure 4.3: Transient component of vertically integrated meridional moisture flux [$\mathrm{kgm^{-1}s^{-1}}$] for extended winter season (April-September) between 1981-2000 for (a,c,e,g) ERA40 and (b,d,f,h) ECHAM5 (ensemble of three runs). Flux is (a,b) not filtered, (c,d) spatially filtered for synoptic wave length, and additionally temporal filtered for (e,f) high and (g,h) low frequencies.

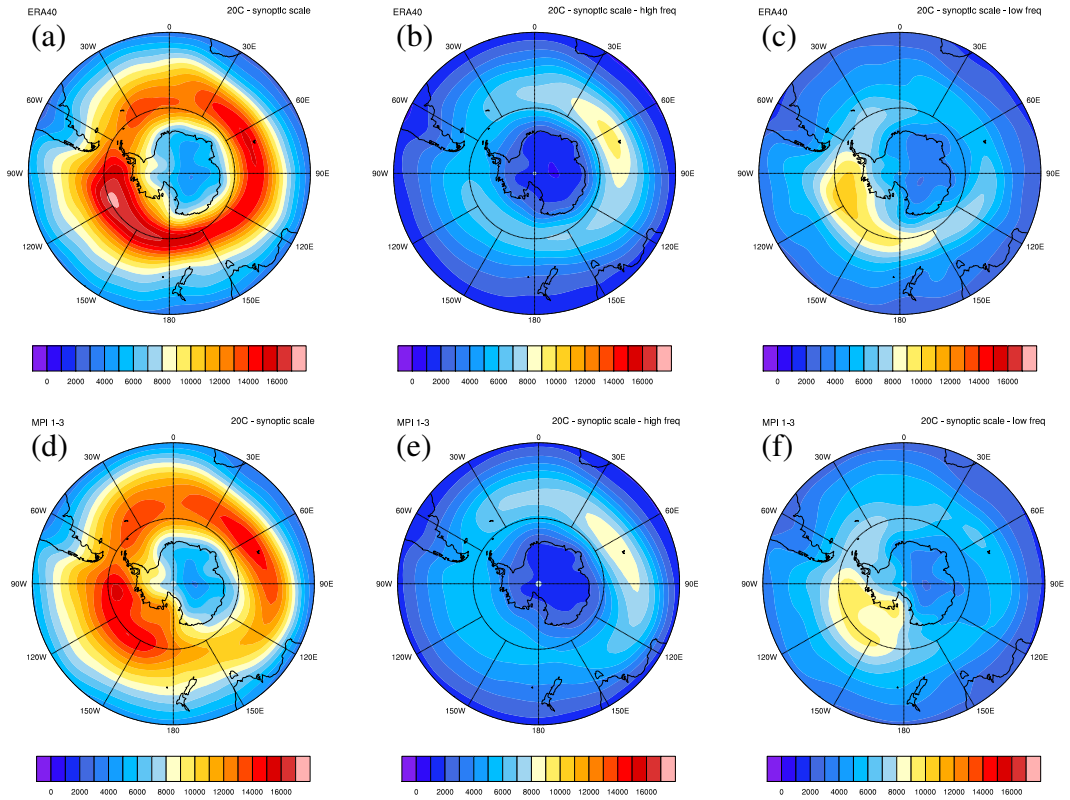

Figure 4.4: Variation of the 500hPa geopotential height anomalies $(z'z')$ [gpm^2] for (a,b,c) ERA40 and (d,e,f) simulated by ECHAM5 (ensemble of three runs) for extended winter season (April-September) between 1981-2000 for (a,d) spatially filtered for synoptic wave length, and additionally temporal filtered for (b,e) high and (c,f) low frequencies.

ity is decreasing. Moisture flux has its highest part in the lower troposphere (Bromwich et al., 1995). The identification of tropospheric wave activity is commonly done at 500hPa (Blackmon, 1976). Due to the fact that maximum moisture transport occurs in the lower troposphere, 500hPa wave activity is assumed to be a good measure for the assignment of transient moisture transport to atmospheric circulation. Variations of geopotential height show different characteristics in terms of length scale and temporal frequency. Synoptic scale variations of the 500hPa geopotential height field in the frequency band between 2.5 and 8 days is known as stormtrack (Blackmon, 1976) and mainly affected by extra-tropical cyclones.

Geopotential height variations are analysed as described in Sec. 4.2. Figure 4.4 shows synoptic scale variations of 500hPa geopotential height in terms of the square of the anomaly for ERA40 and ECHAM5. Maximum variations can be found between 50°S and 60°S in the

Atlantic and Indian Oceans and around 60°S in the Pacific. Decomposition into high (Figure 4.4b) and low frequency variations (Figure 4.4c) highlight different regions. High frequency variations, i.e. the stormtrack, shows more or less zonaly symmetric wave activity with maximum values around 50°S in the Indian ocean for both, reanalysis and the AOGCM. Track density of extra-tropical cyclones is remarkable slightly poleward of the stormtrack whereas strong cyclone activity corresponds to the maximum of the stormtrack in the Indic sector of the Southern Ocean (Figure 4.5). Strong cyclone track density of ERA40 shows another maximum in the Australian Sector of the Southern Ocean off the Antarctic coast (Figure 4.5b), which cannot be found in the stormtrack. The maximum of the low frequency variation is found around 60°S and southward in the Pacific sector of the Souther Ocean (Figure 4.4c and f). Blackmon (1976) discussed NH low frequency variations of synoptic length scale due to blocking situations that are typically more persistent in comparison to low pressure systems. On the SH, synoptic activity of the Pacific Sector of the Southern Ocean is dominated by the Amundsen-Bellingshausen Sea Low (ABSL) (e.g. Fogt et al., 2012). This quasi stationary low steers many cyclones in the direction of West Antarctica (Fogt et al., 2012). Transport of sensible and latent heat is very high in this region (Nicolas and Bromwich, 2011). We assume the ABSL to be the reason for the low frequency variation of the geopotential height field in the Pacific sector of the Southern Ocean.

Meridional moisture flux due to different wave frequencies in the 20th century

A decomposition of the flux into waves of different length scale shows the domination of transport by synoptic scale waves (Fig. 4.3 c-h) in comparison to transient long waves (not shown). This can also be seen by the comparison of the decomposition with the total flux (Fig. 4.3a and b). The synoptic scale waves are split into a high and low frequency components as done for the geopotential height. In the mid-latitudes poleward moisture flux is dominated by the high frequency component. Maximum values can be found in the Atlantic and Indian Sectors of the Southern Ocean. Mid-latitude transport due to low frequency waves is about one order of magnitude smaller in comparison to the high frequency component. This difference becomes smaller in the high-latitudes south of 60°S where the high frequency component is in parts negligible. South of 60°S low frequency component shows maximum values off coast of Adelie land and east of Ross Sea. In these latitude belts, both components are in the same order of magnitude.

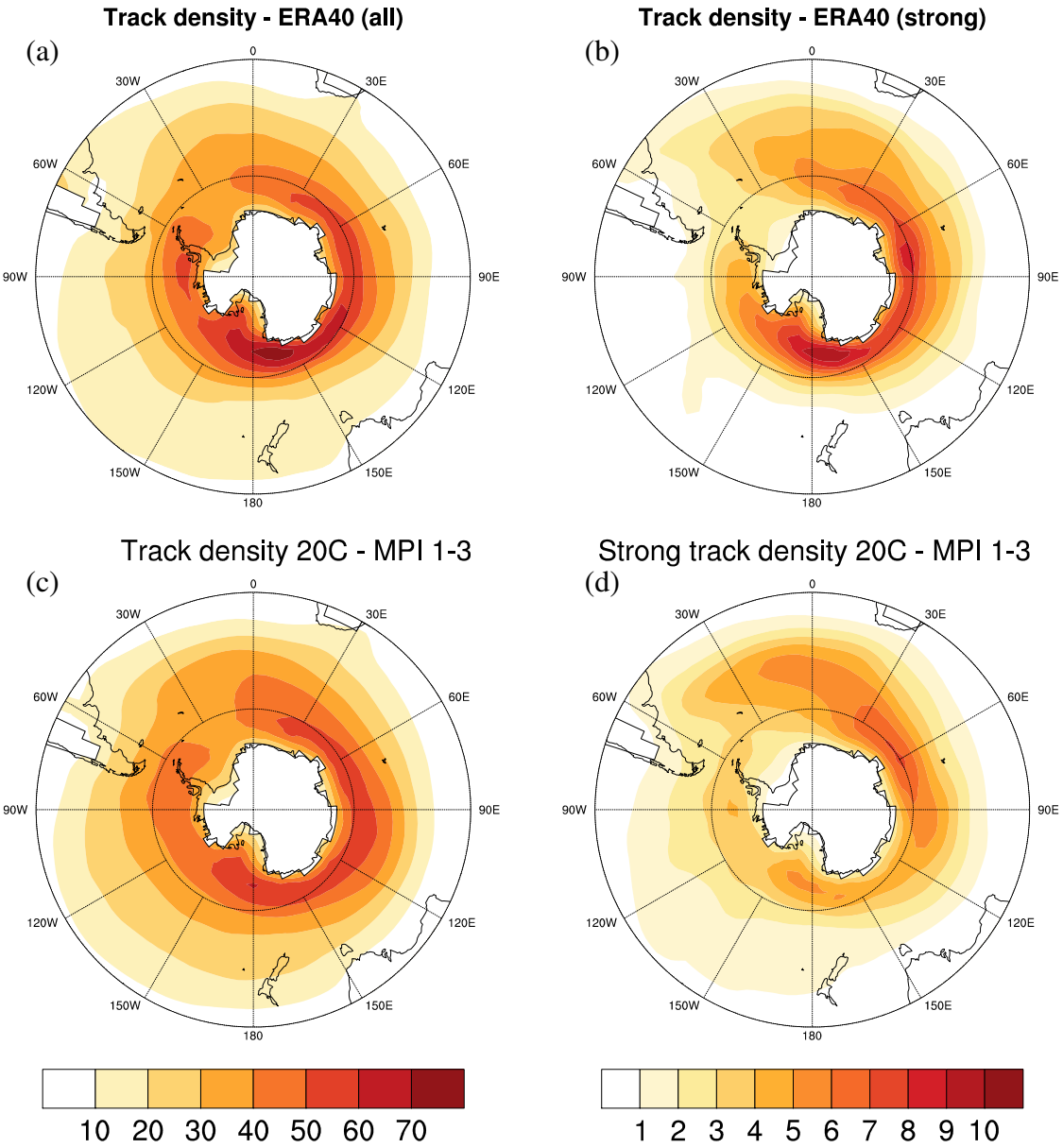

Figure 4.5: Cyclone track density identified for (a,b) ERA40 and (c,d) ECHAM5 (ensemble of three runs) for extended winter season (April-September) between 1981-2000 for (a,c) all and (b,d) strong cyclones.

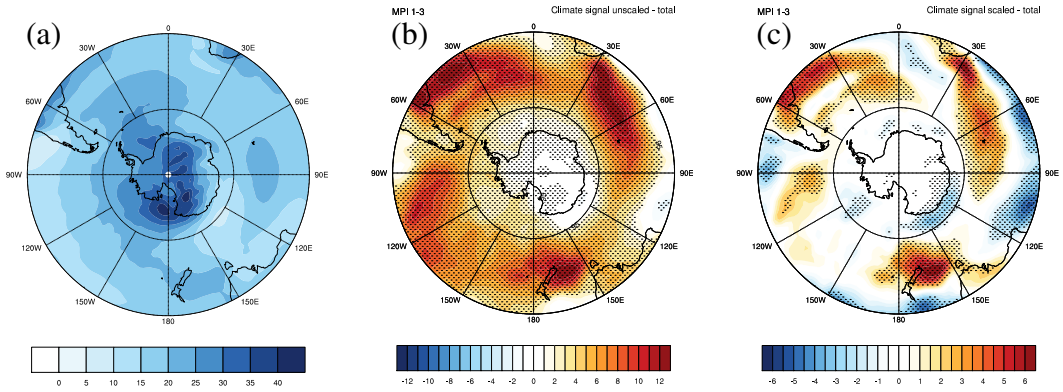

Figure 4.6: Climate change signal of (a) TCWV, (b) transient meridional moisture flux and (c) transient meridional moisture flux due to dynamics. Stippled areas indicate significant changes ($p < 0.05$) with respect to a Student's t-test. Note that the signal of TCWV is significant *everywhere*. Therefore stipples are not shown for TCWV.

4.3.2 Simulated changes in the A1B scenario

Thermodynamical and dynamical change of moisture flux

The AOGCM used in our study shows a distinctive increase of TCWV with respect to the A1B scenario (Figure 4.6a), as suggested by previous studies analysing the model response of the hydrological cycle to temperature changes (Held and Soden, 2006). Higher values of TCWV lead to an increasing signal of the meridional moisture flux in the whole analysed area (Figure 4.6b).

Using Eq. 4.10 enables the possibility to calculate the dynamical change of moisture flux. These climate change signal of the vertically integrated transient moisture flux is dominated by three increasing spots (Figure 4.6c). They are found in the Atlantic and the Indian sectors of the Southern Ocean and south of Tasman Sea. These spots can also be identified in the unscaled total signal as maximum values of the increasing signal (Figure 4.6b). In the following, we concentrate on the discussion of the dynamical changes of moisture flux.

Changes of different wave decompositions

Because of the small influence of transient long waves on meridional moisture transport, we concentrate on the climate change signals of the synoptic length scale. Figure 4.7a shows the climate change signal of synoptic length scale variations of the 500hPa geopotential height

field. Wave activity is enhanced in a circumpolar band between 50°S and 60°S. This is even more pronounced for the high frequency component, i.e. the climate change signal of the stormtrack (Figure 4.7b). The intensification of the stormtrack shows maximum values in the Eastern Atlantic and Indian sectors of the Southern Ocean. Slightly decreasing signals are found north of about 40°S in the Indian and Pacific Oceans. This signal can be interpreted as the commonly named poleward shift of the stormtrack, which can also be seen in previous studies (e.g. Yin, 2005). This characteristic can also be seen in the climate change signal of extra-tropical cyclones (Figure 4.8a) since the stormtrack is an Eulerian measure for cyclone activity. Low frequency wave activity shows a decreasing signal on almost the whole SH but a small region of increase in the Pacific around 45°S and another one south of it. Maximum values of decrease can be seen north and south of Ross Sea, which is assumed to be a shifted and less variable ABSL. On the other hand, following the discussion of Blackmon (1976), who assigned this low frequency variability mainly to atmospheric blockings, the decreasing low frequency variability can be the signal of a future shift towards more frequent situations of low pressure circulation patterns (Lynch et al., 2006).

The dynamical part of the climate change signal of the meridional moisture flux due to synoptic scale waves shows decreasing poleward flux south of 60°S around Antarctica (Figure 4.7d). Increasing poleward flux can be found between 40°S and 60°S, whereas a decrease is seen again north of about 40°S mainly in the Indian and Pacific Oceans. The high frequency component of this signal clearly shows the impact of the shifted stormtrack (Figure 4.7e), i.e. an increasing poleward flux between 40°S and 60°S and decreases north of it. Beside the shift of the stormtrack which can be seen in the change of the variation of the 500hPa geopotential height (Figure 4.7b), maximum values of increases reflect the increasing signal of strong cyclone activity in the South Atlantic, on the Eastern Hemisphere and south of Tasman Sea (Figure 4.8b). The decrease of poleward flux around Antarctica is hardly seen in the high frequency component. The climate change signal of the low frequency part shows more or less decreasing poleward flux on the whole SH. Especially the reduction of poleward moisture transport south of 60°S is due to the climate signal of the low frequency component.

4.3.3 Climate change signal of net precipitation south of the Antarctic Circle

As previously done in Sec. 4.3.1 net precipitation south of a polar spherical cap can be calculated by means of the zonal mean moisture flux at 67.5°S, following equation 4.4. As expected

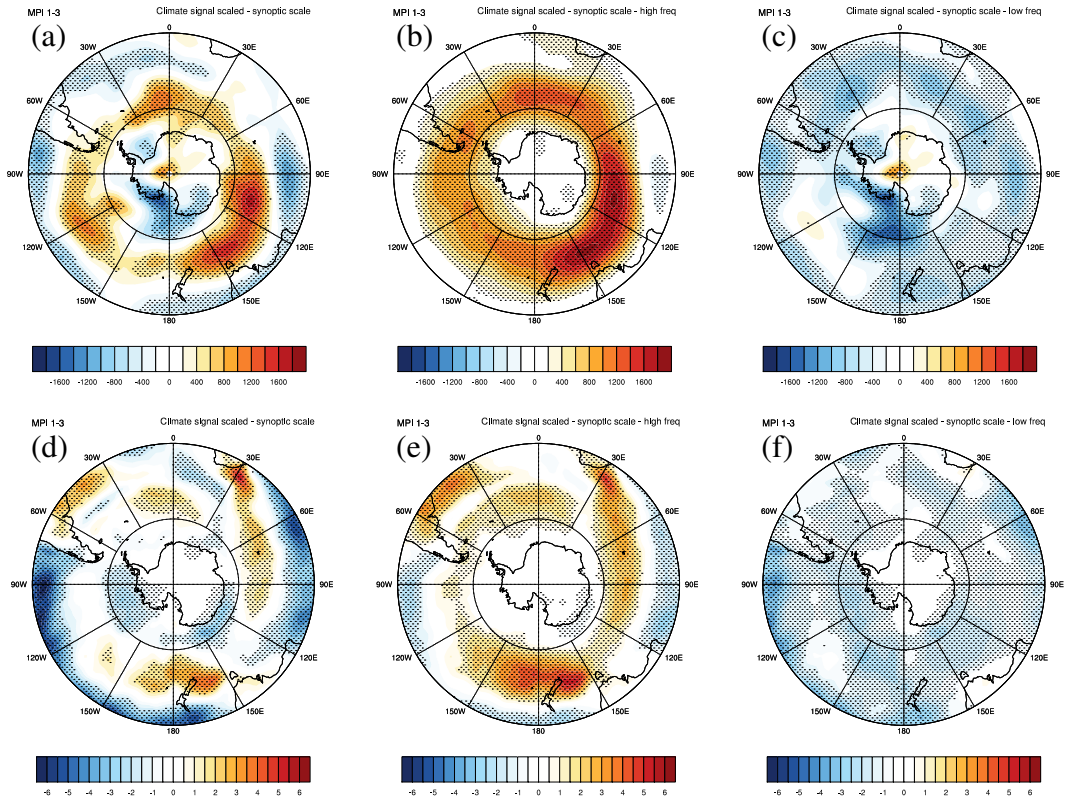

Figure 4.7: Climate change signal of synoptic length scale variations of the 500hPa geopotential height for (a) all frequencies, (b) high frequencies, (c) low frequencies and meridional moisture flux for (d) all frequencies, (e) high frequencies, (f) low frequencies. Stippled areas indicate significant changes ($p < 0.05$) with respect to a Student's t-test.

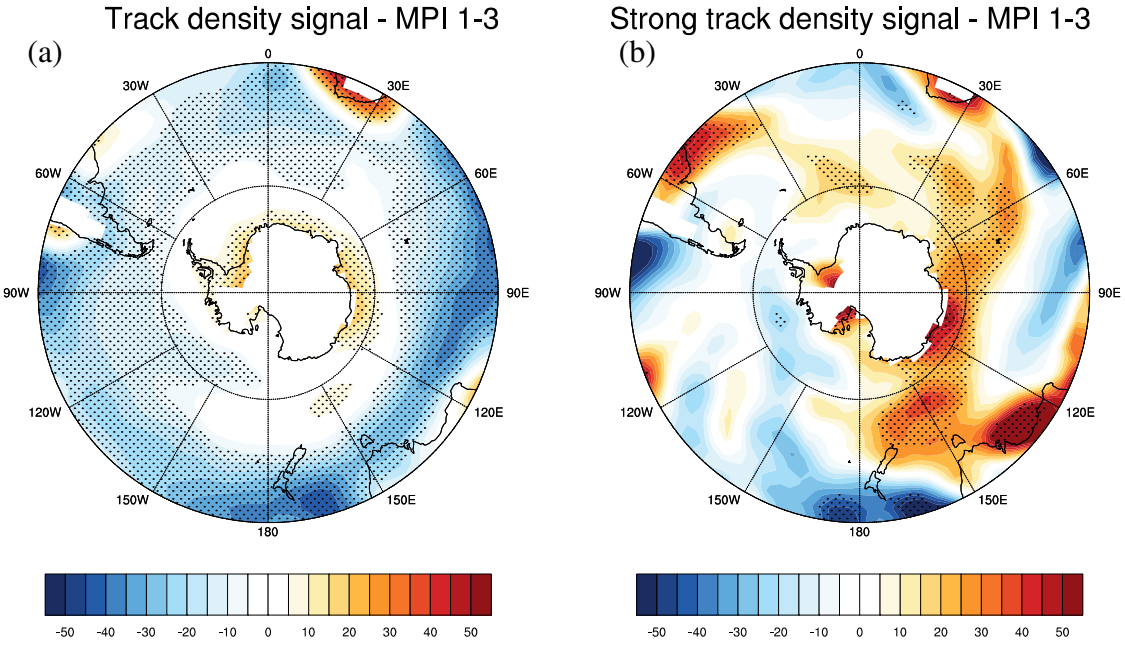

Figure 4.8: Cyclone track density simulated by ECHAM5 for the 20th century for (a) all and (b) strong cyclones. Stippled areas indicate significant changes ($p < 0.05$) with respect to a Student's t-test.

by the climate change signal of meridional moisture flux, which shows increasing poleward transports at almost every location of the SH extra-tropics (Figure 4.6b), increasing values for net precipitation can be found south of 67.5°S (Table 4.2). This is not the case for the dynamical part of the climate signal, which can also be seen for the dynamical signal of the flux (Figure 4.6c). For both, the 20th and 21st century, the synoptic scale component dominates the whole transient flux divergence within the spherical cap. Dividing this part of wavelength into low and high frequency fluctuations leads to an almost balanced ratio of flux divergence with 45% for the low frequency and 55% for high frequency component, whereas the low frequency part of the transient flux in the mid-latitudes is an order of magnitude smaller than its high frequency counterpart (Figure 4.3e-h). South of 60°S, the amount of poleward moisture flux is more similar for low and high frequencies, whereas spacial patterns differ. The high frequency part shows a zonally symmetric behaviour, whereas the main low frequency flux can be found between the Australian Sector of the Southern Ocean (150°E) and the Antarctic Peninsula, where generally the major moisture inflow towards Antarctica takes place.

With respect to the climate change signal, the low frequency component of the flux divergence shows the highest change at all. This can be seen in the high latitude climate change signals of moisture flux itself (Figure 4.7e and f). The high frequency flux component mainly

	20C [mm/y]	A1B [mm/y]	climate change signal [%]
transient	266.5	309.2	+16.0
dynamical		250.6	-6.0
synoptic scale	217.1	193.8	-10.7
synoptic scale - low frequency	98.4	75.3	-23.4
synoptic scale - high frequency	118.7	118.5	-0.2

Table 4.2: Moisture flux convergence simulated by the ensemble of three ECHAM5 runs for different temporal and spacial wave activity south of 67.5°S.

reflects the shift of the SH stormtracks and climate change signal of cyclone activity, respectively (Figure 4.7e), whereas the signal is negligible at the Antartic coast line. The low frequency flux signal is characterised by an opposite sign, i.e. decreasing poleward moisture transport (Figure 4.7f), which mainly leads to the decreasing climate change signal of Antarctic net precipitation due to the dynamical component.

4.4 Summary, discussion and conclusions

This paper analysed SH moisture flux and net precipitation over Antarctica in the 20th and 21st century. For that reason reanalysis data and three runs of ECHAM5/MPIOM integrations were used, which provide 6-hourly output at 11 pressure levels between 1000hPa and 200hPa. Thermodynamical and dynamical components of the climate signal were distinguished by a scaling approach. Furthermore, the dynamical part of the changing signal was analysed by means of spatial and temporal wave decompositions.

This study has found thermodynamical and dynamical parts of the climate change signal of Antarctic net precipitation to be opposing in sign. Although a robust poleward shift of the SH stormtrack can be identified in the future projection, the dynamical component of net precipitation shows a decreasing signal. In parts this can be understood by the climate signal of strong extra-tropical cyclones, which mainly show increasing track density on the Eastern Hemisphere. Furthermore the low frequency variability of geopotential height as well as moisture flux lead to that decrease which is suggested to be attributed to the quasi-stationary lows around Antarctica.

Yin (2005) finds a robust poleward shift of the stormtrack in future projections of a CMIP3 multi-model ensemble. This is consistent with the results of Bengtsson et al. (2006) investi-

gating cyclone activity in the same model runs analysed in our study. Also an examination of a multi-model ensemble which has been investigated in the context of "ENSEMBLES" (van der Linden and Mitchell, 2009) has shown a poleward shift of SH extra-tropical cyclone track density (Grieger et al., 2014). This finding could be reproduced in this paper. Since extra-tropical cyclones are mainly responsible for mid- and high-latitude transport of atmospheric energy (Peixoto and Oort, 1983; Wu et al., 2011), it can be expected that the major parts of moisture flux also shift towards the pole.

Consistent with previous studies, it has been found that the thermodynamical part dominates the climate change of SH moisture flux as well as the changes of Antarctic net precipitation. Counter-intuitively the dynamical component of Antarctic net precipitation change counteracts with the thermodynamical part, although a poleward shift of the SH stormtrack has been identified, as expected. It results in a decreasing signal of moisture transport east of the three climatological low pressure regions off-coast of Antarctica. This is due to the low variability component of spatially synoptic scale waves, which shows a weakened variability across almost the whole analysed area of the SH. As expected the high frequency counterpart of the dynamical moisture flux signal, which can be attributed to SH stormtrack, is shifted poleward and enhanced in the high latitudes. This can be understood by the climate change signal of extra-tropical cyclones, which also show a poleward shift with increasing track density at certain regions of the Antarctic coast. As part of the overall climate change signal there is a particular change pattern for the subset of strong cyclones. These most severe synoptic systems show an increasing track density especially on the Eastern Hemisphere and south of Tasman Sea. They also strongly influence total climate change of moisture flux in the mid-latitudes. On the other hand, south of 60°S the dynamically induced moisture flux change shows decreasing signals which leads to the identified decrease of net precipitation of Antarctica.

Generally, an intensification of atmospheric moisture flux can be identified in future projections of CMIP3 AOGCM simulations (Held and Soden, 2006). Obviously, this is discussed to be due to an increase of atmospheric moisture in a warmer climate. This can be confirmed by our work, since the model projection shows an overall significant increase of TCWV and an increasing signal of moisture flux due to thermodynamics. Held and Soden (2006) discuss the intensification of the hydrological cycle as well as the change of $P-E$ mainly to be a function of global near-surface temperature whereas Lorenz and DeWeaver (2007) relates moisture flux changes with zonal means of 850hPa temperature. Seager et al. (2010) splits the MMC part of moisture transport into thermodynamic and dynamics, which is not possible for the transient component. Since the transient component of moisture flux dominates mid- and high-latitude

transport, this study introduces a scaling approach for the transient part of future moisture flux by means of zonal mean TCWV. Therefore, a climate change component of moisture transport is calculated, which is related to the dynamical climate signal. The major increasing spots of future moisture flux can also be found for the dynamical component, namely in the Atlantic and Indian Sectors of the Southern Ocean and south of Tasman Sea as well as for a small region in the East Pacific. Thermodynamical and dynamical parts show an opposing sign of the climate change signal south of 60°S. This is the key difference of both components, which is important for the climate change signal of net precipitation of Antarctica.

Uotila et al. (2007) investigate Antarctic net precipitation for a multi-model ensemble of CMIP3 AOGCMs. They criticize the temporal and vertical standard resolution of CMIP3 for an analysis of vertically integrated moisture flux to calculate net precipitation. Therefore, they use model output of precipitation and evaporation for their analysis of Antarctic net precipitation. By means of an investigation of circulation weather types they distinguish between thermodynamical and dynamical components of the climate change signal and discuss the thermodynamics to be dominating. In comparison to our results, they do not find a decreasing signal due to dynamics for the whole Antarctica. For the dynamical component of the climate change net precipitation Uotila et al. (2007) find mainly increases for the the Antarctic Peninsula and a small decrease for certain parts, i.e. East Antarctica. This contrasting signal reflects the situation, which can be found in positive phases of the southern annular mode (SAM), where climate models tends to shift to in future projection (Meehl et al., 2007b). SH Westerlies are then increased and suppress meridional exchange of energy towards East Antarctica, whereas the Antarctic Peninsula is more overflowed by the mean circulation (van den Broeke and van Lipzig, 2004). This characteristic is potentially less pronounced in our study since it concentrates on transient transports of moisture whereas the direct impact of SAM as described above is more characterized in the mean meridional circulation. Furthermore, Uotila et al. (2007) uses precipitation and evaporation, where AOGCMs potentially still have problems dealing with the Antarctic region (cf. Genthon and Krinner, 2001).

For a better understanding of geopotential variability in the mid-troposphere Blackmon (1976) has divided variability into different spatial and temporal scales of atmospheric waves. In parts, Wu et al. (2011) have been applied these ideas to atmospheric energy fluxes by means of a bandpass filter between 2.5 and 8 days. Our study uses a low pass filter for fluctuations of 8 days and longer for selection of high and low frequency variability. Spatial filtering is done for waves smaller and larger than wavenumber 7. This approach enables to attribute the major contribution of SH moisture transport to the synoptic length scale. The SH stormtrack

is clearly identified as well as the corresponding part of moisture flux due to high frequency variability. In the SH mid-latitudes the low frequency moisture flux component is an order of magnitude smaller than the high frequency part. Near the Antarctic coast, the low and high frequency moisture fluxes are in the same order of magnitude. On the SH high latitudes, near the Antarctic coast quasi-stationary low pressure patterns can be found (cf. Schwerdtfeger, 1984), whereas the most prominent is the Amundsen-Bellingshausen Sea Low also known as Amundsen Sea Low (ASL) (Turner et al., 2013). Its characterization and variability is important for synoptic activity (Fogt et al., 2012) as well as the climate of West-Antarctica (Hosking et al., 2013). Our analysis seems to cover ASL fluctuations by means of the low frequency geopotential height variability. This can hardly be seen in the corresponding moisture flux part. The climate change signal of the low frequency geopotential height is most pronounced in the ASL sector by decreasing variability. Although the low frequency component of both geopotential height variability and moisture flux shows a decreasing signal for almost the whole analysed area, the changing signal south of about 60°S is highly relevant for Antarctica. The role of the quasi-stationary low pressure patterns around the Antarctic coast are already discussed in previous studies (cf. Turner et al. (2009); Hosking et al. (2013); Turner et al. (2013)). In parts the variability can be also connected to the Southern Oscillation Index (SOI) as well as SAM. The development of the quasi-stationary lows in future climate projections is still ongoing research.

5 Summary, Discussion and Conclusions

The Antarctic ice sheet is the largest contiguous ice mass on globe. This fact makes Antarctica to an important source of sea level rise, with respect to climate change. Estimating Antarctic SMB and its impact on sea level rise is an important issue, which is also discussed in the assessment reports of the Intergovernmental Panel on Climate Change (IPCC) (cf. Meehl et al., 2007b; Church et al., 2013; Collins et al., 2013). Observations as well as model projections underlie various uncertainties. For that reason it is important to better understand mechanisms, which lead to Antarctic mass accumulation and its change in future climate projections. This thesis has investigated the atmospheric branch of Antarctic mass balance, i.e. net precipitation ($P - E$), its representation in reanalysis and AOGCM data. Therefore, this work analysed processes leading to the poleward transport of atmospheric moisture and examined the change these processes in future climate projections.

Since extra-tropical cyclones dominate the moisture flux of SH mid- and high-latitudes (cf. Peixoto and Oort, 1983) this thesis firstly has analysed the representation of Sub-Antarctic cyclones by 30 years of ERA Interim reanalysis. Method uncertainties of objective identification and tracking of extra-tropical cyclones is assessed by means of an intercomparison project introduced by Neu et al. (2013). The thesis used the outcome of 15 different cyclone tracking algorithms to analyse how these methodologies characterize synoptic activity in the Sub-Antarctic region as well as how these algorithms capture processes which are relevant for poleward moisture flux in the SH high-latitudes. It is found that especially the strongest cyclones are similar represented and robustly lead to extraordinary moisture inflow towards Antarctica (chapter 2).

Future projections of AOGCM simulations show a poleward shift of the SH stormtrack (Yin, 2005) as well as extra-tropical cyclone track densities (Bengtsson et al., 2006; Ulbrich et al., 2009). This thesis analysed the robustness of future extra-tropical cyclone change by means of a MME of AOGCMs and specially focussed on strong cyclones which are highly relevant for poleward moisture transport. With respect to different methodologies, the climate change signal of the most severe cyclones is more robust in comparison to the whole intensity

spectrum (Ulbrich et al., 2013). In comparison to all cyclones which show a poleward shift, strong cyclones are found to increase especially on the Eastern Hemisphere, with respect to the climate signal of the MME (chapter 3).

The content of atmospheric moisture will increase in a warmer climate. This results in an intensified hydrological cycle of climate models with respect to climate change (Held and Soden, 2006). Future estimations of $P - E$ are discussed to be mainly a function of atmospheric temperature increase. This thesis takes also into account that the atmospheric circulation shows changing signals, with respect to future projections. Since relevant processes for moisture transport correspond to mid- and high-latitude cyclone activity, this work compares climate change signals of moisture flux and net precipitation with changing extra-tropical cyclone characteristics. For that reason, an approach is introduced to distinguish between thermodynamical and dynamical parts of the climate change signal of moisture flux. The thermodynamical component dominates the climate change signal. The dynamical part decomposed into different spacial and temporal waves. The climate signal of the dynamic component can be understood by a stormtrack shift whereas especially the signal of strong cyclones contribute to a better interpretation. On the other hand, the dynamical component shows a decreasing signal near Antarctica which leads to decreased Antarctic net precipitation due to dynamics. This is explained to be due to low frequency waves which seem to weaken (chapter 4).

The results of the previous chapters are discussed in the following with respect to the thesis objectives introduced in section 1.3.

How are Sub-Antarctic extra-tropical cyclones represented by different tracking schemes in reanalysis data?

This question is analysed by means of the output of 15 objective algorithms for the identification and tracking of extra-tropical cyclones. Tracks have been selected by regional criteria to filter cyclone tracks which mainly exist south of 60°S as well as in three longitudinal sectors, namely the Weddell Sea (WED), East Antarctica (EA), and the ABSL Sector. Statistics of cyclone track counts show large differences for the identified numbers of cyclone tracks, with respect to the 15 objective algorithms. The spread is consistent with findings of Neu et al. (2013), who investigated similar methodologies without a special focus on the Sub-Antarctic region. The separation of three sectors around Antarctica shows the differences of cyclone activity with respect to their occurrence. If the different size of the sectors is taken into account, cyclone activity more frequent for WED and the ABSL sectors in comparison to EA. These

simple statistics have to be discussed with care because some cyclone tracks will be found simultaneously in at least two sectors. Because of the filter criteria they occur in both sectoral datasets. The small sectors, i.e. WED and ABSL should be more influenced by this doubling artefact. Nevertheless, an interesting finding of the track number statistic is the fact that the spread is very similar for the different regions, i.e. methods identifying a number of tracks above average do this in all regions and vice versa. The spread between the identified number of tracks is found to be smaller in summer season when generally less cyclones are identified and the systems are shallower (Simmonds and Keay, 2000; Simmonds et al., 2003). Neu et al. (2013) find the representation of extra-tropical cyclones to be more similar for stronger events, which is counter-intuitive to the smaller spread of identified numbers between the tracks. This is explained to be due to a smaller range of possible cyclone strength in summer.

The analysis of the cyclone system density shows the general representation of different methodologies identifying large and small numbers of cyclone tracks. Different spots of high cyclone activity are expected, i.e. in the Indian and Australian Sectors of the Southern Ocean as well as south of Weddell Sea and Ross Sea, which can in parts attributed to quasi-stationary systems (Simmonds and Keay, 2000; Simmonds et al., 2003). The results of previous studies can be confirmed by different methodologies, whereas differences are found in some details. Southern Weddell and Ross Seas are regions of maximum cyclogenesis whereas around 30°E, north of Amery Ice Shelf as well as off-coast Adelie Land secondary maxima can be found (Simmonds and Keay, 2000; Bromwich et al., 2011). Weddell and Ross Seas are also regions of large cyclolysis. In fact, there can be found many short moving systems in these regions. On the other hand, in the Indian and Australian Sector of the Southern Ocean, the cyclones with the largest radii can be identified (Simmonds et al., 2003) as well as largest mean velocity (Hoskins and Hodges, 2005). The major spots of large cyclone activity is well captured by the different methodologies whereas larger differences occur in the regions of short moving cyclones, i.e. Weddell and Ross Seas.

The most intense 500 cyclones identified in 30 winter seasons are similar represented by the different algorithms. These most severe extra-tropical cyclones have been chosen similar to the study of (Ulbrich et al., 2013). These most intense systems are found in the East Atlantic as well as Indian Sectors where generally large and intense cyclones can be detected (Simmonds and Keay, 2000; Simmonds et al., 2003; Hoskins and Hodges, 2005). Another region of maximum strong cyclone system density in found in the Pacific Sector where cyclone activity is known to be related to the ABSL (Fogt et al., 2012).

How do the identified cyclones contribute to moisture inflow into Antarctica and are the results sensitive on different objective tracking algorithms?

Transient waves are the major contribution to poleward moisture transport in the SH mid- and high-latitudes (Peixoto and Oort, 1983; Tietäväinen and Vihma, 2008; Wu et al., 2011). High poleward energy fluxes in the Antarctic region can be associated with strong cyclone activity (Fogt et al., 2012) as well as extreme Antarctic snowfall events (Turner et al., 1995). To analyse the association of moisture inflow with strong cyclone activity the day of minimum pressure is chosen for the most severe events of each methodology to calculate a composite of transient moisture flux. This composite is compared with the climatological mean transient flux to calculate a flux anomaly. It results in extraordinary poleward moisture transport in the regions of high system density of strong cyclones. This result is robust with respect to the different cyclone tracking methodologies.

In sum a strong method dependency has been found for the general number of identified cyclone tracks. But the representation of strong cyclones as well as their contribution to moisture transport can be robustly analysed by various algorithms for the identification and tracking of extra-tropical cyclones.

How are extra-tropical cyclones represented in a multi-model ensemble?

To address this question a multi-model ensemble of six AOGCMs was investigated which have also been analysed in the context of "ENSEMBLES" (van der Linden and Mitchell, 2009). The objective algorithm for the identification and tracking uses 6-hourly values of MSLP. This parameter has not been CMIP3 standard output, which has been made this study to an important contribution of model evaluation for this generation of AOGCMs. The number of identified cyclone tracks largely differ for the various AOGCMs which is in parts due to the different horizontal resolution (cf. Blender and Schubert, 2000; Pinto et al., 2005). A scaling approach is introduced for a fairer calculation of the MME mean of cyclone track densities. This results in the identification of major cyclone characteristics in the MME, which can also be found in reanalysis data. On the other hand, cyclone intensity in terms of core pressure as well as the Laplacian of MSLP is underestimated by the MME.

Since the cyclone intensity distribution represented by different AOGCMs largely differs an investigation of strong cyclones is done by an analysis of percentile thresholds rather than absolute intensity values. Thus, following the approach of previous studies (Leckebusch and Ulbrich, 2004; Leckebusch et al., 2006, 2008), strong cyclone tracks are defined by means

of the 95th percentile of the Laplacian of MSLP. Therefore, a scaled MME mean of strong cyclone track density has been calculated and compared to reanalysis. As found for all cyclones, intensity of the MME mean is also underestimated for strong cyclones in comparison to reanalysis.

How does the MME simulate climate change of SH extra-tropical cyclones?

The future projections of the AOGCMs have followed the SRES A1B emission scenario (Nakicenovic et al., 2000). Cyclone activity has been investigated for 20 years of each AOGCM run at the end of the 20th and 21st centuries. Each model integration simulates a significant reduction of cyclone activity on the SH for extended winter season. Strong cyclones are found to be increase for 7 of 9 AOGCM runs whereas this hemispheric signal is significant for 3 of them. The climate signal of strong cyclone track numbers for the two models which show decreasing numbers does not depend on the intensity threshold.

Results become more robust for an analysis of track density patterns with respect to the MME mean. All cyclones show a distinct decrease north of 50°S and increases south of 60°S in the Atlantic and Indian Sectors of the Southern Ocean. Strong cyclones show an increasing signal especially on the Eastern Hemisphere with maximum increases south of Tasman Sea. These regions are additionally characterized by an intensification of cyclone tracks (cf. Bengtsson et al., 2006) as well as increase of extreme wind speed (Bengtsson et al., 2009).

The climate change signal of extra-tropical cyclones especially the strong ones is an important result of this study. The MME helps to assess the robustness of the climate change signal. In comparison to the climate signal of all cyclones, the most severe tracks are hardly dependent on the identification methodology (Ulbrich et al., 2013). For that reason the climate change signal of strong cyclones on the eastern Hemisphere can reliably be used for the further interpretation of SH moisture flux change. Certainly the change of all cyclones have also to be taken into account but can discussed to be more dependent on the cyclone identification and tracking algorithm.

How is Antarctic net precipitation represented in an AOGCM?

Net precipitation of a climate model, i.e. the difference between precipitation and evaporation can be calculated by the usage of modelled values for P and E. This is beneficial since the model can do the evaluation of P and E at each internal model integration time step taking into

account all vertical model levels. On the other hand, these benefits can turn into problems for the Antarctic region since the climate model has to deal with the representation of the steep topography, and in general physics of polar region. This can lead to systematic deviations of observational and modelled net precipitation (Genthon and Krinner, 2001). Since observations of Antarctic net precipitation also have to deal with several problems as the general small amount of precipitation and large snow drift, several studies evaluated the atmospheric hydrological cycle for an estimation of $P - E$ by means of radiosonde and numerical analysis (Bromwich, 1988; Bromwich et al., 1995; Cullather et al., 1998; Leckebusch, 1999). Following these ideas, this thesis mainly analysed net precipitation by means of the convergence of vertically integrated moisture flux. Nevertheless at first the three members of an ECHAM5 experiment representing the climate of the 20$^{\text{th}}$ century are analysed and modelled $P - E$ is compared to the output of ERA40 reanalysis. Principal characteristics of SH high-latitude precipitation are captured by the AOGCM although it produces generally more precipitation than ERA40 and shows a more noisy horizontal distribution. The ECHAM5 run which has also been investigated for cyclone activity in chapter 3 has been integrated at T63. In comparison to ERA40, the Antarctic Peninsula seems to be a less intense barrier in the AOGCM, since precipitation is underestimated on the western flank of the Peninsula and overestimated downstream, i.e. north of Weddell Sea. The annual cycle of P, E, and $P - E$ is well represented in the AOGCM for a spherical cap south of 67.5°S. As seen in the horizontal distribution modelled precipitation exceeds the value of ERA40, which results in an higher amount of net precipitation. Nevertheless, the annual cycle is well captured with maximum values in the extended winter season (April-September).

How large is the climate change signal of net precipitation and what is the role of water vapour increase in a warmer climate?

Antarctic net precipitation is simulated to increase in future climate projections (cf. Meehl et al., 2007b; Church et al., 2013; Collins et al., 2013). This is discussed to be due to increasing atmospheric moisture content which leads to increased Antarctic precipitation over the still cold enough ice sheet which does not show significantly increasing evaporation. On the other hand, large differences can be found for East and West Antarctica and in particular the Antarctic Peninsula. The latter region has been affected by huge temperature increases during the last century as well as catastrophic Ice Shelf disintegrations (Turner et al., 2009). This in turn, affects ice sheet dynamics of the adjacent glaciers which has to be taken into account for

a correct estimation of Antarctic SMB (Vaughan et al., 2013).

This thesis investigates the atmospheric branch of SMB, i.e. net precipitation, which is calculated by means of vertically integrated moisture flux. For an analysis of underlying mechanisms of moisture transport and its change, the flux is split into MMC and TE parts. TE has the major contribution to moisture poleward transport. The amount of net precipitation for extended winter is simulated to increase by 16%. This study introduced a scaling approach to distinguish between thermodynamical and dynamical parts of the climate change signal. The dynamical component shows a decreasing signal. In fact, the thermodynamical component is even larger than the totally simulated climate change signal.

What is the role of changed atmospheric circulations for changes in Antarctic net precipitation?

This thesis has used a scaling approach for the extraction of the dynamical part of the climate change signal of Antarctic net precipitation. This part shows a decreasing climate change signal of Antarctic net precipitation. This is counter-intuitive since the climate change signal of the SH atmospheric circulation is characterized by a poleward shift of the stormtrack. This is evaluated by 500hPa geopotential height variability. For a better understanding of the processes geopotential height variability as well as moisture flux is decomposed into different spatial and temporal wavelength (cf. Blackmon, 1976; Wu et al., 2011). The climate change signal of the stormtrack results in a poleward shift which is also be found for moisture flux, although no increases are found south of 60°S. The signal can be better interpreted if strong cyclones are taken into account. Results of chapter 2 for the relevance of strong cyclones as well as the robustness with respect to methodologies motivate this interpretation. The findings of chapter 3 for the robustness of the climate change signal of cyclone activity give importance to the results of dynamical moisture flux changes. The dynamical climate change signal of Antarctic net precipitation is mainly influenced by low frequency eddies in the spatially synoptic wavelength which shows a decreasing signal for almost the whole analysed area. South of 60°S this component can potentially attributed to the climatological low pressure patterns around Antarctica.

The ASL, which has large influences on the climate of West Antarctica (Fogt et al., 2012; Turner et al., 2013) is discussed to be unperfected represented in CMIP5 historical simulations (Hosking et al., 2013). Understanding the climate change signal of the variability is part of current research.

For a better understanding of future Antarctic net precipitation it would be beneficial to apply the approach of this study to a multi-model ensemble of AOGCMs, which requires temporally and vertically high resolution data. The understanding of near Antarctic pressure patterns seem to be crucial for the climate change signal of very high-latitude moisture flux.

Bibliography

M.G. Akperov, M. Yu. Bardin, E. M. Volodin, G. S. Golitsyn, and I. I. Mokhov. Probability distributions for cyclones and anticyclones from the ncep/ncar reanalysis data and the inm ras climate model. *Izvestiya, Atmospheric and Oceanic Physics*, 43:705–712, 2007.

M. Yu. Bardin and A. B. Polonsky. North atlantic oscillation and synoptic variability in the european-atlantic region in winter. *Izvestiya, Atmospheric and Oceanic Physics*, 41: 127–136, 2005.

L. Bengtsson, K. I. Hodges, and E. Roeckner. Storm tracks and climate change. *Journal Of Climate*, 19(15):3518–3543, August 2006.

L. Bengtsson, K. I. Hodges, and N. Keenlyside. Will extratropical storms intensify in a warmer climate? *Journal of Climate*, 22(9):2276–2301, May 2009. doi: 10.1175/2008JCLI2678.1.

N. L. Bindoff, P.A. Stott, K.M. AchutaRao, M.R. Allen, N. Gillett, D. Gutzler, K. Hansingo, G. Hegerl, Y. Hu, S. Jain, I.I. Mokhov, J. Overland, J. Perlwitz, R. Sebbari, and X. Zhang. Detection and attribution of climate change: from global to regional. In T.F. Stocker, D. Qin, G.-K. Plattner, M. Tignor, S.K. Allen, J. Boschung, A. Nauels, Y. Xia, V. Bex, and P.M. Midgley, editors, *Climate Change 2013: The Physical Science Basis. Contribution of Working Group I to the Fifth Assessment Report of the Intergovernmental Panel on Climate Change*, chapter 10. Cambridge Univ. Press, Cambridge, United Kingdom and New York, NY, USA, 2013.

M. L. Blackmon. A climatological spectral study of 500 mb geopotential height of northern hemisphere. *Journal of the Atmospheric Sciences*, 33(8):1607–1623, 1976. doi: 10.1175/1520-0469(1976)033<1607:ACSSOT>2.0.CO;2.

R. Blender and M. Schubert. Cyclone tracking in different spatial and temporal resolutions. *Monthly Weather Review*, 128(2):377–384, February 2000. doi: 10.1175/1520-0493(2000)128<0377:CTIDSA>2.0.CO;2.

R. Blender, K. Fraedrich, and F. Lunkeit. Identification of cyclone-track regimes in the north atlantic. *Quart. J. Roy. Meteor. Soc.*, 123:727–741, 1997.

D. H. Bromwich. Snowfall in high southern latitudes. *Reviews Of Geophysics*, 26(1):149–168, February 1988.

D. H. Bromwich and R. L. Fogt. Strong trends in the skill of the era-40 and ncep-ncar reanalyses in the high and midlatitudes of the southern hemisphere, 1958-2001. *Journal Of Climate*, 17(23):4603–4619, December 2004.

D. H. Bromwich and F. M. Robasky. Recent precipitation trends over the polar ice sheets. *Meteorology and Atmospheric Physics*, 51(3-4):259–274, 1993. doi: 10.1007/BF01030498.

D. H. Bromwich, F. M. Robasky, R. I. Cullather, and M. L. Vanwoert. The atmospheric hydrologic cycle over the southern ocean and antarctica from operational numerical analyses. *Monthly Weather Review*, 123(12):3518–3538, December 1995.

D. H. Bromwich, Z. C. Guo, L. S. Bai, and Q. S. Chen. Modeled antarctic precipitation. part i: Spatial and temporal variability. *Journal of Climate*, 17(3):427–447, February 2004.

D. H. Bromwich, R. L. Fogt, K. I. Hodges, and J. E. Walsh. A tropospheric assessment of the era-40, ncep, and jra-25 global reanalyses in the polar regions. *Journal Of Geophysical Research-Atmospheres*, 112(D10):D10111, May 2007.

D. H. Bromwich, D. F. Steinhoff, I. Simmonds, K. Keay, and R. L. Fogt. Climatological aspects of cyclogenesis near adelie land antarctica. *Tellus Series A-dynamic Meteorology and Oceanography*, 63(5):921–938, October 2011. doi: 10.1111/j.1600-0870.2011.00537.x.

A.M. Carleton. A synoptic climatology of satellite-observed extratropical cyclone activity for the southern hemisphere winter. 27(4):265–279–, 1979. ISSN 0066-6424.

E. K. M. Chang, Y. J. Guo, and X. M. Xia. Cmip5 multimodel ensemble projection of storm track change under global warming. *Journal of Geophysical Research-atmospheres*, 117: D23118, December 2012. doi: 10.1029/2012JD018578.

J.H. Christensen, K. Krishna Kumar, E. Aldrian, S.-I. An, I.F.A. Cavalcanti, M. de Castro, W. Dong, P. Goswami, A. Hall, J.K. Kanyanga, A. Kitoh, J. Kossin, N.-C. Lau, J. Renwick, D.B. Stephenson, S.-P. Xie, and T. Zhou. Climate phenomena and their relevance

for future regional climate change. In T.F. Stocker, D. Qin, G.-K. Plattner, M. Tignor, S.K. Allen, J. Boschung, A. Nauels, Y. Xia, V. Bex, and P.M. Midgley, editors, *Climate Change 2013: The Physical Science Basis. Contribution of Working Group I to the Fifth Assessment Report of the Intergovernmental Panel on Climate Change*, chapter 14, pages 1217–1308. Cambridge Univ. Press, Cambridge, United Kingdom and New York, NY, USA, 2013.

J.A. Church, P.U. Clark, A. Cazenave, J.M. Gregory, S. Jevrejeva, A. Levermann, M.A. Merrifield, G.A. Milne, R.S. Nerem, P.D. Nunn, A.J. Payne, W.T. Pfeffer, D. Stammer, and A.S. Unnikrishnan. Sea level change. In T.F. Stocker, D. Qin, G.-K. Plattner, M. Tignor, S.K. Allen, J. Boschung, A. Nauels, Y. Xia, V. Bex, and P.M. Midgley, editors, *Climate Change 2013: The Physical Science Basis. Contribution of Working Group I to the Fifth Assessment Report of the Intergovernmental Panel on Climate Change*, chapter 13. Cambridge Univ. Press, Cambridge, United Kingdom and New York, NY, USA, 2013.

M. Collins, R. Knutti, J. Arblaster, J.-L. Dufresne, T. Fichefet, P. Friedlingstein, X. Gao, W.J. Gutowski, T. Johns, G. Krinner, M. Shongwe, C. Tebaldi, A.J. Weaver, and M. Wehner. Long-term climate change: Projections, commitments and irreversibility. In T.F. Stocker, D. Qin, G.-K. Plattner, M. Tignor, S.K. Allen, J. Boschung, A. Nauels, Y. Xia, V. Bex, and P.M. Midgley, editors, *Climate Change 2013: The Physical Science Basis. Contribution of Working Group I to the Fifth Assessment Report of the Intergovernmental Panel on Climate Change*, chapter 12. Cambridge Univ. Press, Cambridge, United Kingdom and New York, NY, USA, 2013.

W. M. Connolley and J. C. King. Atmospheric water-vapor transport to antarctica inferred from radiosonde data. *Quarterly Journal of the Royal Meteorological Society*, 119(510): 325–342, January 1993.

R. I. Cullather, D. H. Bromwich, and M. L. Van Woert. Spatial and temporal variability of antarctic precipitation from atmospheric methods. *Journal of Climate*, 11(3):334–367, March 1998. doi: 10.1175/1520-0442(1998)011<0334:SATVOA>2.0.CO;2.

D. P. Dee, S. M. Uppala, A. J. Simmons, P. Berrisford, P. Poli, S. Kobayashi, U. Andrae, M. A. Balmaseda, G. Balsamo, P. Bauer, P. Bechtold, A. C. M. Beljaars, L. van de Berg, J. Bidlot, N. Bormann, C. Delsol, R. Dragani, M. Fuentes, A. J. Geer, L. Haimberger, S. B. Healy, H. Hersbach, E. V. Holm, L. Isaksen, P. Kallberg, M. Kohler, M. Matricardi, A. P. McNally, B. M. Monge-Sanz, J. J. Morcrette, B. K. Park, C. Peubey, P. de Rosnay, C. Tavolato, J. N.

Thepaut, and F. Vitart. The era-interim reanalysis: configuration and performance of the data assimilation system. *Quarterly Journal of the Royal Meteorological Society*, 137(656): 553–597, April 2011. doi: 10.1002/qj.828.

M. G. Donat, G. C. Leckebusch, J. G. Pinto, and U. Ulbrich. European storminess and associated circulation weather types: future changes deduced from a multi-model ensemble of gcm simulations. *Climate Research*, 42(1):27–43, 2010. doi: 10.3354/cr00853.

M. G. Donat, G. C. Leckebusch, S. Wild, and U. Ulbrich. Future changes in european winter storm losses and extreme wind speeds inferred from gcm and rcm multi-model simulations. *Natural Hazards and Earth System Sciences*, 11(5):1351–1370, 2011. doi: 10.5194/nhess-11-1351-2011.

R. L. Fogt, A. J. Wovrosh, R. A. Langen, and I. Simmonds. The characteristic variability and connection to the underlying synoptic activity of the amundsen-bellingshausen seas low. *Journal of Geophysical Research-atmospheres*, 117:D07111, April 2012. doi: 10.1029/2011JD017337.

T. Furevik, M. Bentsen, H. Drange, I. K. T. Kindem, N. G. Kvamsto, and A. Sorteberg. Description and evaluation of the bergen climate model: Arpege coupled with micom. *Climate Dynamics*, 21(1):27–51, July 2003. doi: 10.1007/s00382-003-0317-5.

Q. Z. Geng and M. Sugi. Possible change of extratropical cyclone activity due to enhanced greenhouse gases and sulfate aerosols - study with a high-resolution agcm. *Journal of Climate*, 16(13):2262–2274, July 2003.

C. Genthon and G. Krinner. Antarctic surface mass balance and systematic biases in general circulation models. *Journal of Geophysical Research-atmospheres*, 106(D18):20653–20664, September 2001. doi: 10.1029/2001JD900136.

J. Grieger, G.C. Leckebusch, M.G. Donat, M. Schuster, and U. Ulbrich. Southern hemisphere winter cyclone activity under recent and future climate conditions in multi-model aogcm simulations. *Int. J. Climatol.*, 34(12):3400–3416, 2014. ISSN 1097-0088. doi: 10.1002/joc.3917. URL `http://dx.doi.org/10.1002/joc.3917`.

J. Grieger, G. C. Leckebusch, I. Rudeva, C. C. Raible, and I. Simmonds. Comparison of different tracking algorithms analysing subantarctic cyclones. *in preparation for TELLUS-A*, 2015a.

Jens Grieger, Gregor C. Leckebusch, and Uwe Ulbrich. Net precipitation of Antarctica: thermodynamical and dynamical parts of the climate change signal. *J. Climate*, 2015b. doi: 10.1175/JCLI-D-14-00787.1. URL http://dx.doi.org/10.1175/JCLI-D-14-00787.1.

I. M. Held and B. J. Soden. Water vapor feedback and global warming. *Annual Review of Energy and the Environment*, 25:441–475, 2000. doi: 10.1146/annurev.energy.25.1.441.

I. M. Held and B. J. Soden. Robust responses of the hydrological cycle to global warming. *Journal of Climate*, 19(21):5686–5699, November 2006. doi: 10.1175/JCLI3990.1.

T. D. Hewson and H. A. Titley. Objective identification, typing and tracking of the complete life-cycles of cyclonic features at high spatial resolution. *Meteorological Applications*, 17 (3):355–381, September 2010. doi: 10.1002/met.204.

J. Scott Hosking, Andrew Orr, Gareth J. Marshall, John Turner, and Tony Phillips. The influence of the amundsen–bellingshausen seas low on the climate of west antarctica and its representation in coupled climate model simulations. *J. Climate*, 26(17):6633–6648, March 2013. ISSN 0894-8755.

B. J. Hoskins and K. I. Hodges. A new perspective on southern hemisphere storm tracks. *Journal of Climate*, 18(20):4108–4129, October 2005. doi: 10.1175/JCLI3570.1.

H. Huebener, U. Cubasch, U. Langematz, T. Spangehl, F. Niehorster, I. Fast, and M. Kunze. Ensemble climate simulations using a fully coupled ocean-troposphere-stratosphere general circulation model. *Philosophical Transactions of the Royal Society A-mathematical Physical and Engineering Sciences*, 365(1857):2089–2101, August 2007. doi: 10.1098/rsta.2007.2078.

M. Inatsu. The neighbor enclosed area tracking algorithm for extratropical wintertime cyclones. *Atmos. Sci. Lett.*, 10:267–272, 2009.

M. Inatsu, H. Mukougawa, and S. P. Xie. Tropical and extratropical sst effects on the midlatitude storm track rid a-4239-2012 rid c-1254-2009. *Journal of the Meteorological Society of Japan*, 80(4B):1069–1076, September 2002. doi: 10.2151/jmsj.80.1069.

T. C. Johns, C. F. Durman, H. T. Banks, M. J. Roberts, A. J. McLaren, J. K. Ridley, C. A. Senior, K. D. Williams, A. Jones, G. J. Rickard, S. Cusack, W. J. Ingram, M. Crucifix,

D. M. H. Sexton, M. M. Joshi, B. W. Dong, H. Spencer, R. S. R. Hill, J. M. Gregory, A. B. Keen, A. K. Pardaens, J. A. Lowe, A. Bodas-Salcedo, S. Stark, and Y. Searl. The new hadley centre climate model (hadgem1): Evaluation of coupled simulations. *Journal of Climate*, 19(7):1327–1353, April 2006. doi: 10.1175/JCLI3712.1.

J. H. Jungclaus, N. Keenlyside, M. Botzet, H. Haak, J. J. Luo, M. Latif, J. Marotzke, U. Mikolajewicz, and E. Roeckner. Ocean circulation and tropical variability in the coupled model echam5/mpi-om. *Journal of Climate*, 19(16):3952–3972, August 2006. doi: 10.1175/JCLI3827.1.

E. Kalnay, M. Kanamitsu, R. Kistler, W. Collins, D. Deaven, L. Gandin, M. Iredell, S. Saha, G. White, J. Woollen, Y. Zhu, A. Leetmaa, R. Reynolds, M. Chelliah, W. Ebisuzaki, W. Higgins, J. Janowiak, K. C. Mo, C. Ropelewski, J. Wang, Roy Jenne, and Dennis Joseph. The ncep/ncar 40-year reanalysis project. *Bull. Amer. Meteor. Soc.*, 77(3):437–471, March 1996. ISSN 0003-0007. doi: 10.1175/1520-0477(1996)077<0437:TNYRP>2.0.CO;2.

S. Karelsky. Geographical distribution of pressure in the centres of surface lows and highs in the australian region in january and july, 1952-1963. *Australian Meteorological Magazine*, 43:15–23, 1963.

S. F. Kew, M. Sprenger, and H. C. Davies. Potential vorticity anomalies of the lowermost stratosphere: A 10-yr winter climatology. *Mon. Wea. Rev.*, 138:1234–1249, 2010.

J. Kidston and E. P. Gerber. Intermodel variability of the poleward shift of the austral jet stream in the cmip3 integrations linked to biases in 20th century climatology. *Geophysical Research Letters*, 37:L09708, May 2010. doi: 10.1029/2010GL042873.

J.C. King and J. Turner. *Antarctic meteorology and climatology*. Cambridge University Press, 1997.

S. J. Lambert and J. C. Fyfe. Changes in winter cyclone frequencies and strengths simulated in enhanced greenhouse warming experiments: results from the models participating in the ipcc diagnostic exercise. *Climate Dynamics*, 26(7-8):713–728, June 2006.

Steven J. Lambert. A cyclone climatology of the canadian climate centre general circulation model. *J. Climate*, 1(1):109–115, January 1988. ISSN 0894-8755. doi: 10.1175/1520-0442(1988)001<0109:ACCOTC>2.0.CO;2.

G C Leckebusch. *Meteorological interpretation of depositions in polar ice cores by means of paleoclimate simulations with ECHAM3 global climate model*. PhD thesis, Institute for Geophysics and Meteorology, University of Cologne, 1999.

G. C. Leckebusch, B. Koffi, U. Ulbrich, J. G. Pinto, T. Spangehl, and S. Zacharias. Analysis of frequency and intensity of european winter storm events from a multi-model perspective, at synoptic and regional scales. *Climate Research*, 31(1):59–74, June 2006.

G. C. Leckebusch, M. G. Donat, U. Ulbrich, and J. G. Pinto. Mid-latitude cyclones and storms in an ensemble of european aogcms under acc. *CLIVAR Exchanges*, 13(3):3–5, July 2008.

G. C. Leckebusch, J. Grieger, J. G. Pinto, M. G. Akperov, K. Keay, M. L. R. Liberato, I. F. Trigo, R. Trigo, and U. Ulbrich. Trends and variability of extra-tropical cyclones derived from different tracking schemes. *in preparation for TELLUS-A*, 2015.

Gregor C. Leckebusch and Uwe Ulbrich. On the relationship between cyclones and extreme windstorm events over europe under climate change. *Global and Planetary Change*, 44 (1-4):181–193, December 2004. ISSN 0921-8181.

S. Legutke and R. Voss. The hamburg atmosphere-ocean coupled circulation model echo-g. Technical report 18, German Climate Computer Centre (DKRZ), 1999.

E. P. Lim and I. Simmonds. Southern hemisphere winter extratropical cyclone characteristics and vertical organization observed with the era-40 data in 1979-2001. *Journal Of Climate*, 20(11):2675–2690, June 2007.

E. P. Lim and I. Simmonds. Effect of tropospheric temperature change on the zonal mean circulation and sh winter extratropical cyclones. *Climate Dynamics*, 33(1):19–32, July 2009.

P. Lionello, F. Dalan, and E. Elvini. Cyclones in the mediterranean region: the present and the doubled co2 climate scenarios. *Clim. Res.*, 22:147–159, 2002.

D. J. Lorenz and E. T. DeWeaver. The response of the extratropical hydrological cycle to global warming. *Journal of Climate*, 20(14):3470–3484, July 2007. doi: 10.1175/JCLI4192.1.

A. Lynch, P. Uotila, and J. J. Cassano. Changes in synoptic weather patterns in the polar regions in the twentieth and twenty-first centuries, part 2: Antarctic. *International Journal Of Climatology*, 26(9):1181–1199, July 2006. doi: 10.1002/joc.1305.

E. Manzini and N. A. McFarlane. The effect of varying the source spectrum of a gravity wave parameterization in a middle atmosphere general circulation model. *Journal of Geophysical Research-atmospheres*, 103(D24):31523–31539, December 1998. doi: 10.1029/98JD02274.

S.J. Marsland, H. Haak, J.H. Jungclaus, M. Latif, and F. Röske. The max-planck-institute global ocean/sea ice model with orthogonal curvilinear coordinates. *Ocean Modelling*, 5 (2):91–127, 2003. ISSN 1463-5003.

O. Marti, P. Braconnot, J. Bellier, R. Benshila, S. Bony, P. Brockmann, P. Cadule, A. Caubel, S. Denvil, J.L. Dufresne, L. Fairhead, M.-A. Filiberti, T. Fichefet, M.-A. Foujols, P. Friedlingstein, J.-Y. Grandpeix, F. Hourdin, G. Krinner, C. Lévy, G. Madec, I. Musat, N. De Noblet, J. Polcher, and C. Talandier. The new ipsl climate system model: Ipsl-cm4. *Note du Pôle de Modélisation, IPSL*, 26:1–86, April 2005.

G. M. Martin, M. A. Ringer, V. D. Pope, A. Jones, C. Dearden, and T. J. Hinton. The physical properties of the atmosphere in the new hadley centre global environmental model (hadgem1). part i: Model description and global climatology. *Journal of Climate*, 19(7): 1274–1301, April 2006. doi: 10.1175/JCLI3636.1.

G. A. Meehl, C. Covey, T. Delworth, M. Latif, B. McAvaney, J. F. B. Mitchell, R. J. Stouffer, and K. E. Taylor. The wcrp cmip3 multimodel dataset - a new era in climate change research. *Bulletin of the American Meteorological Society*, 88(9):1383–+, September 2007a. doi: 10.1175/BAMS-88-9-1383.

G.A. Meehl, T.F. Stocker, W.D. Collins, P. Friedlingstein, A.T. Gaye, J.M. Gregory, A. Kitoh, R. Knutti, J.M. Murphy, A. Noda, S.C.B. Raper, I.G. Watterson, A.J. Weaver, and Z.-C. Zhao. Global climate projections. In S. Solomon, D. Qin, M. Manning, Z. Chen, M. Marquis, K.B. Averyt, M. Tignor, and H.L. Miller, editors, *Climate Change 2007: The Physical Science Basis. Contribution of Working Group I to the Fourth Assessment Report of the Intergovernmental Panel on Climate Change*. Cambridge University Press, Cambridge, United Kingdom and New York, NY, USA, 2007b.

A. J. Monaghan, D. H. Bromwich, and S. H. Wang. Recent trends in antarctic snow accumulation from polar mm5 simulations. *Philosophical Transactions of the Royal Society A-mathematical Physical and Engineering Sciences*, 364(1844):1683–1708, July 2006. doi: 10.1098/rsta.2006.1795.

R.J. Murray and I. Simmonds. A numerical scheme for tracking cyclone centres from digital data. part i: developement and operation of the scheme. *Australian Meteorological Magazine*, 39:155–166, 1991a.

R.J. Murray and I. Simmonds. A numerical scheme for tracking cyclone centres from digital data. part ii: Application to january and july general circulation model simulations. *Australian Meteorological Magazine*, 39:167–180, 1991b.

N. Nakicenovic, J. Alcamo, G. Davis, B. de Vries, J. Fenhann, S. Gaffin, K. Gregory, A. Grübler, T.Y. Jung, T. Kram, E.L. La Rovere, L. Michaelis, S. Mori, T. Morita, W. Pepper, H. Pitcher, L. Price, K. Riahi, A. Roehrl, H.-H. Rogner, A. Sankovski, M. Schlesinger, P. Shukla, S. Smith, R. Swart, S. van Rooijen, N. Victor, and Z. Dadi. Special report on emissions scenarios. *Cambridge University Press*, page 599 pp., 2000.

Urs Neu, Mirseid G. Akperov, Nina Bellenbaum, Rasmus Benestad, Richard Blender, Rodrigo Caballero, Angela Cocozza, Helen F. Dacre, Yang Feng, Klaus Fraedrich, Jens Grieger, Sergey Gulev, John Hanley, Tim Hewson, Masaru Inatsu, Kevin Keay, Sarah F. Kew, Ina Kindem, Gregor C. Leckebusch, Margarida L. R. Liberato, Piero Lionello, Igor I. Mokhov, Joaquim G. Pinto, Christoph C. Raible, Marco Reale, Irina Rudeva, Mareike Schuster, Ian Simmonds, Mark Sinclair, Michael Sprenger, Natalia D. Tilinina, Isabel F. Trigo, Sven Ulbrich, Uwe Ulbrich, Xiaolan L. Wang, and Heini Wernli. Imilast - a community effort to intercompare extratropical cyclone detection and tracking algorithms. *Bull. Amer. Meteor. Soc.*, 94(4):529–547, 2013. ISSN 0003-0007. doi: 10.1175/BAMS-D-11-00154.1.

J. P. Nicolas and D. H. Bromwich. Climate of west antarctica and influence of marine air intrusions. *Journal of Climate*, 24(1):49–67, January 2011. doi: 10.1175/2010JCLI3522.1.

F. Niehörster, I. Fast, H. Huebener, and U. Cubasch. The stream one ensembles projections of future climate change. ENSEMBLES Technical Report 3, 2008.

K. M. Nissen, G. C. Leckebusch, J. G. Pinto, D. Renggli, S. Ulbrich, and U. Ulbrich. Cyclones causing wind storms in the mediterranean: characteristics, trends and links to large-scale patterns. *Natural Hazards and Earth System Sciences*, 10(7):1379–1391, 2010. doi: 10.5194/nhess-10-1379-2010.

J. P. Peixoto and A. H. Oort. The atmospheric branch of hydrological cycle and climate. In

Alayne Street-Perrott, editor, *Variations in the global water budget*, pages pp. 5–65. Reidel, 1983.

J. P. Peixoto and A. H. Oort. *Physics of climate*. Springer, 1992.

A. B. Pezza, T. Durrant, I. Simmonds, and I. Smith. Southern hemisphere synoptic behavior in extreme phases of sam, enso, sea ice extent, and southern australia rainfall. *Journal of Climate*, 21(21):5566–5584, November 2008. doi: 10.1175/2008JCLI2128.1.

A. B. Pezza, H. A. Rashid, and I. Simmonds. Climate links and recent extremes in antarctic sea ice, high-latitude cyclones, southern annular mode and enso. *Climate Dynamics*, 38 (1-2):57–73, January 2012. doi: 10.1007/s00382-011-1044-y.

J. G. Pinto, T. Spangehl, U. Ulbrich, and P. Speth. Sensitivities of a cyclone detection and tracking algorithm: individual tracks and climatology. *Meteorol. Z.*, 14(6):823–838, 2005.

J. G. Pinto, U. Ulbrich, G. C. Leckebusch, T. Spangehl, M. Reyers, and S. Zacharias. Changes in storm track and cyclone activity in three sres ensemble experiments with the echam5/mpi-om1 gcm. *Climate Dynamics*, 29(2):195–210, August 2007.

C. C. Raible, P. M. Della-Marta, C. Schwierz, H. Wernli, and R. Blender. Northern hemisphere extratropical cyclones: A comparison of detection and tracking methods and different re-analyses. *Mon. Wea. Rev.*, 136:880–897, 2008.

M. A. Ringer, G. M. Martin, C. Z. Greeves, T. J. Hinton, P. M. James, V. D. Pope, A. A. Scaife, R. A. Stratton, P. M. Inness, J. M. Slingo, and G. Y. Yang. The physical properties of the atmosphere in the new hadley centre global environmental model (hadgem1). part ii: Aspects of variability and regional climate. *Journal of Climate*, 19(7):1302–1326, April 2006. doi: 10.1175/JCLI3713.1.

E. Roeckner, G. Bäuml, L. Bonaventura, R. Brokopf, M. Esch, M. Giorgetta, S. Hagemann, I. Kirchner, L. Kornblueh, E. Manzini, A. Rhodin, U. Schlese, U. Schulzweida, and A. Tompkins. The atmospheric general circulation model echam 5. part i: Model description. *Max Planck Institute for Meteorology Report*, 349, 2003.

I. Rudeva and S. K. Gulev. Climatology of cyclone size characteristics and their changes during the cyclone life cycle. *Mon. Wea. Rev.*, 135:2568–2587, 2007.

D. Salas-Mélia, F. Chauvin, M. Déqué, H. Douville, J. F. Gueremy, P. Marquet, S. Planton, J. F. Royer, and S. Tyteca. Description and validation of the CNRM-CM3 global coupled model. Technical Report CNRM working note 103, Météo-France, 42 Avenue Gaspard Coriolis, 31057 Toulouse Cedex, France, 2005.

Mareike Schuster. Die Bedeutung von Änderungen der SST-Gradienten und der obertroposphärischen Temperatur für die Verlagerung der südhemisphärischen Zyklonenzugbahnen im Klimaszenario. Master's thesis, Institut für Meteorologie, Freie Universität Berlin, 2012.

W. Schwerdtfeger. *Weather and Climate of the Antarctic*. Elsevier Science Bv, 1984.

R. Seager, N. Naik, and G. A. Vecchi. Thermodynamic and dynamic mechanisms for large-scale changes in the hydrological cycle in response to global warming. *Journal of Climate*, 23(17):4651–4668, September 2010. doi: 10.1175/2010JCLI3655.1.

M. C. Serreze. Climatological aspects of cyclone development and decay in the arctic. *Atmosphere-Ocean*, 33(1):1–23, March 1995.

Steven R. Silberberg and Lance F. Bosart. An analysis of systematic cyclone errors in the nmc lfm-ii model during the 1978-79 cool season. *Mon. Wea. Rev.*, 110(4):254–271, April 1982. ISSN 0027-0644. doi: 10.1175/1520-0493(1982)110<0254:AAOSCE>2.0.CO;2.

I. Simmonds and K. Keay. Mean southern hemisphere extratropical cyclone behavior in the 40-year ncep-ncar reanalysis. *Journal Of Climate*, 13(5):873–885, March 2000.

I. Simmonds and R. J. Murray. Southern extratropical cyclone behavior in ecmwf analyses during the frost special observing periods. *Weather And Forecasting*, 14(6):878–891, December 1999.

I. Simmonds, R. J. Murray, and R. M. Leighton. A refinement of cyclone tracking methods with data from frost. *Australian Meteorological Magazine*, (SI):35–49, June 1999.

I. Simmonds, C. Burke, and K. Keay. Arctic climate change as manifest in cyclone behavior. *Journal of Climate*, 21(22):5777–5796, November 2008. doi: 10.1175/2008JCLI2366.1.

Ian Simmonds, Kevin Keay, and Eun-Pa Lim. Synoptic activity in the seas around antarctica. *Monthly Weather Review*, 131(2):272–288, 2003. doi: 10.1175/1520-0493(2003)131<0272:SAITSA>2.0.CO;2.

Mark R. Sinclair. An objective cyclone climatology for the southern hemisphere. *Monthly Weather Review*, 122(10):2239–2256, 1994. doi: 10.1175/1520-0493(1994)122<2239:AOCCFT>2.0.CO;2.

Mark R. Sinclair. Objective identification of cyclones and their circulation intensity, and climatology. *Weather and Forecasting*, 12(3):595–612, 1997. doi: 10.1175/1520-0434(1997)012<0595:OIOCAT>2.0.CO;2.

J. J. Taljaard. Development, distribution and movement of cyclones and anticyclones in the southern hemisphere during the igy. *J. Appl. Meteor.*, 6(6):973–987, December 1967. ISSN 0021-8952. doi: 10.1175/1520-0450(1967)006<0973:DDAMOC>2.0.CO;2.

H. Tietäväinen and T. Vihma. Atmospheric moisture budget over antarctica and the southern ocean based on the era-40 reanalysis. *International Journal of Climatology*, 28(15):1977–1995, 2008.

I.F. Trigo. Climatology and interannual variability of storm-tracks in the euro-atlantic sector: a comparison between era-40 and ncep/ncar reanalyses. *Climate Dynamics*, 26:127–143, 2006.

J. Turner, T. A. Lachlan-Cope, J. P. Thomas, and S. R. Colwell. The synoptic origins of precipitation over the antarctic peninsula. *Antarctic Science*, 7(3):327–337, September 1995.

J. Turner, R. Bindschadler, P. Convey, G. di Prisco, E. Fahrbach, J. Gutt, D. Hodgson, Mayewski P., and C. Summerhayes, editors. *Antarctic climate change and the environment*. Cambridge: Scientific Committee on Antarctic Research, Scott Polar Research Institute, 2009.

John Turner, Tony Phillips, J. Scott Hosking, Gareth J. Marshall, and Andrew Orr. The amundsen sea low. *Int. J. Climatol.*, 33(7):1818–1829, June 2013. ISSN 1097-0088.

U. Ulbrich, G. C. Leckebusch, and J. G. Pinto. Extra-tropical cyclones in the present and future climate: a review. *Theoretical and Applied Climatology*, 96(1):117–131, April 2009.

Uwe Ulbrich, Gregor C. Leckebusch, Jens Grieger, Mareike Schuster, Mirseid Akperov, Mikhail Yu. Bardin, Yang Feng, Sergey Gulev, Masaru Inatsu, Kevin Keay, Sarah F. Kew, Margarida L. R. Liberato, Piero Lionello, Igor I. Mokhov, Urs Neu, Joaquim G. Pinto,

Christoph C. Raible, Marco Reale, Irina Rudeva, Ian Simmonds, Natalia D. Tilinina, Isabel F. Trigo, Sven Ulbrich, Xiaolan L. Wang, and Heini Wernli. Are greenhouse gas signals of northern hemisphere winter extra-tropical cyclone activity dependent on the identification and tracking algorithm? *Meteorologische Zeitschrift*, 22(1):61–68, 2013. doi: doi:10.1127/0941-2948/2013/0420.

P. Uotila, A. H. Lynch, J. J. Cassano, and R. I. Cullather. Changes in antarctic net precipitation in the 21st century based on intergovernmental panel on climate change (ipcc) model scenarios. *Journal of Geophysical Research-atmospheres*, 112(D10):D10107, May 2007. doi: 10.1029/2006JD007482.

S. M. Uppala, P. W. Kallberg, A. J. Simmons, U. Andrae, V. Da Costa Bechtold, M. Fiorino, J. K. Gibson, J. Haseler, A. Hernandez, G. A. Kelly, X. Li, K. Onogi, S. Saarinen, N. Sokka, R. P. Allan, E. Andersson, K. Arpe, M. A. Balmaseda, A. C. M. Beljaars, L. Van De Berg, J. Bidlot, N. Bormann, S. Caires, F. Chevallier, A. Dethof, M. Dragosavac, M. Fisher, M. Fuentes, S. Hagemann, E. Holm, B. J. Hoskins, L. Isaksen, P. A. E. M. Janssen, R. Jenne, A. P. Mcnally, J.-F. Mahfouf, J.-J. Morcrette, N. A. Rayner, R. W. Saunders, P. Simon, A. Sterl, K. E. Trenberth, A. Untch, D. Vasiljevic, P. Viterbo, and J. Woollen. The era-40 re-analysis. *Quarterly Journal of the Royal Meteorological Society*, 131(612):2961–3012, 2005. doi: 10.1256/qj.04.176.

M. R. van den Broeke and N. P. M. van Lipzig. Changes in antarctic temperature, wind and precipitation in response to the antarctic oscillation rid f-7867-2011. *Annals of Glaciology, Vol 39, 2005*, 39:119–126, 2004. doi: 10.3189/172756404781814654.

P. van der Linden and J.F.B. Mitchell. Ensembles: Climate change and its impacts: Summary of research and results from the ensembles project. *Met Office Hadley Centre, Exeter, UK*, page 160pp., 2009.

H. van Loon. A climatological study of the atmospheric circulation in the southern hemisphere during igy, part i: 1 july 1957 - 31 march 1958. *Journal of Applied Meteorology*, 4:479–491, 1965.

D.G. Vaughan, J.C. Comiso, I. Allison, J. Carrasco, G. Kaser, R. Kwok, P. Mote, T. Murray, F. Paul, J. Ren, E. Rignot, O. Solomina, K. Steffen, and T. Zhang. Observations: Cryosphere. In T.F. Stocker, D. Qin, G.-K. Plattner, M. Tignor, S.K. Allen, J. Boschung,

A. Nauels, Y. Xia, V. Bex, and P.M. Midgley, editors, *Climate Change 2013: The Physical Science Basis. Contribution of Working Group I to the Fifth Assessment Report of the Intergovernmental Panel on Climate Change*, chapter 4. Cambridge Univ. Press, Cambridge, United Kingdom and New York, NY, USA, 2013.

X. L. L. Wang, V. R. Swail, and F. W. Zwiers. Climatology and changes of extratropical cyclone activity: Comparison of era-40 with ncep-ncar reanalysis for 1958-2001. *Journal of Climate*, 19(13):3145–3166, July 2006. doi: 10.1175/JCLI3781.1.

XiaolanL. Wang, Y. Feng, G.P. Compo, V.R. Swail, F.W. Zwiers, R.J. Allan, and P.D. Sardeshmukh. Trends and low frequency variability of extra-tropical cyclone activity in the ensemble of twentieth century reanalysis. *Climate Dynamics*, pages 1–26, 2012. ISSN 0930-7575. doi: 10.1007/s00382-012-1450-9. DOI:10.1007/s00382-012-1450-9.

H. Wernli and C. Schwierz. Surface cyclones in the era-40 data set (1958–2001). part i: Novel identification method and global climatology. *J. Atmos. Sci.*, 63:2486–2507, 2006.

Y. T. Wu, M. F. Ting, R. Seager, H. P. Huang, and M. A. Cane. Changes in storm tracks and energy transports in a warmer climate simulated by the gfdl cm2.1 model. *Climate Dynamics*, 37(1-2):53–72, July 2011. doi: 10.1007/s00382-010-0776-4.

Koji Yamazaki. Moisture budget in the antarctic atmosphere. *Proceedings of the NIPR Symposium on Polar Meteorology and Glaciology*, 6:36–45, 1992. ISSN 09142037.

J. H. Yin. A consistent poleward shift of the storm tracks in simulations of 21st century climate. *Geophysical Research Letters*, 32(18):L18701, September 2005. doi: 10.1029/2005GL023684.

O. Zolina and S. K. Gulev. Improving accuracy of mapping cyclone numbers and frequencies. *Mon. Wea. Rev.*, 130:748–759, 2002.

Acknowledgments

Zunächst möchte ich Gregor Leckebusch und Uwe Ulbrich danken, dass sie es mir ermöglichten diese Arbeit anzufertigen. Ohne die stetigen Diskussionen und die Betreuung der letzten Jahre wäre diese Arbeit nicht zustande gekommen. Ich möchte darüber hinaus allen Mitarbeiter_innen der Arbeitsgruppe Clidia für das gute Arbeitsumfeld danken. Des Weiteren bedanke ich mich bei Markus und Mareike für die gute Zusammenarbeit und bei Tim, Tobias, Robert und Christopher für die guten Worte in der stressigen Schlussphase meiner Arbeit. Ich möchte meinen Eltern, Großeltern, Schwiegereltern und meiner Schwester und Manu für ihre Unterstützung danken. Ein besonderer Dank gilt Celine, Milo und Emmi, die viel Verständnis für die Zeit, die ich in diese Arbeit steckte, aufbrachten. Sie zeigten mir, dass es viele wichtige Dinge im Leben gibt, was mir eine nötige Ablenkung schaffte und mich die Motivation an meiner Arbeit nicht verlieren ließ.